3-13-2007

Portable Diode Pumped Femtosecond Laser

David A. Jones

PORTABLE DIODE PUMPED FEMTOSECOND LASERS

THESIS

David A. Jones, Captain, USAF

AFIT/GAP/ENP/07-04

DEPARTMENT OF THE AIR FORCE
AIR UNIVERSITY

AIR FORCE INSTITUTE OF TECHNOLOGY

Wright-Patterson Air Force Base, Ohio

The views expressed in this thesis are those of the author and do not reflect the official policy or position of The United States Air Force, Department of Defense, or the United States Government.

AFIT/GAP/ENP/07-04

PORTABLE DIODE PUMPED FEMTOSECOND LASERS

THESIS

Presented to the Faculty

Department of Engineering Physics

Graduate School of Engineering and Management

Air Force Institute of Technology

Air University

Air Education and Training Command

In Partial Fulfillment of the Requirements for the

Degree of Master of Science in Applied Physics

David A. Jones, B.S.

Captain, USAF

March 2007

AFIT/GAP/ENP/07-04

PORTABLE DIODE PUMPED FEMTOSECOND LASERS

David A. Jones, B.S.
Captain, USAF

Approved:

Matthew J. Bohn (Chairman)	13 Mar 07 Date
Michael A. Marciniak (Member)	13 Mar 07 Date
Timothy H. Russell (Member)	13 MAR 07 Date

Abstract

Ultrashort pulse laser technology is receiving increased focus around the world, and as the size and expense are reduced, their applications will receive more attention. This thesis discusses the work to make ultrashort pulsed lasers smaller and more economical. Possibilities of these pulses include creation of terahertz radiation, characterization of materials through ablation, enhanced ring laser gyroscopes, ultrastable atomic clocks and fast ignition fusion. While sharing many of the basic properties of normal beam optics there are some specific properties in both creating and exploiting those pulses that must be understood. The discussion will focus on mode locking as the primary way of producing ultrashort pulses. Particular attention will be paid to intracavity group velocity dispersion and how to correct it inside the cavity. The discussion then turns to the basis of our work including initial cavity design and component selection with a focus on the specific crystals used in the solid state laser. The primary focus for the rest of the experiment setup is based on the evolution of the designs in order to get the systems lasing and then mode locked. Results from the work on the small cavity systems are then compared to data taken from a commercial titanium-sapphire laser with an emphasis on current measurement techniques. Overall conclusions include the impact of both equipment and the crystals used in the solid state cavity to generate ultrashort pulses. While not fully successful, the groundwork has been laid for future research on portable, diode pumped femtosecond lasers.

Acknowledgements

I owe a large debt of gratitude to my advisor. He provided the guidance and direction that made my laboratory experience both rewarding and successful. He also kept me focused when the frustrations and monotony threatened to derail my efforts. Thanks also to the lab technicians who were wonderful, reacting to changes in the research plan and making it work. I would kiss your feet but that would mean asking for something again. If my work has any future impact much credit belongs to the members of my advisory board. Finally, to my wife and daughters, thanks for the patience and understanding. Daddy doesn't have any homework tonight...

David A. Jones

Table of Contents

Page

List of Figures

List of Tables

List of Abbreviations

Abbreviation		Page
m	meters	45
mW	milliwatts	45
Yb:KGW	Yb:KGd$(WO_4)_2$	47
Yb:vanadate	Ytterbium orthovanadate	49
ROC	radius of curvature	61
TEC	thermoelectric cooler	69
SHG	second harmonic generation	74
RF	real-time Fourier transform	74
FFT	fast Fourier transform	74
ps	picosecond	74
SHG	second harmonic generation	74

PORTABLE
DIODE PUMPED
FEMTOSECOND LASERS

I. Introduction

In just over forty years, the laser has gone from crude laboratory experimentation to an essential technology in the health, communication, and military arenas. The cutting edge of the continued advances in laser optics are ultrashort pulsed lasers. Dubbed "extreme light" by *Scientific American* in May 2002, pulsed lasers have garnered interest because of their unique properties and their effect on matter. [28] However, there are challenges in producing these ultrashort and ultrafast pulse rates. Some technologies, such as the mode locked titanium-sapphire (Ti:sapphire) laser, are relatively mature but other ways to produce the pulses are being explored. This thesis focuses on several of these new sources, emphasizing the size and results when used in a cavity design.

1.1 Extreme Applications

As a leading edge optical technology, useful applications are continually being proposed. The biggest advantage of this technology is its promise of adaptability. It is possible to design a system to have a faster repetition rate while another can be designed for more intensity by shortening the pulse width. Even better, current research is leading towards the ability to do both of those things with the same system. This is being done by reducing the size of the cavity and using the higher power diode lasers now becoming available at the proper wavelengths. Ben Agate *et al.* has done a large amount of work on reducing cavity size and motivated much of this thesis. [1]

The goal of systems having both of the qualities noted above has an immense impact on current efforts at system development and design. For example, a significant

effort within the homeland security arena is the development of detection systems. A specific example of current research, which is also being studied at AFIT, is on producing terahertz radiation by impacting these ultrashort pulses on a nonlinear crystal or photoelectric switch. [28] This terahertz radiation has some unique detection capabilities in both solid materials and the human body. Another detection oriented example is proton-radiography in which ultra-intense pulses are directed on to a thin metallic surface, causing the release of protons that can be then directed to a detector. [28] This technology is promising because protons are good at looking through complex systems without having to physically dismantle the items being scanned.

Another interesting development is looking at the particles being ablated from a material with a spectrometer. This is done by laser-induced breakdown spectroscopy (LIBS), which uses a laser pulse to ablate and ionize a target. [32] However, the intensity on target decreases dramatically with distance from the target due to diffraction. [32] This results in problems when observing targets where it is dangerous or inconvenient to be in close proximity. There is promise that ultrashort pulses can solve some of these problems. Because ultrashort pulses are subject to a limited Kerr effect in air (see Chapter II), self-focusing of the beam can occur resulting in filaments being created in the air. These filaments can then be used to ionize a target, which is known as remote filament-induced breakdown spectroscopy (R-FIBS). [27, 32] Figure 1.1 shows a typical setup and pattern created on the target. While a short distance was used for the experiment, it is believed that ultimately the effect can be created at distances of up to several kilometers, a clear advantage for a sensor system. [32] Another advantage, though of less importance, is that enough power is put on target to cause ablation but due to the changes in the atmosphere over time the filaments move causing no obvious markings. [27] This can be advantageous is many situations when discretion is necessary.

Of specific interest to the USAF is the possible development of enhanced laser gyroscopes. There are still a number of mechanical inertial navigation units being used in aircraft systems. Ring laser gyroscopes are becoming more popular due to the

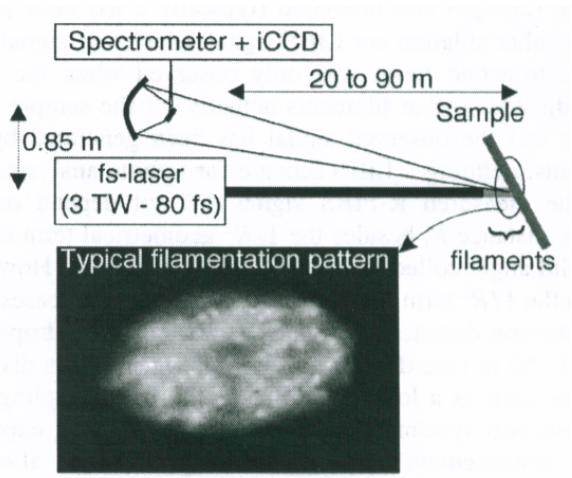

Figure 1.1: Experimental R-FIBS setup with sample signal showing approximately 30 filaments across the overall beam. [41]

lack of moving parts. They work similar to a Sagnac interferometer like that shown in Figure 1.2. [40, 41] As the ring is moved, the beams in the two directions end up with different path lengths and as a result the interference pattern changes. The problem with ring laser gyroscope is that they have difficulty registering changes when angular velocities are very slow. [40] Low angular velocity aerial systems such as unmanned aerial reconnaissance vehicles could benefit from inertial systems built around smaller and faster pulse rates, providing back-up navigation capabilities if global positioning system (GPS) guidance is unavailable due to jamming or systems failures. It can also further advance GPS systems by using this type of gyroscope in satellites to increase accuracy of placement in orbit and reduce deviations.

Along the same lines as the laser ring gyroscopes is the possibility of ultra-stable atomic clocks. This can be an advantage in the continual tug of war to reduce the size, while making more accurate and more economical clocks. Ultrashort pulses enable a relatively simple and cheap method to link optical spectra with the current microwave spectra standard. [37] The key is that at these optical frequencies are calibrated down to the radio frequency standard. [37] The Air Force interest for this is primarily GPS related. More accurate clocks in the GPS receivers and satellites increase the precision that the signal times are calculated. Current commercial systems have

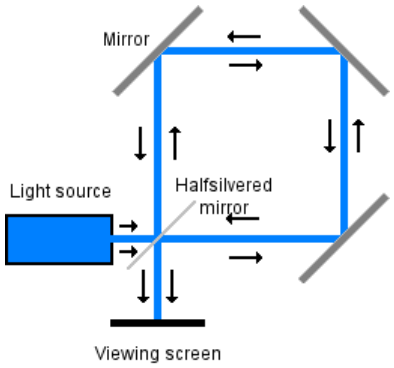

Figure 1.2: Example of a Sagnac ring interferometer. As the beam enters the interferometer it is split into two opposite paths and the pattern of interference can be analyzed. [41]

precision around 20 meters without local digital correction. [20] The possibility of getting precision from space below a meter is becoming a reality.

Another leading edge technology research is "Fast Ignition" fusion technology. Michael Perry *et al.* at the Lawrence Livermore National Laboratory have had success working on this aspect of research. Essentially, this consists of using an ultraintense pulse beam, dividing it into separate parts, and then focusing them from multiple angles onto a compressed fusion fuel. [13, 28] Specifically, they were using the aptly named Petawatt laser, which was able to provide 680 joules of energy in 440 femtoseconds resulting in a power over 1.5 peta or 10^{15} W. While they were not able to create fusion, their work provided enough information to show that there is a future for this research. [21] The most current research is looking at effects on plasmas which are leading into the compressed fuels. The implications of success would have an effect on everything from energy production to space travel. [28] As always, however, new ideas and new research must continue to be followed.

1.2 Current System Limitations

1.2.1 Size, Support and Price. One of the biggest limitations on current extreme light sources is the size of the system. Most mature systems have large laboratory footprints. This is due to a combination of the lasers and the tremendous

amount of support equipment needed. The primary reason for the large size is the need to correct for dispersion or pulse broadening. In mature systems, this is accomplished by multiple prisms which most often have to be separated over 50 cm with the proper angles corresponding to the Brewster's angle for the peak wavelength. [14, p.105-117] An example of the support equipment needed is that most Ti:sapphire lasers are pumped with a high power argon-ion laser. [14, p.361] This then requires both a high current driver and a cooling system for the laser cavity. Due to the high pump power portions of the solid state section of the system, namely the crystal, need to be cooled, adding many more pieces to an already complex system.

Behind all of this is the cost of the laser system. Most industrial and commercial lasers are very expensive due to the precision that must be used in manufacturing these systems. This, combined with necessary peripherals such as nitrogen purging, special humidity considerations, and required ventilation, adds upkeep and construction costs to the system and often pushes the overall costs for these systems into the millions of dollars. The increased availability of diode lasers and new crystals is rapidly bringing the price down. The availability of these less expensive technologies made the research in solid state lasers possible for this thesis.

1.2.2 Capability. It is in the aspect of capability that the biggest deviation is present in mature systems compared to the research systems. Specifically, commercial systems, while relatively inefficient, have very high output powers due to the availability of high power pump lasers. When working with smaller systems, specifically those pumped with diode lasers, the pump powers are a major limitation. While output power goals are not specifically addressed the general goal is efficiency for the system due to the portability goal expressed below. As the continued growth in the semiconductor laser industry booms this problem should be overcome.

Recently, and where the research systems outclass the commercial systems, is the push to create faster pulse repetition rates for various applications. The biggest factor is that the repetition rate is directly related to the length of the laser cavity.

[31, p.1042] [14, p.279] Due to design limitations and necessary corrections for group velocity, most mature systems require cavities over 150 cm. The result is that it takes longer for a pulse to travel through the cavity and make it out through the output coupler. Specific discussions of how it is possible to shorten the cavity will be discussed more in Chapter III.

1.2.3 Portability. This, by far, is the biggest limit to the use of ultrashort pulsed lasers outside of the laboratory and is an important focus of this thesis. As previously discussed, size is the primary reason that portability is almost impossible. Many applications require that the size of the system be small in order to fit into a required space or be able to move freely. The second reason is that these types of laser systems usually need to be powered by large current sources, which can be a problem even for modern batteries. Such a current draw would require frequent battery changes or a large capacity system both of which are detrimental to use in external, and in the case of military hardware, extreme environments.

1.3 Goals

This research has three primary goals. The first goal is an introduction into the study of ultrashort pulsed lasers and the related lab techniques. Work in this field is a new level of optics and while the basics of electrodynamics and beam propagation are the same there are some very specific properties that have to be used in order to achieve proper pulsing. This bleeds over into lab techniques because there are a large number of specialty components used in the laser and very specialized measurement equipment that must be used in order to analyze the pulses being produced. This basic experience is important and needs to be passed on to the future researcher using this system.

The second goal is to analyze the components of the system and their role in producing ultrashort pulses. The purpose is to provide a baseline understanding of the advances that are allowing the reduction is size of the system. This includes a

discussion of the different types of solid state crystals being used, the equipment to induce mode locking, and group velocity dispersion correction components. Closely related to this discussion is an examination of system portability. Critical to researching this goal is the reduction in laser cavity size and though not completely explored, there are suggestions for more detailed future research.

Along the lines of future research, the last goal for this thesis is to provide a baseline capability for AFIT and AFRL/SN for future research. Neither institution has much experience with small cavity ultrashort pulsed lasers and as more of the possibilities of this type of laser are formulated that experience needs to grow. The key was providing a system and system design that is robust and easily duplicated for researchers anywhere to use as a basis.

II. Background

The overall story of the laser and optics are well beyond the scope of this thesis. What is important is the physics behind pulsed lasers, and its application to the current research in short-pulsed solid state lasers.

2.1 Why Pulse?

The science of pulsing lasers has moved quickly along with continuous wave (cw) lasing techniques. In fact, the first ruby laser was a pulsed laser due to the properties of the flashlamps being used and the ruby itself. [31, p.60-61] The overriding reason for pulsing a laser is to create a very short and very intense burst of laser power which is often much higher than normal cw lasing. [31, p.1004] It must be noted, however, that in order to extract the energy stored in the laser crystal, the pulse mechanism must be placed inside the cavity. As shown in Figure 2.1, if the system is pulsed outside the cavity, the maximum power that is going to be achieved is the cw power. [30, p.522] When pulsing from inside the cavity, the difference is that the time of the pulses needs to be taken into account. This is shown by the differences between Equations (2.1) and (2.2) where $\langle I \rangle$ is the cw intensity, Δt is the time between pulses, τ_p is the pulse width and I_p is the intensity of each pulse assuming a square pulse. [34, p.285]

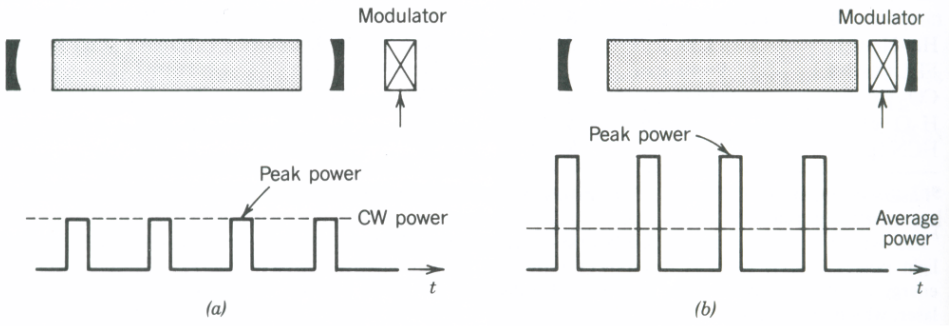

Figure 2.1: The difference between pulsing systems (a) outside and (b) inside of the cavity. [30, p.522]

$$\langle I \rangle = \frac{Power}{Area}. \tag{2.1}$$

$$I_p = \frac{\langle I \rangle \times \Delta t}{\tau_p}. \tag{2.2}$$

For example, using numbers close to those expected from the designed system, assume a 0.1 watt average power cw laser with a beam diameter of 0.2 cm. The cw intensity is $\langle I \rangle = 0.1$ W/($\pi \times 0.1$ cm^2/2) = 6.366 W/cm^2. A cavity with a length, L, of 1 meter using Equation (2.3) will allow a pulse frequency of 149.9 MHz, which is the amount of time it takes for a pulse round trip inside the cavity, or a pulse every 6.671 ns. [31, p.1042] [14, p.279]

$$\nu = \frac{c}{2 \times L} \tag{2.3}$$

$$T = \frac{2 \times L}{c}.$$

Using this calculation and a pulse width of 150 femtoseconds, and plugging this into Equation (2.2) gives a pulse intensity of I_p = 6.6366 W/cm^2×6.671 ns/0.0001 ns = 442.7 kW/cm^2. This major jump in target power allows the use of lower power (and cheaper) lasers to investigate pulsed phenomena with the possibility of extrapolating results to higher power systems, thus, enabling some of the fascinating technologies mentioned in Chapter I

2.2 Solid State Lasers for Pulse Production

Solid state lasers are becoming the standard type of laser for ultrashort pulse production. Early work in this field was primarily done with dye lasers. [14, p.371] The problem with those types of lasers is that they can be very messy and the support equipment for flow and concentration control is rather bulky along with very low average powers. Solid state lasers have allowed the size of the systems to decrease to the point that an entire system, including power supply, was put onto a 22 cm×28 cm optical breadboard. [2] This is a big step toward making these systems more portable,

and thus, useful. The focus here is on overall properties of solid state lasers and the impact of the Ti:sapphire laser with the specific choices made in Chapter III.

2.2.1 Gain Media. Generally, the solid state gain media used for ultrashort pulse generation are rare-earth ions doped into glass or crystal, normally from 0.5% to 5%. [31, p.61] The dopant usually needs to have a carrier lifetime longer than typical cavity round trip lifetimes. [14, p.358] Most often, the dopant is chosen for the wavelength produced and specific qualities that allow useful interaction with other parts of the system. An example of this is having a low quantum defect, such as ytterbium doped crystals, which lends itself to high efficiency with properly tuned pump lasers. [14, p.358] The choice of the crystal or glass is a little more arbitrary. Most often, they are chosen for either their thermal properties or their emission cross section size both of which result from the lattice properties. [35] Appendix A contains a short list from Viana *et al.* of common dopants and the different types suspension materials that are used. It is important to note that the gain for these crystals is low compared to most dye lasers due to a smaller gain cross section so the crystals are usually several mm long compared to several hundred μm for dye lasers. [14, p.359] This has a large effect on the width of the pulse and will be discussed more with group velocity dispersion.

2.2.2 Pump Lasers. The rapid progress in the evolution of pump lasers is the main reason that advancement in this field has been so exponential. The dopant in the glass or crystal is often very pump wavelength restricted due to the proper energy levels for stimulated emission. The primary result is that the researcher is limited to a dopant that has a matching pump laser wavelength. There normally is some form of pump available but it is often severely restricted in power. This changed however with advances in optical storage and optical communications laser technologies. [5, 24] This push has encouraged semiconductor laser design in many different wavelengths. The first result has been that more dopants have become usable and second it creates a relatively low cost pump system that does not require a large footprint. The specific

type of semiconductor laser has little effect on performance of the systems. The main problem with some of these diodes, however, is that the output beam is not circular but a line so focusing down to the small spot sizes necessary can be troublesome. Despite this flaw, it looks like almost all ultrashort pulse lasers in the future are going to be pumped by a semiconductor laser.

2.2.3 Titanium Sapphire Laser. The titanium doped Sapphire (Ti^{3+}:Al_2O_3) laser is the bedrock and most popular solid state system for creating ultrashort pulses, and as such, needs to be discussed as background. [14, p.360] This type of system is very mature because there is an immediate high power pump available in the form of the argon-ion laser which has an output wavelength of 514.5 nm. [5, 10, 43] Using a gas laser as a pump versus a semiconductor laser results in a decrease of efficiency but a solution is being formed for Ti:sapphire by using a frequency doubled neodymium-vanadate laser (Nd:vanadate)(Nd:YVO_4) which has the benefit of improved efficiency. [14, p.361] A typical Ti:sapphire laser is shown in Figure 2.2. [14, p.361] These lasers are popular because of their controllability (as illustrated in Figure 2.2). Critical is the ability to adjust the output wavelength. Most Ti:sapphire systems have a tunability from 650-1200 nanometers allowing for considerable effects testing. [5, 10] [30, p.480] This is accomplished using the wavelength dispersion from the second prism and an aperture. [14, p.362] The other controllers allow adjustment of the dispersion, and resulting group velocity dispersion and mode selection. [14, p.362] Work will no doubt continue into the immediate future on the Ti:sapphire laser.

2.3 Common Pulsing Schemes

Overall, there are four primary ways to pulse a system inside the cavity. Each has their own advantages and disadvantages and can be used actively, passively, or both. We will assume a solid state laser being pumped by an outside source of flashlamps or another laser.

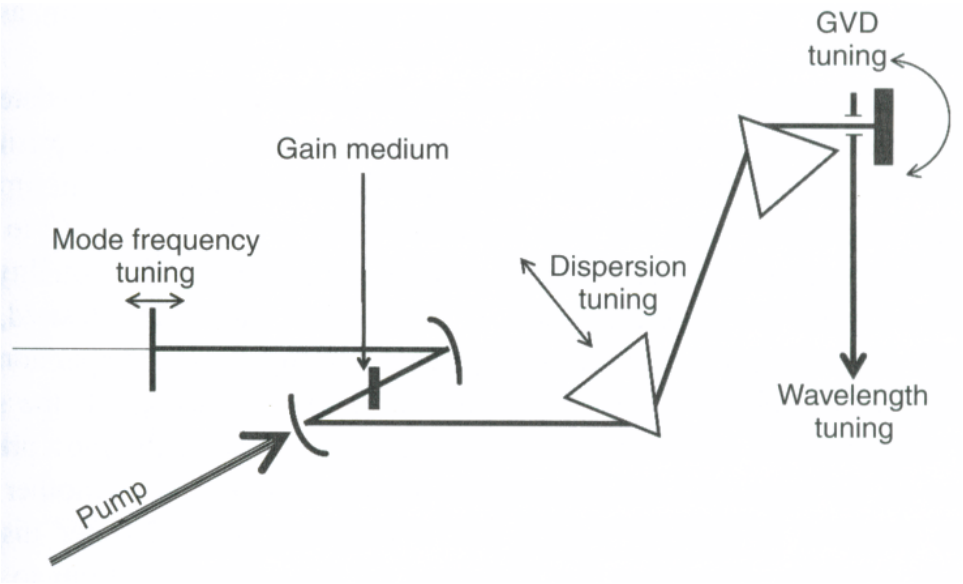

Figure 2.2: Typical Ti:sapphire laser cavity with possible controls indicated. [14, p.361]

2.3.1 Gain Switching. Gain switching is essentially turning the pump on and off. [30, p.521] [31, p.966] This is the simplest way to pulse a system and is completely actively accomplished. The goal when doing this is to rapidly overcome the threshold of the system by creating a high population inversion and gain resulting in more inversion than photons. [34, p.240] [31, p.967] A graphical example from is shown in Figure 2.3. [30, p.523] The major disadvantage of this technique is that it is limited by the speed that the pump can be turned on and off with the required intensity. The most logical use of this technique is in pulsing semiconductor lasers and it is not much use for this research.

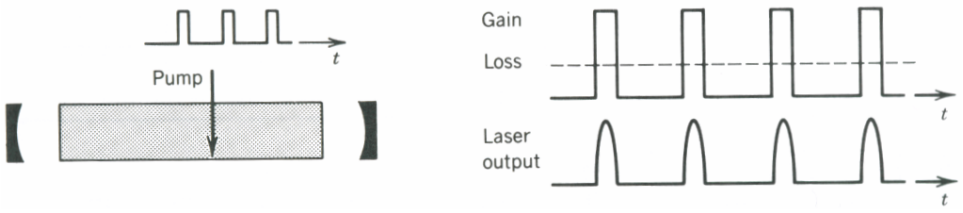

Figure 2.3: Profile of the effects of gain switching. [30, p.523]

2.3.2 Cavity Dumping. Cavity dumping is essentially the opposite of gain switching in that instead of releasing the stored inversion it releases stored photons. [30, p.524] This is done by either removing one of the mirrors of the cavity or using another system to rapidly open the cavity. The reaction of the system in shown in Figure 2.4. [30, p.524] An example of a system that does not physically remove the mirror is shown in Figure 2.5 which works by using a Pockels cell to induce a rapid quarter-wave plate reaction dumping the photons out of the system. [31, p.976] The advantage of this type of setup is that unlike a normal output coupled system it has the ability to release almost all of the built up intensity at one time. The disadvantage is that this technique is completely active and not very useful for this research.

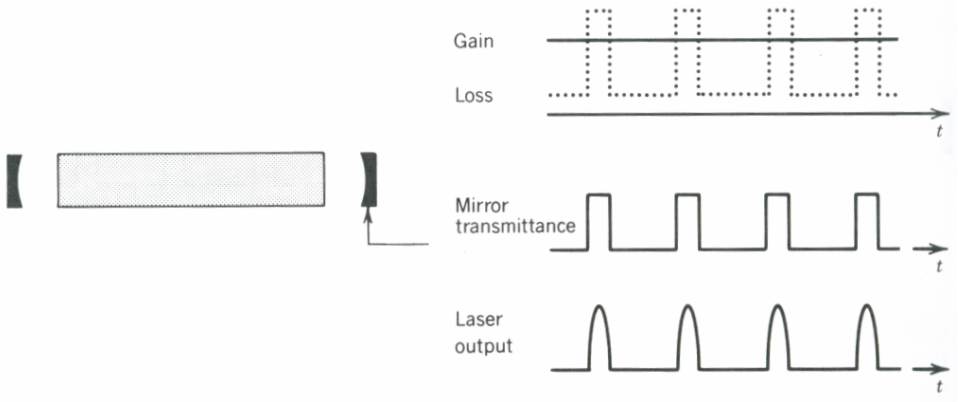

Figure 2.4: Cavity dumping described as removing the mirror at one end of the cavity dumping the stored photons. [30, p.523]

2.3.3 Q-switching. This type of pulsing relates more to gain switching in that it stores the energy of the system in the population inversion of the system. This is done by causing a large loss until a desired time and then lowering the loss in order to allow a brief oscillation in the cavity. [30, p.527] This type of pulsing has the advantage in that it can be accomplished both actively and passively. An overall example is shown in Figure 2.6 and several specific ways to accomplish this are shown in Figure 2.7. [30, p.523] [31, p.1006] What is relevant to this research is the saturable absorber technique since this leads to the same ideas as a saturable absorbing mirror which will be described in more detail in the next section. The primary disadvantage

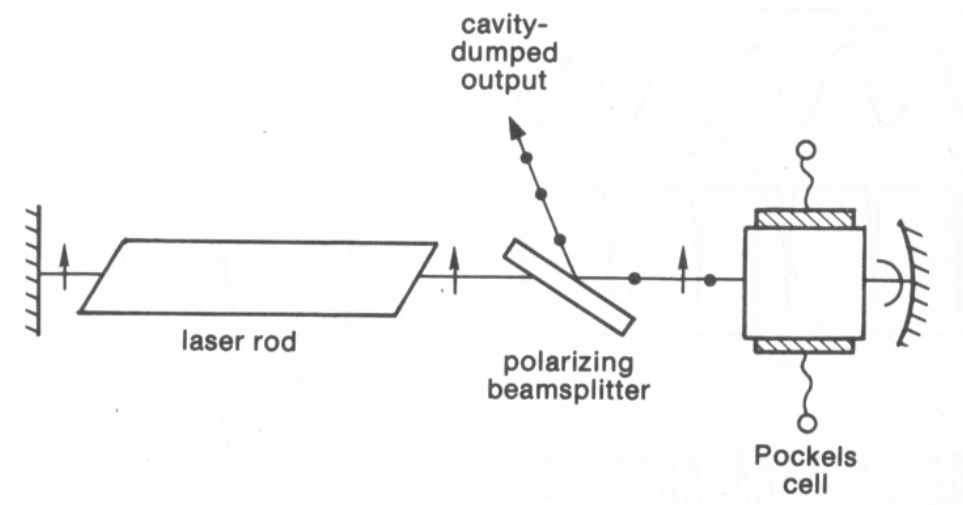

Figure 2.5: Example of an electroptic cavity dumping system. [31, p.976]

of Q-switching is that the pulse train is not necessarily constant and that pulses can be different temporal distances apart. Despite this problem Q-switching can produce ultrashort pulses and steps into the next form of pulsing.

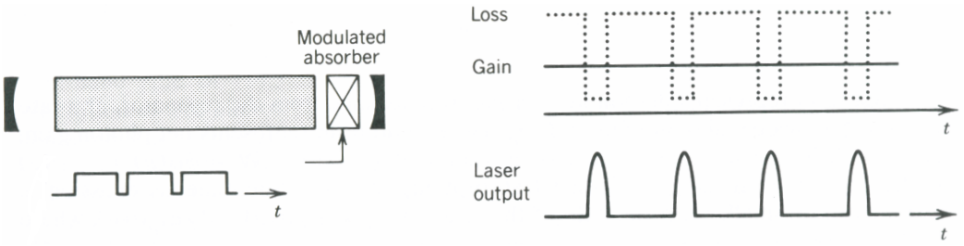

Figure 2.6: General Q-switching setup. [30, p.523]

2.3.4 Mode Locking. Mode locking is the standard method of creating pulses in modern ultrafast and ultrashort pulse research and as such needs to be fully explained. The usefulness of this technique is that, while it has less energy per pulse than Q-switching, its pulse rate is faster and the pulse widths are shorter. [34, p.311] The basis of mode locking is, "to establish a phase relationship between longitudinal modes," per Diels and Rudolph. [14, p.277] Essentially, this means that the goal is to get most of the phases of the modes of the cavity to be equal at the same time and form a large pulse of energy. As a side note, the radial modes generally contribute

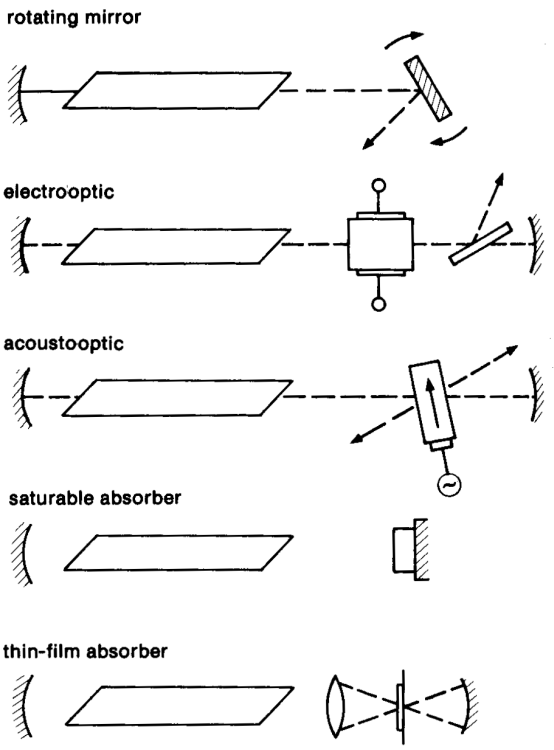

Figure 2.7: Common laser Q-switching systems. [31, p.976]

to amplitude noise. [14, p.325] Accomplishing this task is more complex than that statement implies so a better description is required.

The general description of the fields of N modes within an oscillating system is shown in Equation (2.4) where the taking the real part is assumed. [31, p.1044] [34, p.298]

$$\mathcal{E}(t) = \sum_{n=1}^{N} E_n e^{i(\omega_n t + \phi_n)} \tag{2.4}$$

The overall goal is to get *most*, since for a "real" laser it is impossible to get all, of the phases ϕ_n aligned together at the same time to create an overall greater field. The modes then become complimentary and create an intense short pulse with an overall field intensity of $|\mathcal{E}(t)|^2$. [31, p.1054] The adding of these modes remains true no matter what their amplitudes. Two examples are shown in Figure 2.8 and Figure 2.9. [31, p.1047-1049] It is important to note that the intensity is the square of the field, so

the addition of different modes can cause the pulse to quickly out grow noise. For example, if two modes are added the intensity would be four times the single mode, but if five modes are added, it would be 25 times stronger than the single mode. For a typical 100-femtosecond pulsed laser, there are over 100,000 modes contributing resulting in an intensity 10^10 greater than a single mode. [14, p.291]

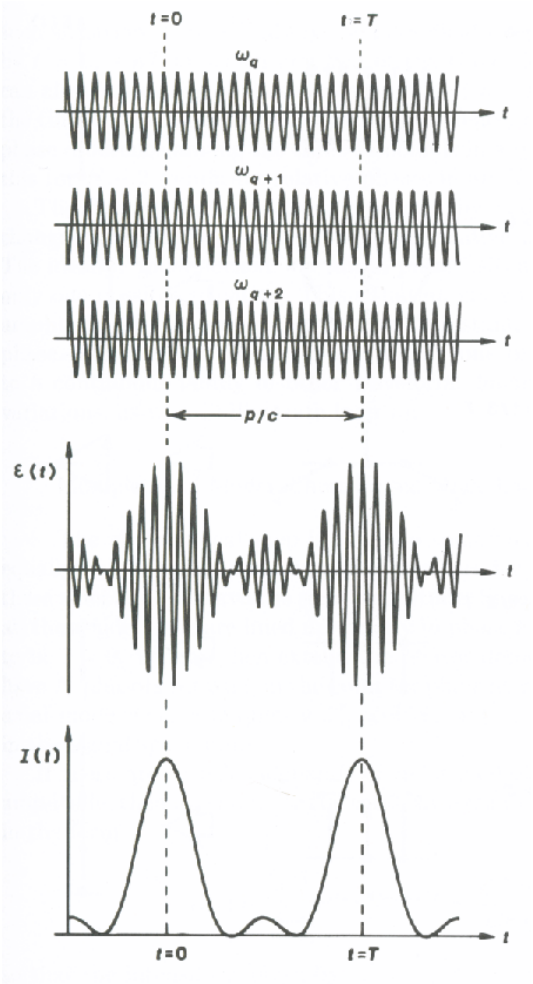

Figure 2.8: Superposition of 3 equally spaced frequency components in phase at $t = 0$ and $t = T$. [31, p.1047]

2.3.4.1 Time and Frequency Domain Analysis. Primary analysis for the cavity effects, pulse train, and pulse properties can be completely characterized in either the time or frequency domain. The one that seems most intuitive is looking at

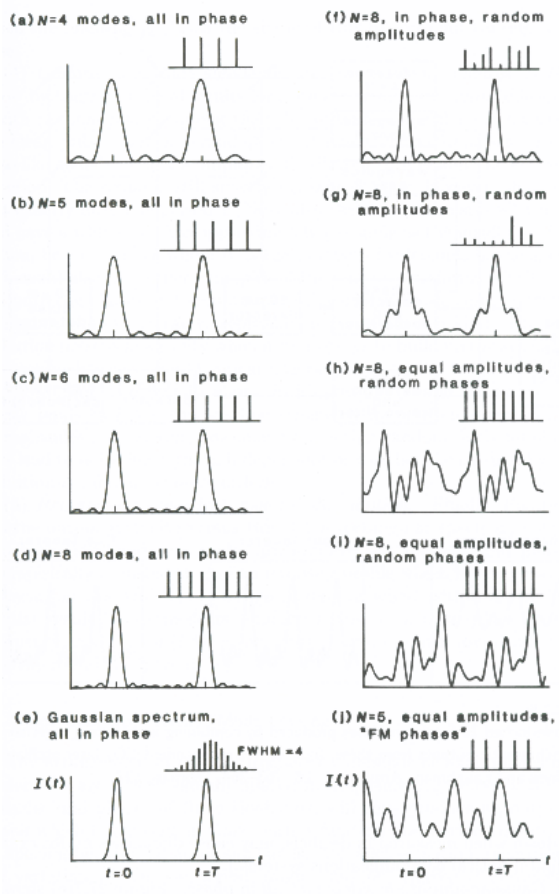

Figure 2.9: Various intensity examples for different modes, amplitudes and phases. [31, p.1051]

this information in the time domain with the real field $E(t)$, having pretty much any shape. [31, p.1043] With a Fourier transform, this can be taken into the frequency domain as shown in Equation (2.5) where Ω is the frequency, $|\tilde{E}(\Omega)|$ is the spectral amplitude, and the important factor $\Phi(\Omega)$ is the spectral phase. [14, p.2]

$$\tilde{E}(\Omega) = \mathcal{F}\{E(t)\} = \int_{-\infty}^{\infty} E(t)e^{-i\Omega t}dt = |\tilde{E}(\Omega)|e^{i\Phi(\Omega)} \tag{2.5}$$

Analysis often jumps between the two interchangeably and care needs to be taken that the proper data form is being looked at in order to make the proper conclusions. Importantly, if you have the frequency data, you can interpolate back to the field via Equation (2.6) since $E(t)$ is real and $\tilde{E}(\Omega) = \tilde{E}^*(-\Omega)$ is true. [14, p.2]

$$E(t) = \mathcal{F}^{-1}\{\tilde{E}(\Omega)\} = \frac{1}{2\pi}\int_{-\infty}^{\infty} \tilde{E}(\Omega)e^{i\Omega t}d\Omega \tag{2.6}$$

Time domain analysis is based on looking at the signal passing a specific reference point and how that signal changes over successive round trips, noting that the reference point can be inside or outside the cavity. [31, p.1043] An example of this is shown in Figure 2.10 with the periodic signal on the left and its power spectrum on the right. [31, p.1044] The advantages of time domain analysis are in looking at how different parts of the cavity affect the pulse shape. [14, p.291] Parts that have extra effects are the mirrors and any type of absorbers in the cavity. This will become more evident in Chapter III and Chapter IV when discussing the component properties.

The frequency domain analysis is most effective when talking about the overall cavity and the pulse train, but not the pulses themselves. Usually, this is due to the desire to know more about the longitudinal modes of the system than the exact shape of the field. Most of the time this is an approximation because the number and magnitude of the modes is constantly changing. [14, p.291] An excellent example of the transition between the time and frequency domains is shown in Figure 2.11 from Verdeyen. [34, p.297] The example shows how it is possible to characterize the signal in either time or frequency and have good characterization which becomes better with help from phasor analysis described in the next section.

2.3.4.2 Phasor Analysis. Another popular analysis technique is the phasor analysis technique. Essentially, this is an extended version of the frequency domain analysis. The basic premise is that each mode of the cavity has a phase amplitude and phase angle, ϕ_n, in Equation 2.4. Normally, the phase amplitude and angle are represented as a vector in mode space. An assignment is then made that the centermost mode component is stationary in time with the other modes rotating at the beat frequency of the center mode. [31, p.1047] Modes then rotate in different directions depending if they are higher or lower in frequency. The modes further away from the central frequency rotate at a higher rate than the ones closer. [31, p.1048] The

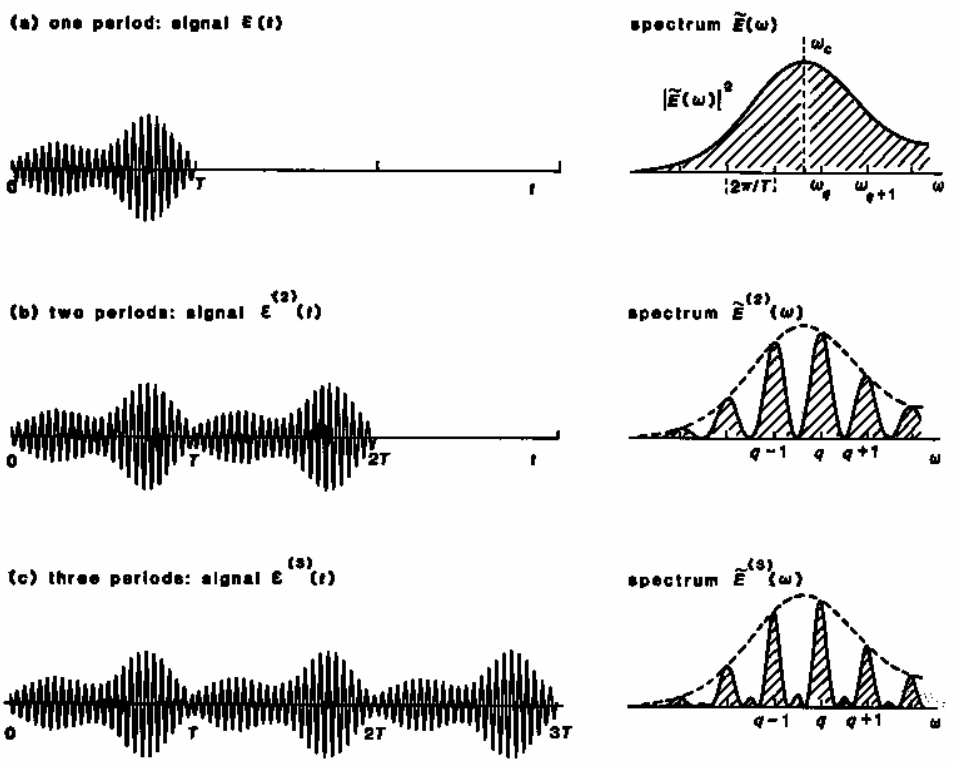

Figure 2.10: Time signal $E(t)$ and power spectrum for a periodic signal. [31, p.1044]

overall amplitude is then the added magnitude of these phaser vectors. Two examples are shown in Figure 2.12 and Figure 2.13. [31, p.1048] [34, p.299] Figure 2.12 shows an example where all of the modes have equal amplitudes and Figure 2.13 have more realistic differing amplitudes. Overall, this is kind of a crude method of analysis but provides a good visual example of how all of these modes need to align.

2.3.5 Methods of Mode Locking. There are many ways to induce mode locking in a cw laser, including both active and passive means. Active examples include the use of amplitude modulators operating at the round trip frequency of the cavity or phase modulators which act as frequency modulators. An example of an amplitude modulator setup is shown in Figure 2.14. [31, p.1056] More useful, especially for small cavity systems, is the use of passive techniques. There are several ways to do this, but I am going to concentrate on Kerr-lens mode locking and saturable absorber mode locking. These are currently the most popular types used, are the ones that are

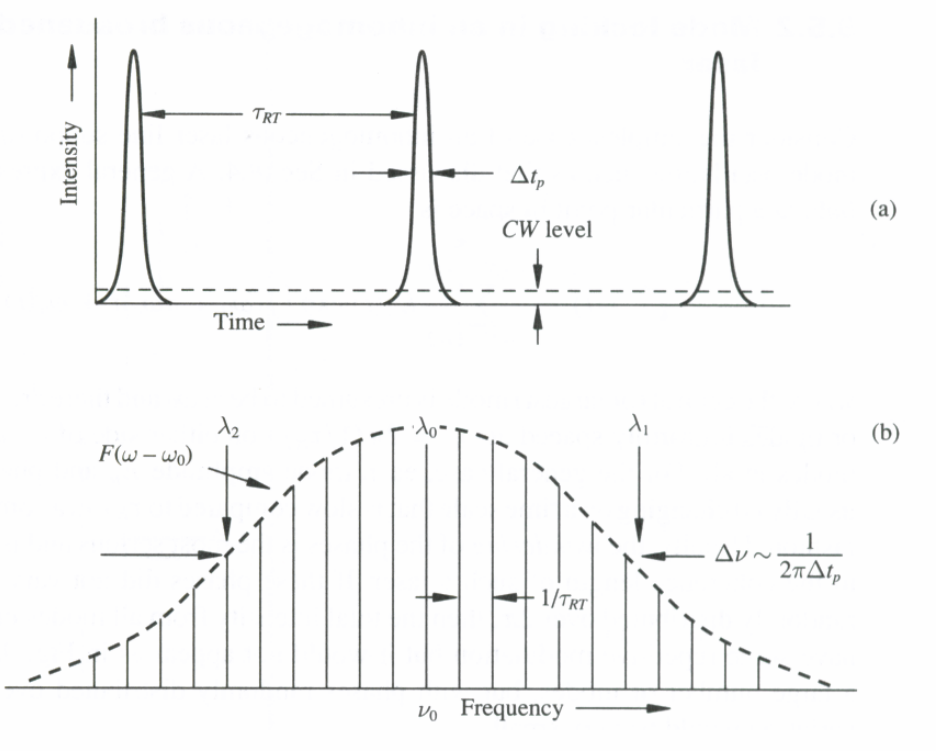

Figure 2.11: Time (a) and frequency (b) domain representation of a modelocked laser. [34, p.297]

used in this research, and have the unique advantage in that they allow the shortest pulses seen. [31, p.1058]

2.3.5.1 Kerr-lens Mode Locking. The basis for KLM is use of the optical Kerr effect. This is a property of a third-order nonlinear reaction in a medium. [30, p.752] In order for the effects to become appreciable, however, the light impacting on this medium needs to be strong enough to induce an effect by this reaction. [31, p.379] Once that limit has been surpassed, the result is a nonlinear polarization effect, shown in Equation (2.7), effecting the *original* frequency of light by the intensity. [30, p.752]

$$P_{NL}(\omega) = 3\chi^{(3)}|E(\omega)|^2 E(\omega) \tag{2.7}$$

This results in a change in susceptibility, $\Delta\chi$, at the original frequency which causes a change in the index of refraction as noted in Equation (2.8), where η is the impedance

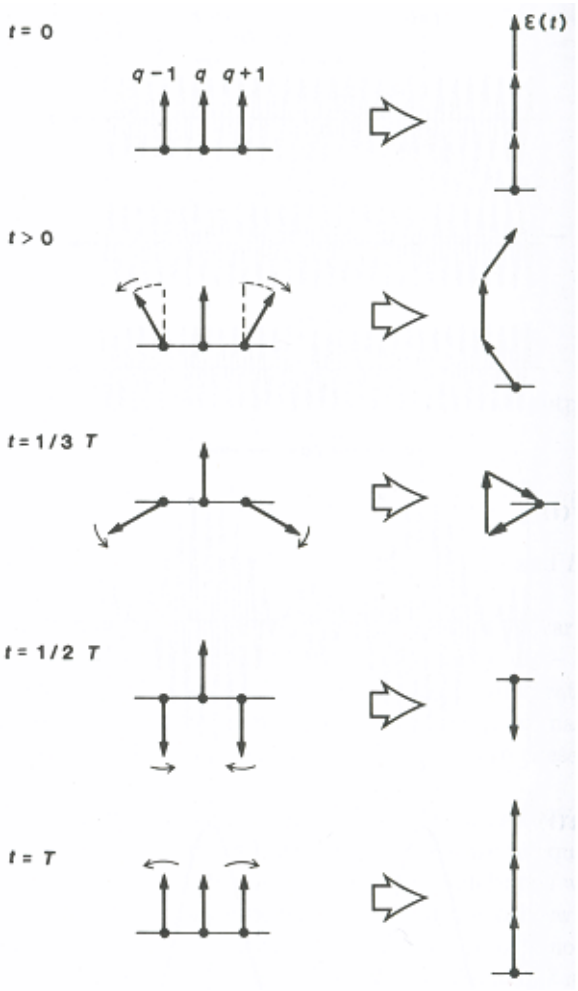

Figure 2.12: Rotation phasor example for three equal amplitude phases. [31, p.1047-1048]

of the dielectric medium and ϵ is the electric permittivity. [30, p.752]

$$\Delta n = \frac{3\eta}{\epsilon_o n}\chi^{(3)} I = n_2 I \tag{2.8}$$

The overall result is that the index of refraction becomes a function of intensity, $n(I) = n + n_2 I$. [30, p.752]

What then occurs, and what is most important, is that there is a self-phase modulation that begins to have an effect. [30, p.753] This effect is dependent on the power of the beam, the area that it fills, and the length of the medium. The change

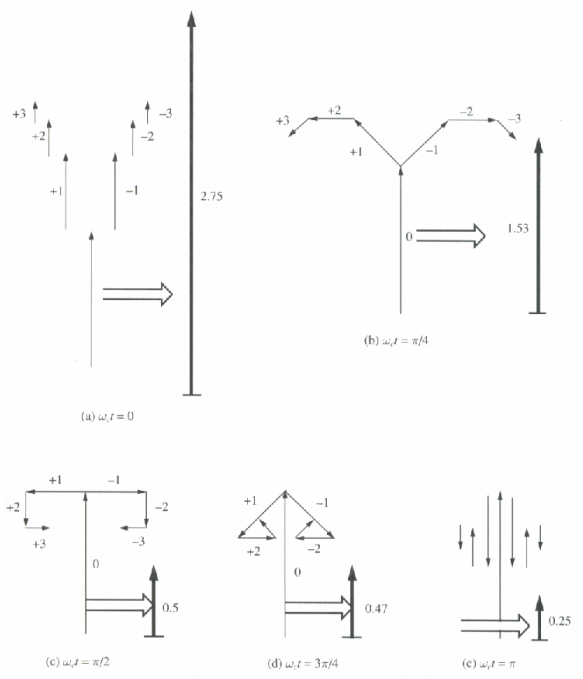

Figure 2.13: Rotation phasor example of a mode locked laser with different mode amplitudes. [34, p.299]

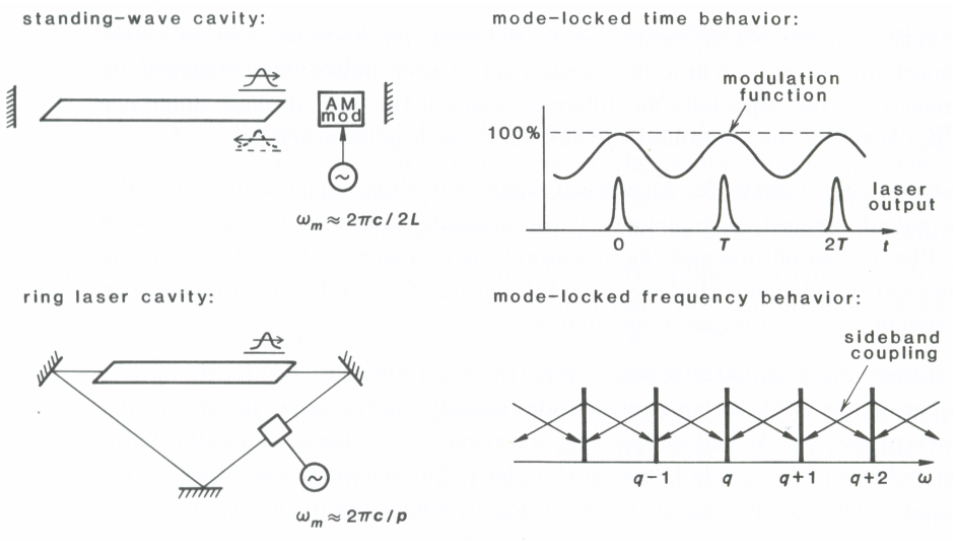

Figure 2.14: Active amplitude mode locking in a standing wave or ring laser cavities with description in time and frequency domain. [31, p.1056]

in phase of the high power location is given by Equation (2.9) where n_2 is the index defined before, L is the length of the medium, A is the area of the spot size, λ_o is the

carrier wavelength, and P is the power of the beam. [30, p.753]

$$\delta\varphi = 2\pi n_2 \frac{L}{\lambda_o A} P \tag{2.9}$$

Maximizing this change incurs maximizing L and P while minimizing A. This effect is most useful when light is controlling light in terms of intensity. [30, p.753]

The effect that is most useful for mode locking is directly related to the phase modulation. If n_2 is positive and finite, the higher the intensity ,the higher the index of refraction. [31, p.380] The result, if the center of the beam has the most intensity, is that there is an amount of self-focusing since the edges of the beam will see a smaller index of refraction. A visual example is shown in Figure 2.15. [39] An aperture is then put into place to cause the cw lasing modes to see more loss than the phase locked modes. Due to the higher gain the phase-locked modes see, more of the unlocked modes align themselves to achieve this gain. Again, it is impossible to get all of the modes in phase but those that are easily overshadow the random modes. Over time, the repeating field inside the cavity builds up and creates a pulse that travels the cavity when these modes are in alignment. At the output coupler, a little bit of the pulse is let out while the rest repeats its trip in the cavity. As a result, the pulse rate is very consistent, and if other factors such as pump power and temperature remain constant, the pulse energy is consistent. Due to these properties, this is the most common way to mode lock mature systems such as the Ti:sapphire laser.

2.3.5.2 Saturable Absorber Mode Locking. The saturable absorber is becoming the standard and easiest way to accomplish mode locking. Saturable absorbers work essentially the same way as KLM in that the cw modes see more loss than the phase locked modes. This begins with a small increase in noise which is able to partially saturate the absorber. [31, p.1118] This then allows the energy to increase for that noise turning it into a pulse that then begins to align more modes to it. There are two reasons why it is the standard. The first is that it is completely passive. There is no worry about parts moving properly and how the rest of the system is affected.

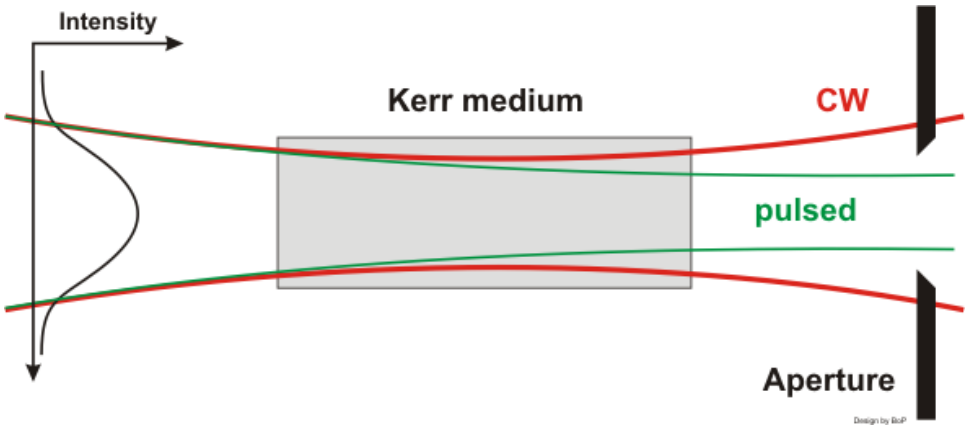

Figure 2.15: Example of Kerr-lens mode locking using a Kerr material and a hard aperture. [39]

The second is because the advancement in saturable absorber technology has been very rapid.

Saturable absorbers can be any type of gas, liquid, or crystal of which the key is that it absorbs constantly at low intensities, but as the intensity rises, the absorber becomes "saturated" and transparent to the light. [31, p.1057] Equation (2.10) is how the saturation intensity is calculated with $h\nu$ as the photon energy, σ_A is the material absorption cross section, and T_A is the absorber recovery time. [15]

$$I_{sat} = \frac{h\nu}{\sigma_A T_A} \tag{2.10}$$

It is important to remember that the saturation is a nonlinear process and, as such, has unique qualities as the initial saturation is building. [15] [14, p.316] Figure 2.16 shows an example for an absorber on a mirror which will be described more later. [15]

Originally, these absorbers were usually dyes that were injected across the beam using the ability to control the density of the absorbing particles in the dye. [31, p.1118] [14, p.315] The push more recently has been into the use of semiconductor absorbers primarily due to the ability to tailor the absorption to specific wavelengths and intensities. [15] For this research the designed systems use this type of absorber. The main disadvantage of semiconductor absorbers, however, is that they can be

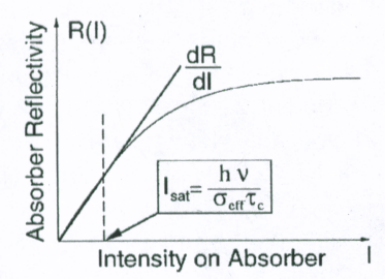

Figure 2.16: Nonlinear buildup of reflection from an absorber mounted on a mirror. As the absorber is saturated more light gets to and is reflected by the mirror. [15]

damaged by too much intensity. Care needs to be taken to provide a balance between the needed intensity and maximum intensity on the material.

There are two general types of semiconductor absorbers. The primary constraint on both types is that the recovery time be less than the round trip time for a pulse in the cavity. [14, p.315] The first is a fast absorber which relaxes much faster than the width of the pulse. [31, p.1105] An example of this type of absorber is a Kerr lens material in which the effect is almost instantaneous and acts like a soft aperture. [14, p.315] The other types are slow absorbers in which the relaxation time is more than the width of the pulse. This is useful in that it not only provides the mode locking capability but also can work on the shape of the pulse due to the attenuation at the leading edge of the pulse before saturation is obtained with little effect on the trailing edge. [14, p.317]

Of recent advent is the semiconductor saturable absorbing mirror or SESAM. Essentially, a SESAM is a saturable absorber over a high efficiency Bragg reflector. [12,15] The absorber on the top performs the function of inducing the system to pulse with the full mode locking done by KLM within the gain medium itself. The Bragg reflector beneath acts as a high quality reflector to those pulses that get through. A time line of designs is shown in Figure 2.17 by Keller *et al.* [15] Like the nonlinearity shown in Figure 2.16, there is an analogous action for pulsing except the term looked at is the incident pulse energy, E_p. Figure 2.18 shows the buildup past the saturation

fluence given in Equation (2.11). [15]

$$E_{sat} = \frac{h\nu}{\sigma_A} \tag{2.11}$$

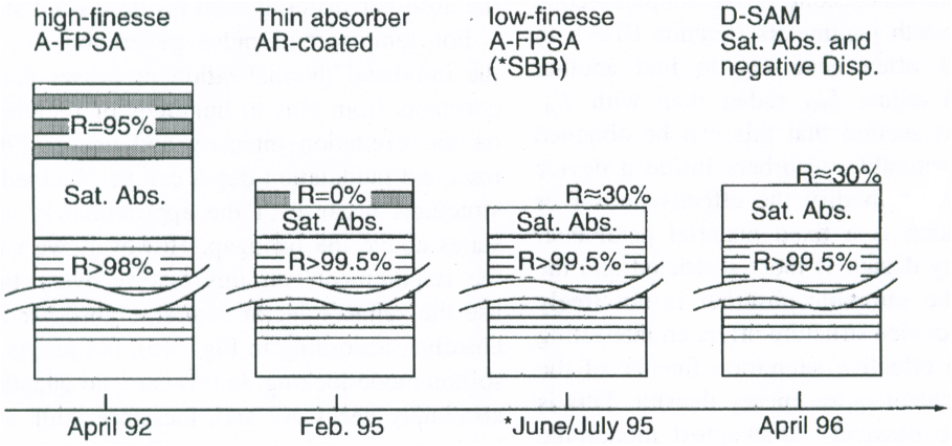

Figure 2.17: Evolution of the initial designs for saturable absorbing mirrors. [15]

The SESAM has two major advantages over other saturable designs. The first is size. A SESAM essentially just takes the place of one of the four mirrors needed in a solid state cavity. This makes it simple to place into an established cw lasing setup. A comparison can be shown between Figure 2.19 from Siegman [31, 1118] and Figure 2.20 from Agate. [2] Aligning the system from Agate would be much easier since the angle of the absorber would be critical. The second and probably most

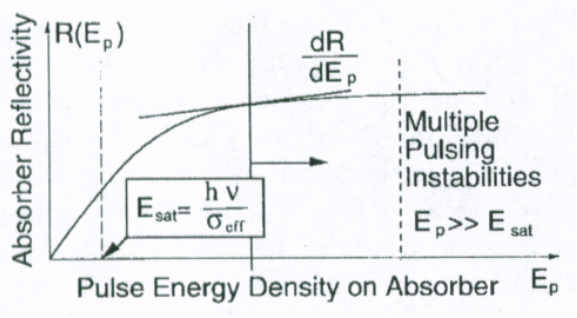

Figure 2.18: Nonlinear energy density buildup of reflection from an absorber mounted on a mirror. [15]

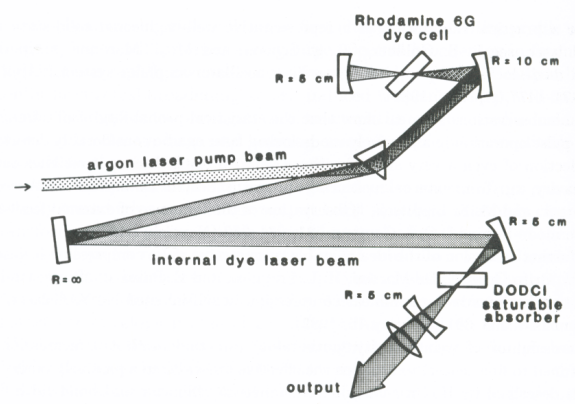

Figure 2.19: Layout for a cw passively mode locked Argon-ion pumped dye laser. [31, 1118]

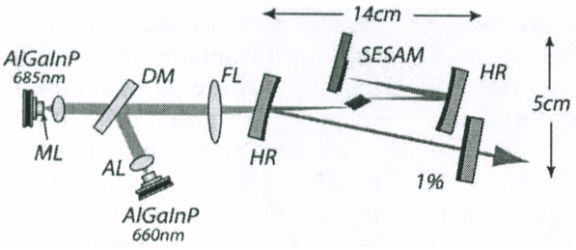

Figure 2.20: Example of a diode pumped compact femtosecond laser cavity. [2]

important advantage of a SESAM is that it can be tailored to the specific wavelength and relaxation times desired by the researcher. [15]

As noted, there are several different designs of SESAMs which have different usable properties. Most common are the antireflection (AR) coating as shown in Figure 2.21 using multi quantum wells (MQW). [15] This type has the advantage in that the AR coating provides some protection for the components underneath. A subset of this design is also important to note. This is termed by Keller *et al* the dispersion-compensating saturable absorbing mirror or (D-SAM) shown as the far right type in Figure 2.17. [15] What this type of SESAM does is provide a small amount of negative group velocity dispersion which will be discussed more later.

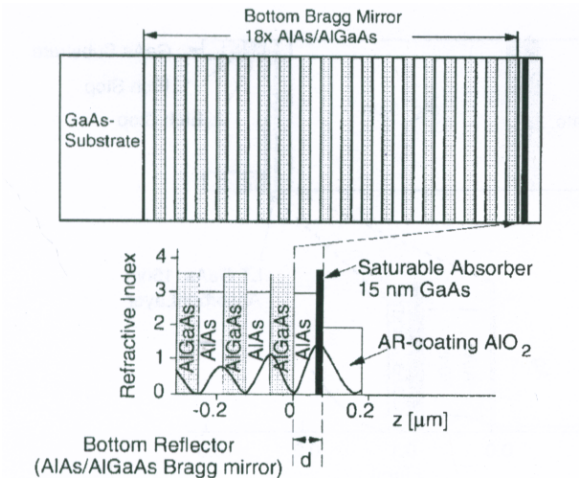

Figure 2.21: General design of an AR coated SESAM. [15]

2.4 Group Velocity Dispersion

Once mode locked, the key behind performance of systems is the pulses themselves. The biggest thing that effects these pulses is dispersion. Dispersion occurs due to an index of refraction that is frequency, and therefore wavelength, dependent, resulting in effects on the difference between the higher and lower frequencies of a pulse. [30, p.176] This analysis is going to stay in the frequency domain but the same description could be applied to wavelength analysis. Most optical components have a positive dispersion coefficient, which means that a pulse will spread temporally due to the velocity difference between the "blue" and "red" portions of the pulse. There are cases, however, where it is possible to create a negative dispersion. To understand this, a deeper understanding of dispersion and specifically group velocity dispersion (GVD) needs to be made.

The initial setup comes in the form of Equation (2.12) which is the reduced wave equation in the frequency domain with its general solution, Equation (2.13). [14, p.22]

$$\left[\frac{\partial^2}{\partial z^2} + \Omega^2 \epsilon(\Omega)\mu_0\right]\tilde{E}(z,\Omega) = 0 \tag{2.12}$$

$$\tilde{E}(z,\Omega) = \tilde{E}(0,\Omega)e^{-ik(\Omega)z} \tag{2.13}$$

What is important to note here is the $k(\Omega)$ which is the dispersion relation, $k(\Omega) = \Omega n(\Omega)/c$, which can then be expanded into Equation (2.14) where ω_l is the carrier frequency. [14, p.22] [11, p.298]

$$k(\Omega) = k(\omega_l) + \delta k \tag{2.14}$$

Now there is a need to step back and look at the big picture. What this is really showing is that the dispersion relation is, obviously, frequency dependent since the index of refraction is frequency dependent. It is then possible to split the information present into the carrier or center frequency and the portion away from that point which is affected by the different index. This can be expanded as shown in Equation (2.14). This expanded relation can then be further expanded by the derivative of δk in terms of Ω expanded around ω_l via a Taylor's series expansion due to the need for Equation (2.12) to obey the conventional transmission line relation shown in Equation (2.15). [34, p.110]

$$\frac{\partial \tilde{E}(\Omega, z)}{\partial z} = -ik(\Omega)\tilde{E}(\Omega, z) \tag{2.15}$$

The result is shown in Equation (2.16) with the understanding that the first term has already been pulled out in Equation (2.14) and has been truncated to two terms under the assumption that the overall envelope of k is small compared to the $k(\omega_l)$. [14, p.23]

$$\delta k = \frac{dk}{d\Omega}\Big|_{\omega_l} (\Omega - \omega_l) + \frac{1}{2}\frac{d^2k}{d\Omega^2}\Big|_{\omega_l} (\Omega - \omega_l)^2 + ... \tag{2.16}$$

Taking the derivatives described keeps things moving forward. The $k(\omega_l)$ is just the phase constant of the system at the carrier frequency. The derivatives begin to specify the difference. Recalling $k(\Omega) = \Omega n(\Omega)/c$ and using this in the first term gives Equation (2.17) where n_g is the group index of refraction and v_g is the group velocity. [34, p.111]

$$\frac{\partial k}{\partial \Omega} = \frac{n}{c} + \Omega\frac{dn}{d\Omega} = \frac{n_g}{c} = \frac{1}{v_g} \tag{2.17}$$

The second part of Equation (2.16) is what becomes important for what we are concerned. The result is shown in Equation 2.18 introducing the shorthand notation $k"_l$. [34, p.111] [14, p.25,32]

$$\frac{\partial^2 k}{\partial \Omega^2} = \frac{2}{c}\frac{\partial n}{\partial \Omega} + \Omega\frac{d^2 n}{d\Omega^2} = -\frac{1}{v^2{}_g}\frac{dv_g}{d\Omega} = k"_l \tag{2.18}$$

Overall this leads to a generalized form of Equation (2.13) shown in Equation (2.19).

$$\tilde{E}(\Omega, z) = \tilde{E}(\Omega, 0)\exp\Big(-\imath\big(k(\omega_l) + \frac{1}{v_g} - \frac{1}{v^2{}_g}\frac{dv_g}{d\Omega}\big)\Big) \tag{2.19}$$

This is important because it gives the rate of change of the group velocity in terms of the frequency. This is the term described as the group velocity dispersion parameter which mathematically shows the reaction of a pulse in a dispersive medium. Of note it is possible to move this to the wavelength description of the system by the relation in Equation (2.20) of which a similar relation will be used later. [14, p.25]

$$\frac{d^2 k}{d\Omega^2} = \frac{2\pi c}{d\Omega^2}\frac{dv_g}{d\lambda} \tag{2.20}$$

With $k"_l$ present, an initially small bandwidth pulse will develop a spectral phase with a quadratic frequency dependence. [14, p.31] The overall result of which is that an element of chirp is introduced and since, as noted in Equation (2.19), the intensity, $|\tilde{E}(\Omega, z)|^2$, is unchanged, the pulse has to broaden. [14, p.31] The overall conclusion is that if $k"_l$ is positive when multiplied by a certain distance traveled, the pulse will broaden. [14, p.32] In almost all cases, $k"_l$ is defined with units of fs^2 per distance, since when multiplied by the propagation distance, it gives the frequency dependence of group delay. [14, p.32]

Every medium that a pulse traverses through, with the exception of a perfect vacuum, will have an effect of the spread of a pulse. A general visual example is shown in Figure 2.22 showing how over time the pulse spreads. [30, p.178] This figure also notes the index of refraction based on wavelength which better shows the pull

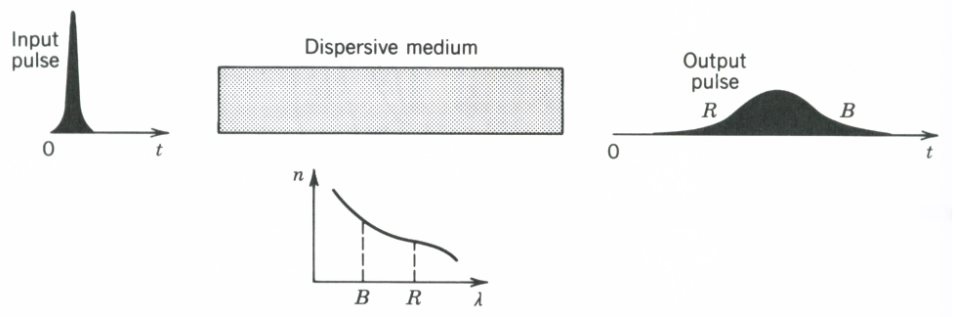

Figure 2.22: General visual example of a pulse traveling in a dispersive medium. Note the index of refraction as a function of wavelength is included. [30, p.178]

on the different frequencies present. For many types of glasses, the general pattern shown in the bottom of Figure 2.22 with a high index of refraction in the visual and near infrared, which then continues to decrease in the mid infrared and beyond, is prevalent. [7] In most known materials, dispersion is positive and are normally described using a set of empirically determined equations. Most often, a form of the Sellmeier equation shown in Equation (2.21) is used, however if the substance is biaxial, such as crystalline quartz, a Laurent series like Equation (2.22) is used. [14, p.63] Equation (2.21) is the definition used by Schott Glass but many other forms exist. [42]

$$n^2(\lambda_l) = 1 + \frac{B_1\lambda_l^2}{\lambda_l^2 - C_1} + \frac{B_2\lambda_l^2}{\lambda_l^2 - C_2} + \frac{B_3\lambda_l^2}{\lambda_l^2 - C_3} \tag{2.21}$$

$$n^2(\lambda_l) = A + B\lambda_l^2 + \frac{C}{\lambda_l^2} + \frac{D}{\lambda_l^4} + \frac{E}{\lambda_l^6} + \frac{F}{\lambda_l^8} \tag{2.22}$$

2.4.1 Positive GVD in the Laser Cavity. Overall in the cavity there are three primary sources of GVD. The first is the dispersion from the air traveled through in the cavity. This, while small, does have enough of an effect to be of relevance and becomes important when introducing negative GVD. The second major source of dispersion is the mirrors within the cavity due to the properties of the mirrors themselves. The reason for this effect is because of the phase shift upon reflection of the mirror. [14, p.70] A good visual example in terms of wavelength is shown in Figure 2.23 with the dashed line representing a high reflector and the solid line a

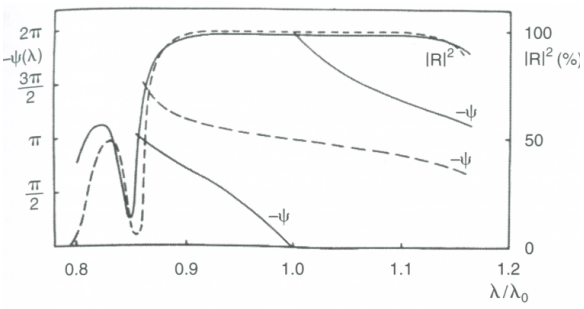

Figure 2.23: Phase change due to reflection off of a layered dielectric high reflector mirror (dashed line) and weak output coupler (solid line). [14, p.71]

weak output coupler. [14, p.71] The relation to the designed wavelength is what is important, and further away from λ_0, the effect can be drastic. Recent advancements have produced improvement and will be explained in the next section.

By far, the highest contributor to dispersion in a solid state cavity is the gain medium itself. There are several reasons for this but the most important is that the crystal or glass usually has a high index of refraction which, when combined with its frequency dependence, has an increased effect. Specific properties of the crystals used in this research will be described in Chapter III. Another factor is the amount of glass that the pulse has to travel through when output coupled.

As a short example, look at borosilicate crown glass (BK7), also known as Pyrex, which is by far the most popular optical glass and makes up most of our glass components. [14, p.63] [38] The coefficients, $B_1, C_1, B_2, C_2, B_3, C_3$ are shown in Table 2.4.1 which, when input, result in Equation (2.23). [14, p.63] [6]

$$n(\lambda) = \sqrt{1 + \frac{1.01046945 \times \lambda^2}{\lambda^2 - 103.560652999} + \frac{0.231792344 \times \lambda^2}{\lambda^2 - 0.0200179144} + \frac{1.03961212 \times \lambda^2}{\lambda^2 - 0.00600069867}} \tag{2.23}$$

The index of refraction as a function of wavelength is shown in Figure 2.24 with the wavelength determined in μm. [6] It is very obvious that parts of the pulse with a shorter wavelength, and higher frequency, will progress through the glass much more slowly.

Table 2.1: Sellmeier coefficients for BK7, which is the most commonly used optical glass. [6, 42]

Coefficient	Value
B_1	1.03961212
B_2	2.31792344×10-1
B_3	1.01046945
C_1	6.00069867×10-3 μm^2
C_2	2.00179144×10-2 μm^2
C_3	1.03560653×10^2 μm^2

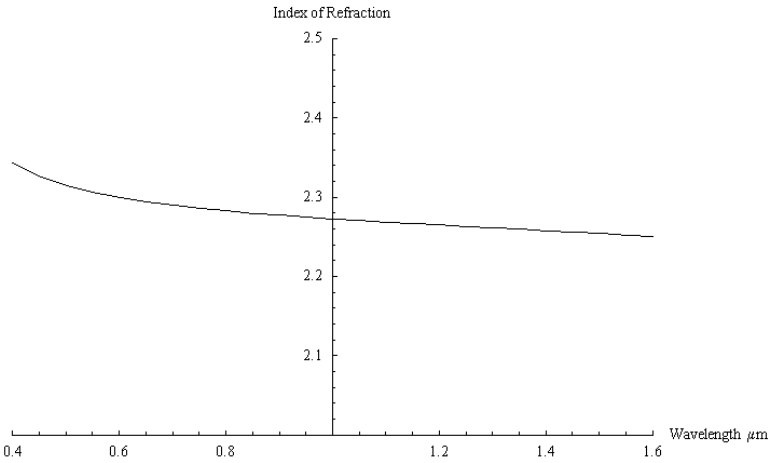

Figure 2.24: Index of refraction of BK7 as a function of wavelength λ in μm. [6]

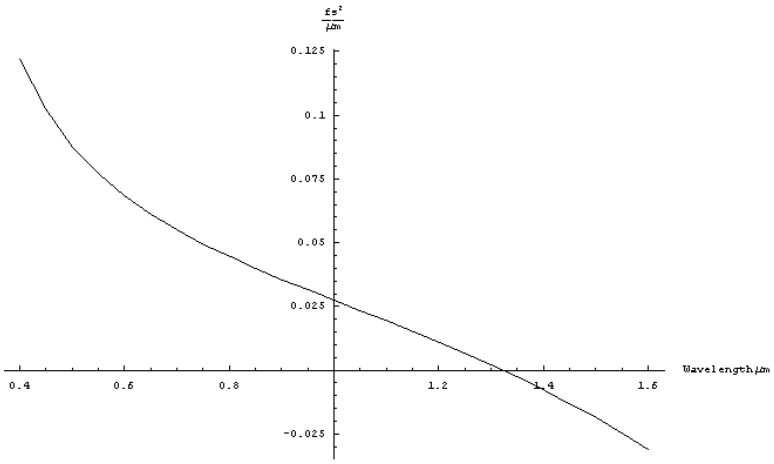

Figure 2.25: GVD as a function of wavelength λ in $\frac{fs^2}{\mu m}$.

Lurking behind the implications of having a different velocity in the glass for different wavelengths is the amount of change in the pulse width over a certain distance traveled in a medium. The first part of accomplishing this is to use the Sellmeier equation noted above to find a function for the GVD in terms of a wavelength. The general equation that provides this information is Equation (2.24) ,of which, the wavelength dependent portion will be used. [14, p.32]

$$\frac{d^2k}{d\Omega^2} = \frac{2}{c}\frac{dn}{d\Omega} + \frac{\Omega}{c}\frac{d^2n}{d\Omega^2} = \left(\frac{\lambda}{2\pi c}\right)\frac{1}{c}\left(\lambda^2\frac{d^2n}{d\lambda^2}\right) \tag{2.24}$$

Applying this to Equation (2.23) results in a plot like that in Figure 2.25 again in terms of wavelength in μm. The result is a term in $fs^2/\mu m$ of the GVD at each specific wavelength. From the example, the GVD for BK7 glass at 850 nm is 40.0 fs^2/mm, whereas it is 25.7 fs^2/mm at 1023 nm. Overall, these are relatively low compared to other portions of the cavity, but they still have an effect.

The next step is to determine the characteristic length. This is essentially the pulse equivalent of the Rayleigh range common to lasers, of which a general visual representation is shown in Figure 2.26. [30, p.187] The same general idea applies in that the useful range is $\sqrt{2} \times \tau_{G0}$ where τ_{G0} is the input pulse width. The result is

Equation (2.25) where L_d is the characteristic length. [14, p.34]

$$L_d = \frac{\tau_{G0}^2}{2|k"_l|} \tag{2.25}$$

For the example, assuming a 100 fs pulse at 1032 nm, the resulting characteristic length is 194.9 mm noting again that the GVD is small for BK7. Once this value is obtained, further determination can be made about how the pulse reacts traveling in the medium. If the distance traveled is going to be close to the characteristic length, it is necessary to use Equation (2.26) to determine the pulse width after traveling a distance, z. [14, p.34]

$$\tau_G(z) = \tau_{G0}\sqrt{1 + (\frac{z}{L_d})^2} \tag{2.26}$$

If, however, $z >> L_d$, it is possible to use Equation (2.27). [14, p.34]

$$\frac{\tau_G(z)}{\tau_{G0}} \approx \frac{z}{L_d} = \frac{2|k"_l|}{\tau_{G0}^2} z \tag{2.27}$$

In the example, assuming 1 cm of BK7, it is possible to use the first equation, resulting in a pulse width change to 100.13 fs. So, as expected in a general purpose glass there is low dispersion, especially at the longer wavelength.

It is important to note that these equations tell nothing about the pulse before entering the medium. In order to use this properly an initial pulse width must be provided. This causes the need for a certain amount of guessing as far as the amount of GVD that is occurring in the system without directly measuring the pulse width in the cavity because it would destroy the oscillation. What then becomes important is how much to correct in terms of the GVD in order to either correct the pulse width or adjust it as desired.

2.4.2 GVD Dispersion Correction. The first method of correction is actually the newest. Recent advances allow using mirrors with layered substrates to induce chirping of the input pulse. Essentially, the layers of the substrates reflect different

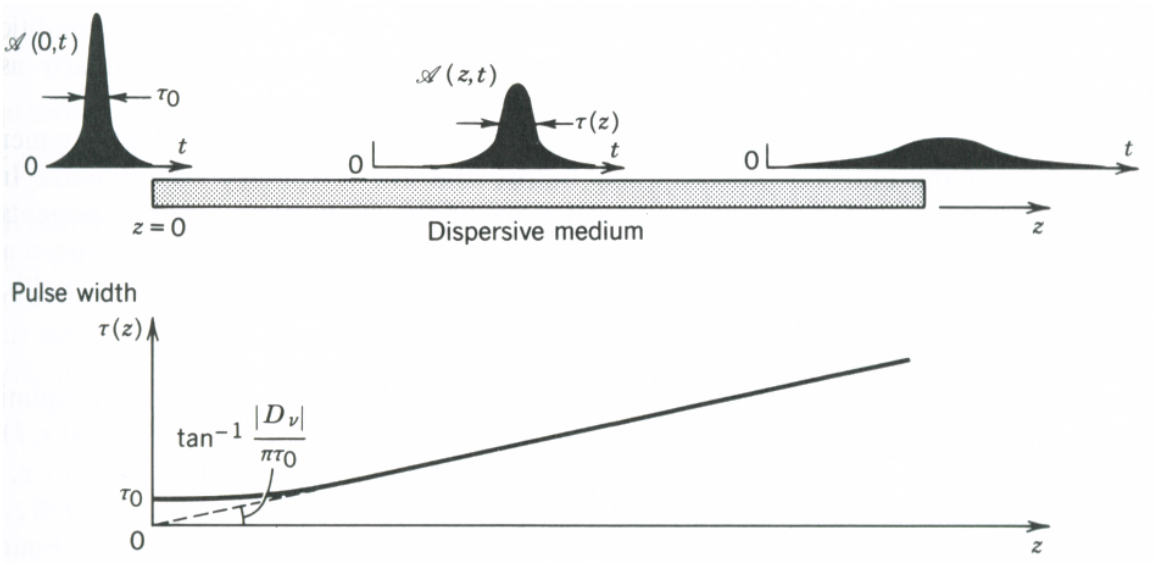

Figure 2.26: General representation of a pulse width in a dispersive medium comparable to the Rayleigh range in laser optics. [30, p.187]

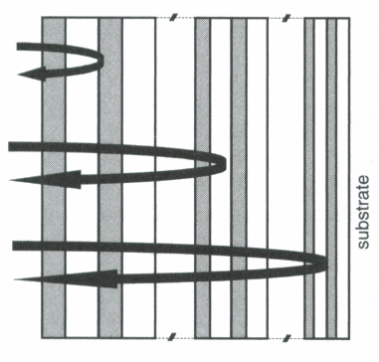

Figure 2.27: General view of a chirped dielectric mirror and how it works. [14, p.82]

frequencies at different places resulting, at least, in phase correction noted above but also can compress the pulse. [7] A simple visual example is shown in Figure 2.27. [14, p.82] Normally, the GVD correction is relatively weak, around 100 fs^2 per bounce off of the mirror, until wavelengths get into mid-infrared range. [7] As a result, multiple bounces have to be accomplished to achieve the desired correction. An example of this type of cavity using only negative GVD mirrors is shown in Figure 2.28. [7]

The most popular and more mature dispersion correction process is based off of the ability to get negative GVD through angular dispersion. [14, p.100] The basis of

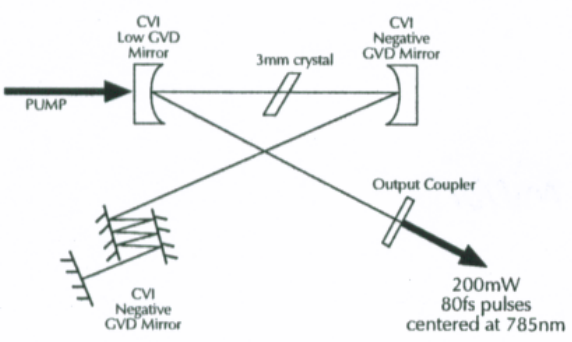

Figure 2.28: An example of a cavity that uses only negative GVD mirrors. [7]

this technique is the optical path lengths (OPL) that different frequencies of the pulse travel. A general description is shown in Figure 2.29 which shows a beam impacting an optical element that causes angular dispersion. [14, p.101] The solid line is the carrier frequency and the dashed line is an arbitrary frequency. The response of a linear medium has the form of Equation (2.28) and that the phase delay, Ψ, between the two frequencies is related to the path length, P_{OL}, by Equation (2.29). [14, p.100]

$$R(\Omega)e^{-i\Psi(\Omega)} \tag{2.28}$$

$$\Psi(\Omega) = \frac{\Omega}{c}P_{OL}(\Omega) \tag{2.29}$$

Using the figure, it is possible to determine the difference in path lengths. The arbitrary frequency travels a distance of $Lcos(\alpha)$ compared to the carrier frequency, resulting in the phase delay given by Equation (2.30). [14, p.101]

$$\frac{\Omega}{c}Lcos(\alpha) \tag{2.30}$$

From there, the second derivative of $\Psi(\Omega)$ with respect to Ω is used to determine the effect on the pulse envelope. The result is Equation (2.31). [14, p.101]

$$\frac{d^2\Psi}{d\Omega^2} = -\frac{L}{c}\Big\{sin(\alpha)\big[2\frac{d\alpha}{d\Omega} + \Omega\frac{d^2\alpha}{d\Omega^2}\big] + \Omega cos(\alpha)\big(\frac{d\alpha}{d\Omega}\big)^2\Big\} \approx -\frac{L\omega_l}{c}\Big(\frac{d\alpha}{d\Omega}\Big)^2 \tag{2.31}$$

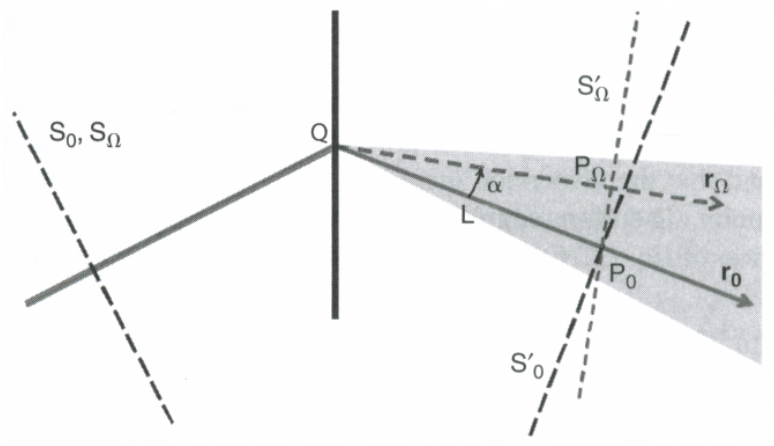

Figure 2.29: Angular dispersion causing GVD. The solid line is the carrier frequency and the dashed line is an arbitrary frequency dispersed differently. [14, p.101]

The approximation is made by assuming that α is very small, resulting in $sin(\alpha) = 0$ and $cos(\alpha) = 1$. A couple of things that should be noted are that the dispersion is negative no matter what side of the carrier frequency the arbitrary frequency is on, and that it gets more negative the more distance, L, you get from the diffraction point. [14, p.102] The goal now is to harness the capability to compress the pulses in the cavity by using a multi-arm cavity and correcting along one of these arms.

The most common setup for using angular dispersion correction is using a dual prism setup inside the cavity. A cavity example is shown in Figure 2.30 and a general setup of the prisms is shown in Figure 2.31. [17] [14, p.107] The key behind this type of correction is geometry. The pulse is compressed because the path lengths of the different frequencies work out to get closer together. One of the most important aspects to using this technique is working with matched isosceles prisms. This is because the faces of the prisms need to be parallel in order to get proper realignment after the second prism. [14, p.106]

The path of the frequencies can be split into four major areas. The first is the OPL in the first prism. The second is the OPL traveled through the air between the prisms. The third is the path through the second crystal, and the last is the air after the second prism. The overall correction can be described better by looking

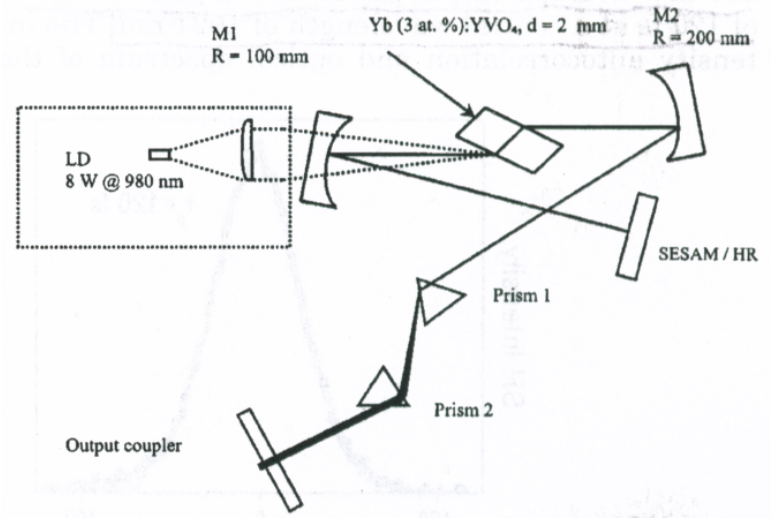

Figure 2.30: Laser cavity of a Yb:YVO_4 solid state laser showing the prisms for dispersion correction. [17]

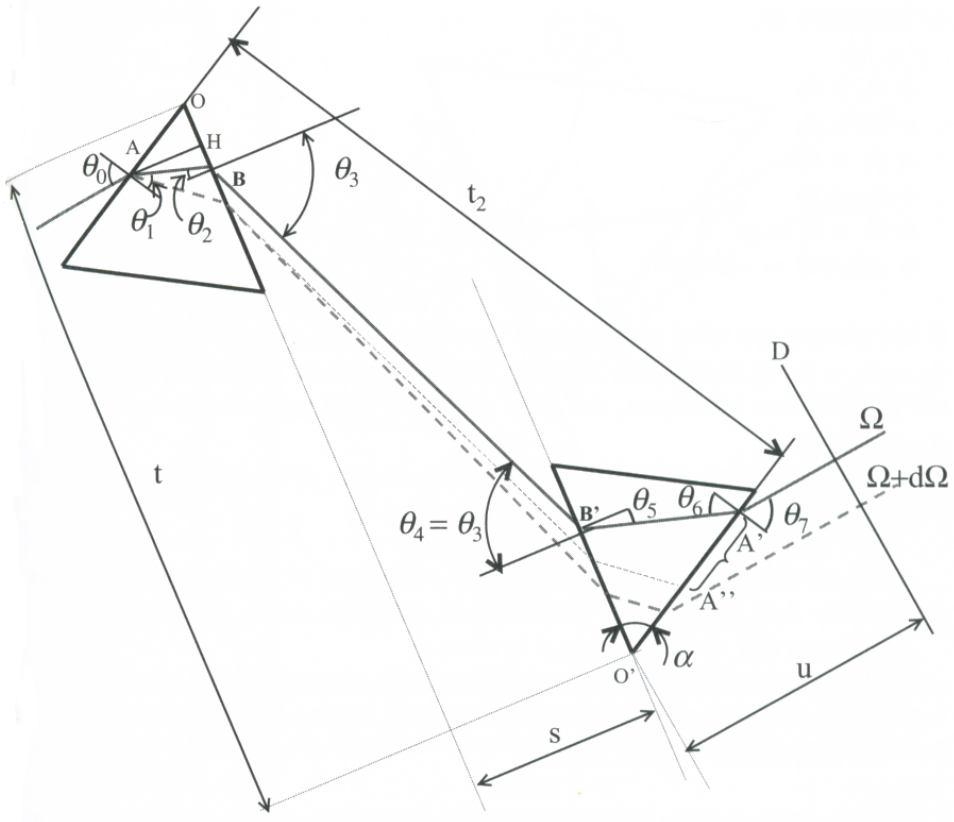

Figure 2.31: Typical two prism setup used in ultrashort systems. [14, p.107]

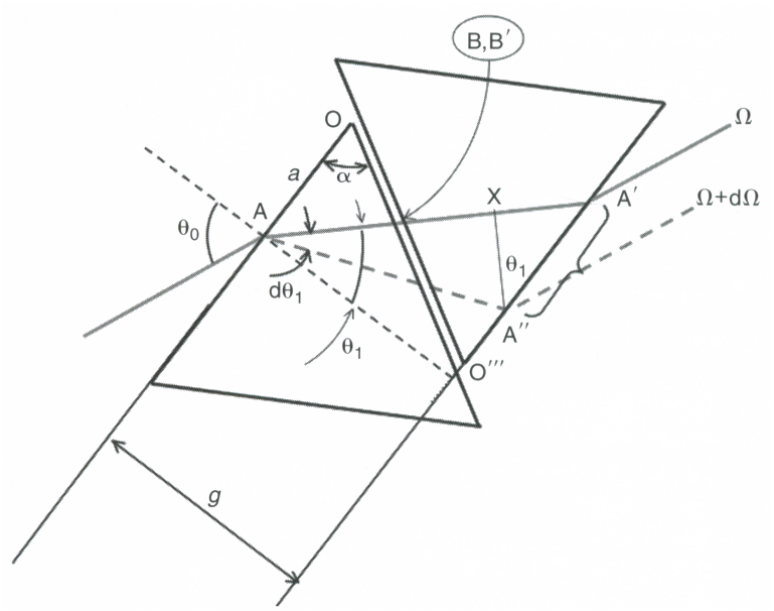

Figure 2.32: Enhanced view of the beam passage through 2 prisms. [14, p.109]

at Figures 2.32 and 2.33. [14, p.109] The OPL differences are easy to notice. The first is the difference between $\overline{AA''}$ and $\overline{AA'}$, as shown in Figure 2.32, and the second is the shorter OPL via $\overline{B'''A'''}$ due to the further dispersion by air of the distance, T, after the first prism, as shown in Figure 2.33. Several different sources work through the same type of analysis shown above and it is not worthwhile to reiterate their analysis. [14, p.105-117] What is important is the general solution derived for negative GVD as shown in Equation (2.32) which is then transferred to wavelength in Equation (2.33). [14, p.115]

$$\frac{d^2\Psi}{d\Omega^2} = \frac{L_g}{c}\left[2\frac{dn}{d\Omega} + \omega_l \frac{d^2n}{d\Omega^2}\right] - \frac{\omega_l}{c}\left(4L + \frac{L_G}{n^3}\right)\left(\frac{dn}{d\Omega}\right)^2 \tag{2.32}$$

$$\frac{d^2\Psi}{d\Omega^2} = \frac{\lambda_l^3}{2\pi c^2}\left[L_g \frac{d^2n}{d\lambda^2} - \left(4L + \frac{L_g}{n^3}\right)\left(\frac{dn}{d\lambda}\right)^2\right] \tag{2.33}$$

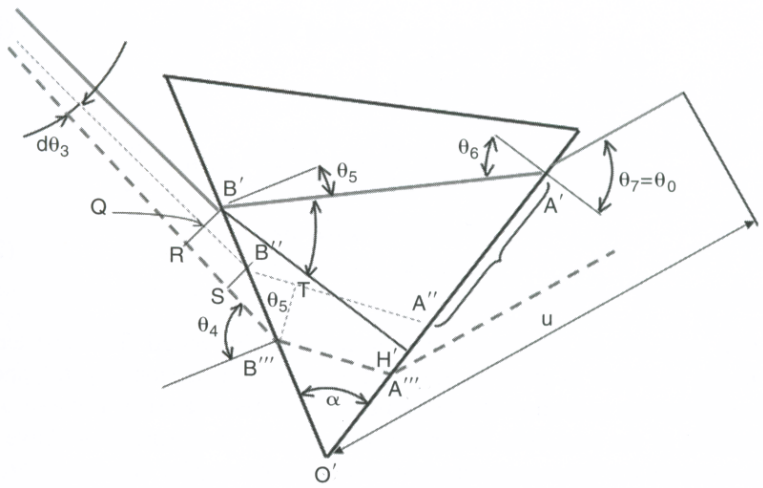

Figure 2.33: Details of a beam through the second prism of the pair. [14, p.109]

One of the best ways to show this is through an example. A common glass used in prisms is N-SF18, of which Equation (2.34) is the resulting Sellmeier equation.

$$n(\lambda) = \sqrt{2.85778 + \frac{0.0000120785}{\lambda^8} - \frac{0.0000740644}{\lambda^6} + \frac{0.00171433}{\lambda^4} + \frac{0.0330238}{\lambda^2} - 0.00948893\lambda^2} \tag{2.34}$$

Using this equation with Equation 2.33 and several assumptions allows a thorough example. The general assumptions are a lasing wavelength of 1023 nm, 1 cm total of path length through the prisms, the angle of the sides of the prisms are at Brewster's angle for the wavelength, and the angle of deflection is the minimum angle of incidence. A graphical example of the result is shown in Figure 2.34. Obviously, it is possible to adjust the desired correction by prism separation and this is where a little of the guessing portion comes in on how much correction is needed. This type of setup has overall advantage of chirping up or down as desired comparable to having a certain number of bounces off of a chirped mirror. The disadvantage of this setup is that the separation has to be large. For this example a separation of 21.2 cm is needed even before the correction becomes negative. For useful corrections the separations are often over 40 cm which provides a distinct disadvantage over chirped mirrors.

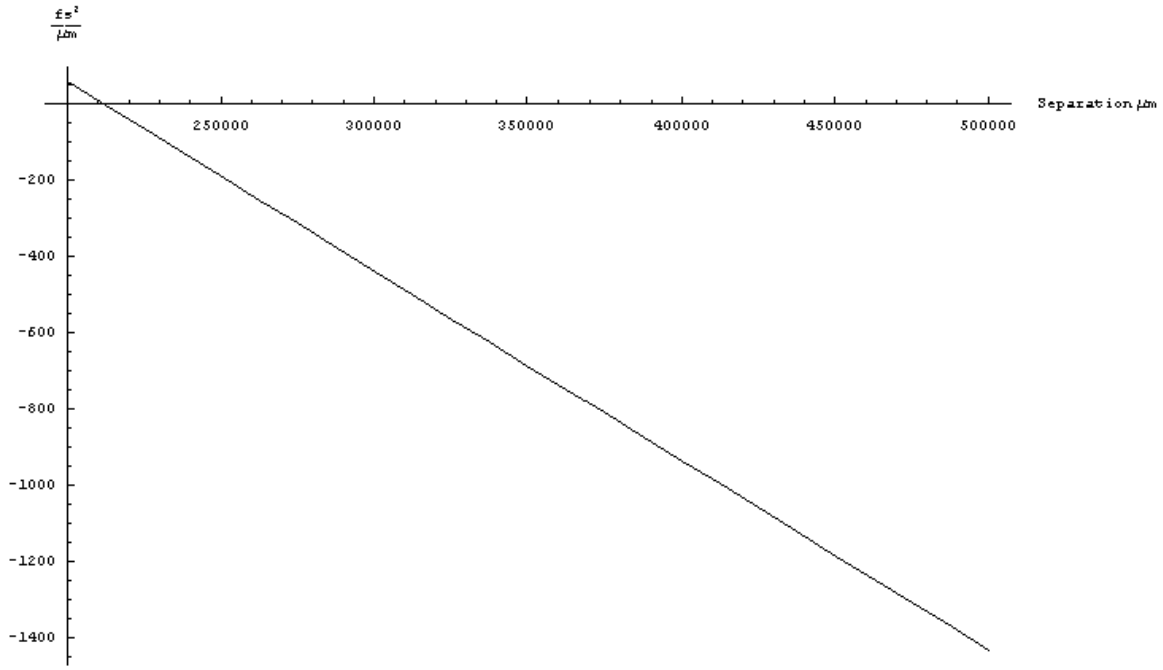

Figure 2.34: GVD as a function of separation, in μm, of two N-SF18 Brewster angle prisms at a wavelength of 1023 nm.

2.5 Summary

The unique aspects of pulsing lasers can seem quite complex but the basics have been presented. Even with general assumptions noted they are usually quite accurate. This background sets the stage for experimental setup described in Chapter III.

III. Design, Construction, and Initial Setup

Most of the experimental setup for this research concerned cavity design. Each design had to be tailored to a specific crystal in order to produce proper nonlinear effects and pulsing phenomena. This resulted in individual designs, reflecting each crystal's unique properties. The designs changed over time due to the purchase of improper parts and manufacturer errors.

3.1 Gain Crystals

As discussed in Chapter II, there is a large number of gain media that can be used in these types of solid state systems. Using desired system properties and well-documented successes by other researchers in the field the gain media types were narrowed down to three crystals. The focus was on creating a baseline system for future research, but also the desire to improve on existing designs by using better materials.

3.1.1 Cr:LiSAF. Of the three chosen crystals, the Cr^{3+}:$LiSrAlF_6$ (Cr:LiSAF) research is the most mature. The availability of chromium doped materials and the early availability of diode lasers at the required pump wavelength (corresponding directly to the GaInP/AlGaInP band gap) encouraged early experimentation. [1, 24] The principal reason for choosing this crystal is the continuing research reducing both the size and power requirements, developments that will contribute to portable systems. [2] A thin Cr:LiSAF crystal has been shown to lase with just 2 mW of pump power, extremely low for a solid state system be it pulsed or not. [14, p.366] When combined with the mass production of efficient diode lasers operating around the peak absorption wavelength, this allows the economic selection of the optimum diode for a specific application. The combination of low pump power and diode selection has resulted in a small cavity Cr:LiSAF laser being pulsed for over 12 hours using just six AA batteries averaging 130 fs per pulse and 14 mW. [2] This easily shows that a truly portable system is achievable in the short term.

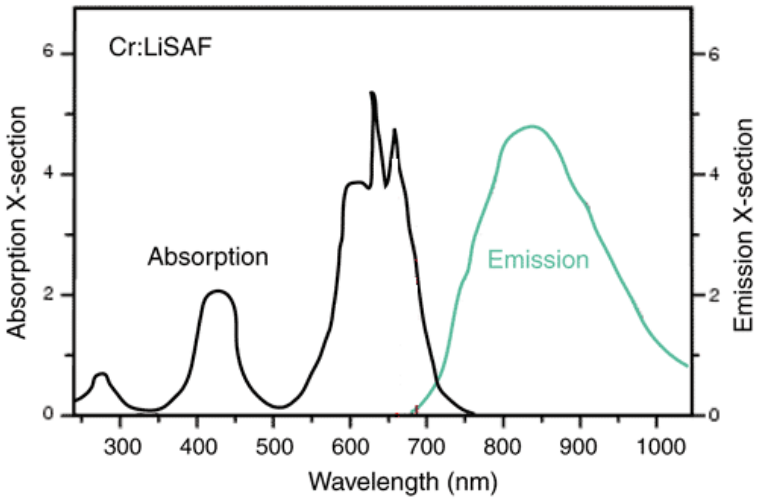

Figure 3.1: Absorption and emission spectra of a Cr:LiSAF laser crystal. [24]*et al*

In order to provide a good measure of the cavity design, an understanding of the crystal's basic properties is necessary. This crystal has a colquiriite structure, with lasing occurring from the normally 1-5% doped Cr^{3+} atoms. [19, 24] The primary absorption of Cr:LiSAF is between 630-680 nm with an emission peak around 850 nm [1, 19, 24] It has been shown, however, that tuning of the output wavelength is possible between 780-990 nm as emphasized in Figure 3.1. [1, 24] Due to this output wavelength and tunability, there are a large number of applications available. The major advantage of this material is the very broad absorption spectrum, allowing for the use of a wide range of pump lasers. Other advantages include a balance between the cross section, $4.8 \times 10^{-20} \text{cm}^2$, fluorescence lifetime, 67μs, and the emission bandwidth as noted above. [24, 35] These advantages, combined with little or no availability of a diode laser at the direct wavelength necessary for the Ti:sapphire crystal, provide a distinct advantage over the more mature commercial system.

A 3mm long circular crystal with Brewster-angle-cut windows doped at 5% was chosen for this work. A schematic of the crystal is shown in Figure 3.2. The index of refraction at the peak wavelength of 850 nm is shown with the Brewster's angle of 54.6° for an index of refraction of n=1.41. [36] The index of refraction as a function of wavelength is shown in Figure 3.3. It is obvious that the index of refraction

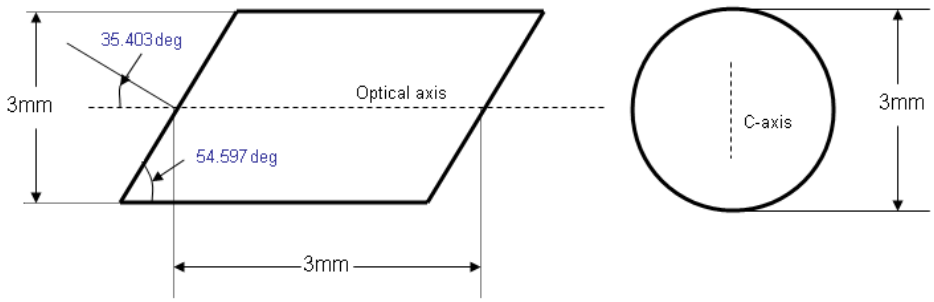

Figure 3.2: Design of Cr:LiSAF crystal showing Brewster angle of 54.6°.

is low as comparable to many other glasses and crystals. For instance, the index of refraction for LiSAF at 850 nm is 1.41, as noted above, whereas the index of refraction of BK7 at the same wavelength is 1.51. This figure also emphasizes how little the index of refraction changes across the wavelengths for both pumping and emission. This has a noticeable result on the GVD which is shown in Figure 3.4. This crystal shows a similar result as BK7 in that, as the wavelength increases, the GVD can become negative. The specific GVD at the peak emission wavelength was calculated to be 11.0 fs^2/mm which actually turns out to be less than the BK7. This number is a little misleading, however. While not directly stated the GVD of Cr:LiSAF is dopant dependent, a property that is suspected for all of the crystals used in these experiments. The dependence is shown in Figure 3.5. [33] This property is the only thing that keeps a linear cavity from being possible for this crystal.

However, there are a several limitations when using Cr:LiSAF. The first is low thermal conductivity. As a reference point, Cr:LiSAF has a thermal conductivity of 3.1 W m^{-1} K^{-1} versus 25 W m^{-1} K^{-1} in a Ti:sapphire crystal. At 69° C, the fluorescence lifetime of Cr:LiSAF is reduced by half. [14, p.366] [2] The result is that optimal use of this crystal occurs below 100 mW of pump power, below which, it is not necessary to cool the crystal. [2] The second problem is that when using a Brewster-angle-cut crystal, there has to be a high astigmatism correction in the cavity. [2] [14, p.366] This becomes necessary to get a small spot size within the crystal for proper gain since the gain cross section is relatively low compared to other

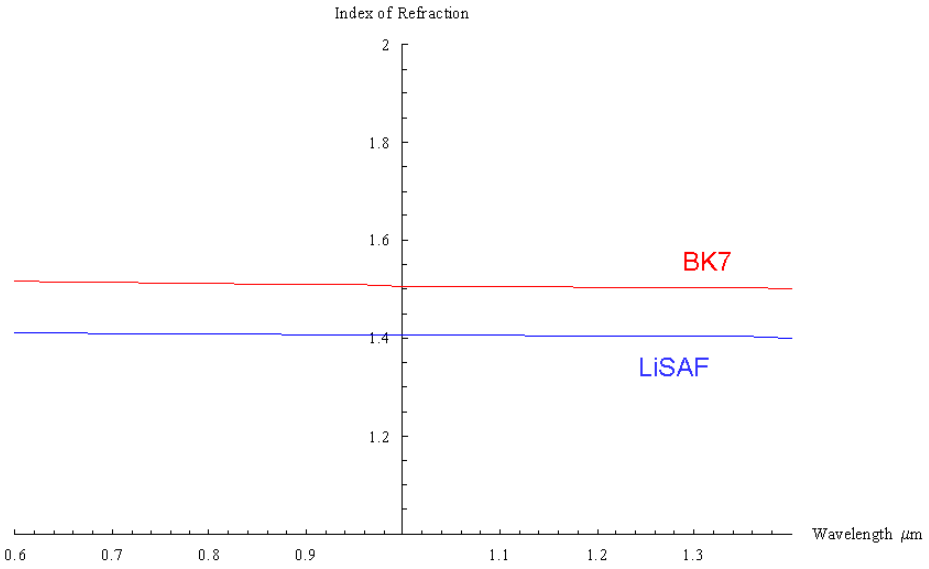

Figure 3.3: Index of refraction of LiSAF (blue) and BK7 (red) as a function of wavelength.

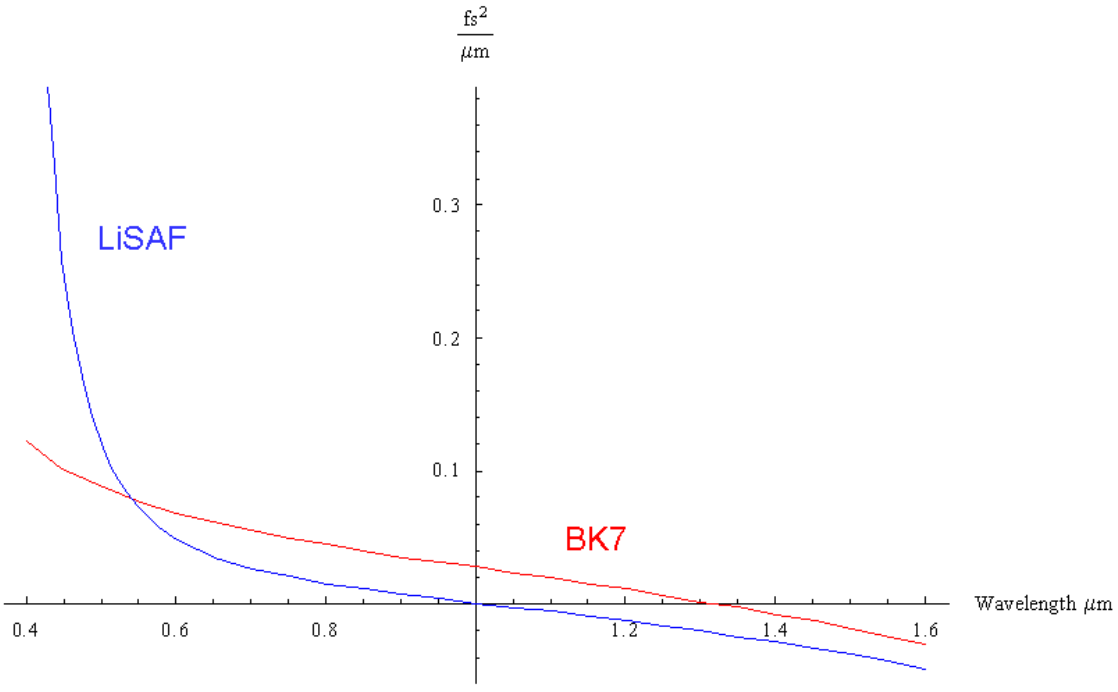

Figure 3.4: GVD of LiSAF (blue) and BK7 (red) as a function of wavelength.

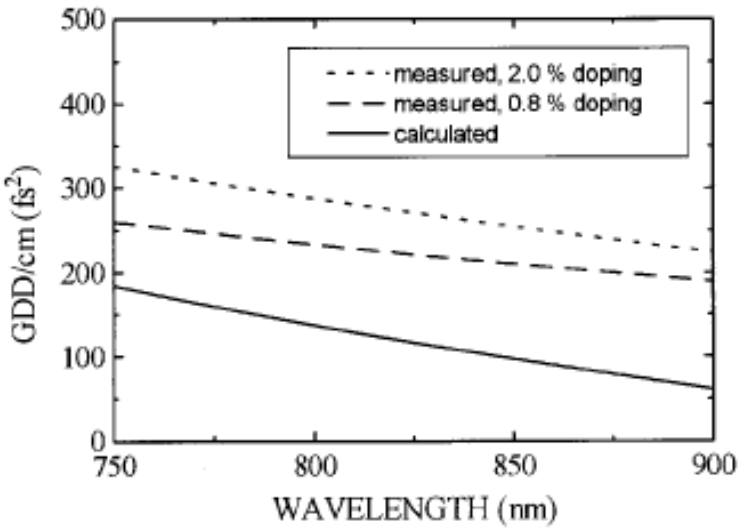

Figure 3.5: GVD of LiSAF as calculated, for 0.8% doping, and 2.0% doping. [33]

lasers, like dye lasers, used for pulsing. [14, p.365] Another factor is that, while diodes for the pump wavelength have existed for an extended period, these diodes have remained at low powers. The last disadvantage is that it has a unique but not well understood property, a negative thermal expansion coefficient in one direction. [19] As a result, more care must be used in designing a mount to keep the crystal from cracking. These, however, are minor issues, and for properly designed systems, the effects are negligible.

3.1.2 Yb:KGW. While research with Yb:$KGd(WO_4)_2$ or Yb:KGW is not as mature as Cr:LiSAF, it is rapidly gaining a following. Many of the general properties of Yb:KGW are similar to that of the Cr:LiSAF crystal. The main reason for using this crystal is for high power applications due to the availability of high power diodes at the pump wavelength. The crystal's use for high power applications, however, is not due to its thermal conductivity, which is on par with Cr:LiSAF at 3.8 W m^{-1} K^{-1}, but is instead due to a low quantum defect which causes less heat buildup in the crystal. [35] Lastly, it is used for high powers due to the simple energy level scheme which limits parasitic processes including up-conversion, exited state absorption and concentration quenching. [23]

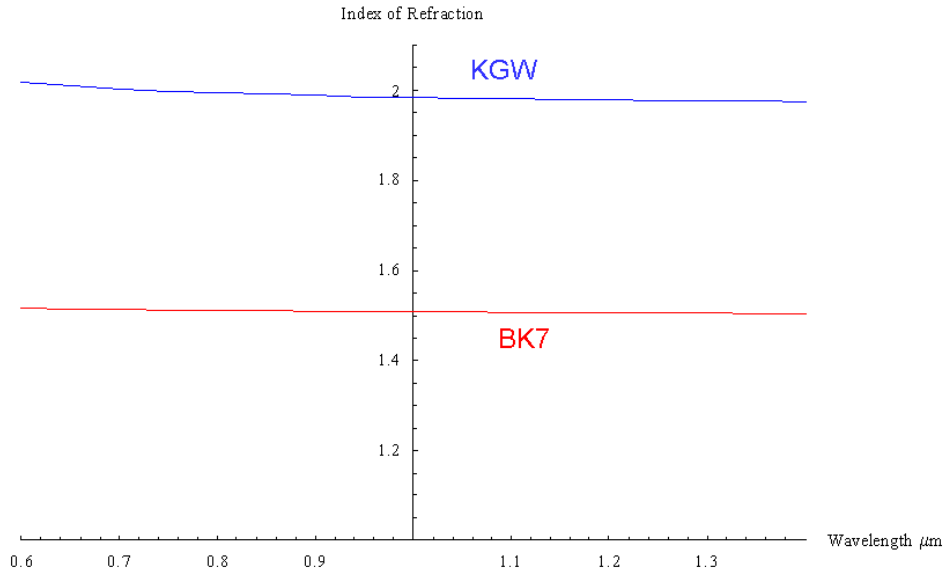

Figure 3.6: Index of refraction of KGW (blue) and BK7 (red) as a function of wavelength.

Basic properties begin with a primary gain region of 1023 nm when pumped at 981 nm with a ytterbium doping normally between 0.5-5.0%. It is possible to dope at higher levels, but a certain amount of loss at the lasing wavelength becomes evident resulting in reduced efficiency. [9] The overall gain bandwidth is around 25nm with an absorption bandwidth of ± 3.5 nm from the peak pump noted above. [8] The crystal has a monoclinic structure with a stimulated emission cross section of 2.8×10^{-20} cm^2 and a fluorescence lifetime of 600 μs. [25, 35] These provide a good baseline of comparison between all of the crystals. The index of refraction based off of the Sellmeier equation for this crystal is shown in Figure 3.6, noting that it is much higher than Cr:LiSAF. [26] The resulting GVD in the system is shown in Figure 3.7. Overall, at the peak wavelength of 1023 nm, the GVD is 167.4 fs^2/mm.

Two different sizes for this crystal were chosen. The first size crystal chosen is used for higher power applications, and was a 5mm height×5mm width×3mm thick Brewster angle cut crystal doped at 5% ytterbium. The second is a 4mm height×10mm width×1mm thick crystal also doped at 5%. It is important to note that KGW crystals are very birefringent, causing a very polarized gain in the medium.

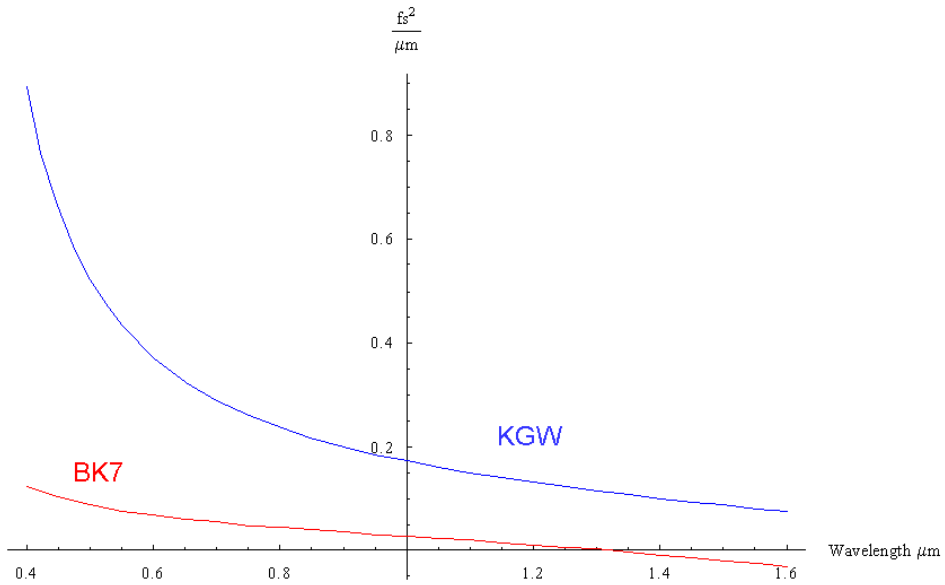

Figure 3.7: Group velocity dispersion of KGW (blue) and BK7 (red) as a function of wavelength.

[23] The Brewster angle cut helps with this effect and has the advantage in that it reduces intracavity losses. The first crystal is for pumping from 1 W to 4 W and the second crystal is for pumping below 500 mW.

As always, there are several disadvantages to this crystal. The most significant disadvantage is the quasi-three-level structure of the laser. This structure leads to a high re-absorption of the emitted photons due to the short wavelength separation of the pump and gain. [23, 35] Figure 3.8 gives a visual explanation of their overlap. [23] The other disadvantage is the long fluorescence lifetime which causes trouble in generating mode-locking due to energy storage and the favoring of a Q-switched regime. [35] These disadvantages are relatively minor and are further minimized by the availability of high power semiconductor lasers at the pump wavelength.

3.1.3 Yb:vanadate. Ytterbium orthovanadate (Yb^{3+}:YVO_4) or Yb:vanadate is essentially an extension of Yb:KGW and one of the most recent advances in small cavity solid state lasers. The basic absorption and emission spectra are the same as Yb:KGW due to the same doping material. The difference is with the thermal

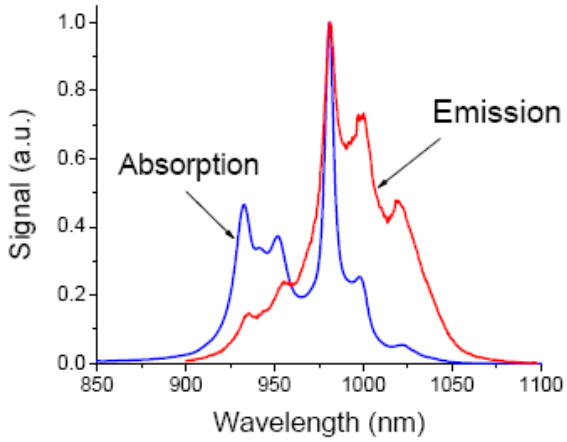

Figure 3.8: Absorption and emission spectra of a Yb:KGW crystal. [23]

conductivity and the ability to shorten the pulse duration. [17] While the thermal conductivity is 3.8 W m^{-1} K^{-1} for Yb:KGW, it is 5.23 W m^{-1} K^{-1} for Yb:vanadate which, combined with the low quantum defect, results in much more thermal transfer efficiency that Yb:KGW or Cr:LiSAF. [17] The other attractive part of Yb:vanadate is its pump-versus-lasing efficiency. It has been shown that it is possible to KLM Yb:vanadate with only 190 mW of absorbed pump power resulting in 130 fs pulses and 8 mW average output power. The index of refraction for vanadate is shown in Figure 3.9 with a corresponding GVD shown in Figure 3.10. As with Yb:KGW the index of refraction is high and the GVD at 1023 nm is 203.1 fs^2/mm. Thus it is obvious that the crystal itself is the main portion of the cavity causing dispersion. For this experiment a 10mm height×10mm width×2mm thickness Brewster-cut crystal doped at 2.6% Yb was chosen. This choice was based off of current documented research specifically noting efficiency. [22]

3.2 Initial Designs

Femtosecond pulsed lasers are maturing rapidly and the bridge is beginning to be built between research and application. The need for smaller and more robust sources is one area that is lacking, so the primary goal of the initial design was to reduce the overall footprint of the system. The robustness was partially taken care

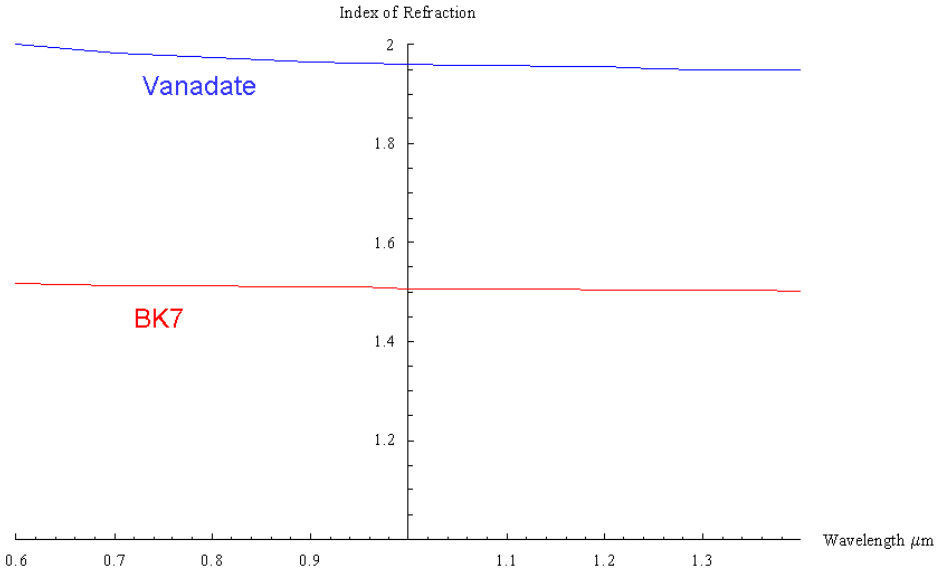

Figure 3.9: Index of refraction of vanadate (blue) and BK7 (red) as a function of wavelength.

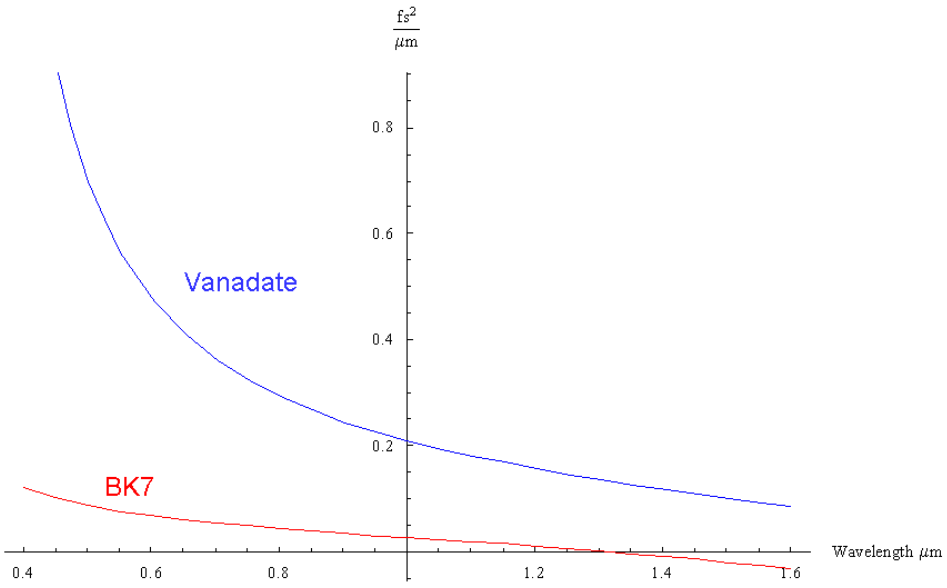

Figure 3.10: GVD of vanadate (blue) and BK7 (red) as a function of wavelength.

of by using diode pumped solid state laser systems and enhanced by the stability of a small optical breadboard. This, combined with the ability to run the diode lasers being used for the Cr:LiSAF system off of batteries, provides a portability which can be exploited. That leaves the cavity design to allow forward progress necessary to future refinement.

Even though three crystals were used, there really only needed to be two systems designed since the Yb:vanadate and Yb:KGW are so similar. The initial designs of both systems are essentially the same with the major exception of the different ways of providing GVD correction. The design of the Cr:LiSAF system is based on being able to use chirped mirrors for correction, while the Yb-based system is designed around the prism correction described in Chapter II. Other differences were in the base components of the system and that will be summed up later.

The first primary design decision concerned the type of cavity to use. To meet the requirements of a small footprint size and multiple passes of the laser light through the crystal, a z-type, ring, or bow tie cavity were determined to be the best solution. All three have been used by many other researchers, but a bow tie cavity design, as shown in Figure 3.11, was determined to be the best starting point for both systems. [7, 17] The reason that the bow tie cavity was determined to be the best was due to the reduction in footprint size over a z cavity and the astigmatism control unable to be reached in a ring cavity.

3.2.1 Astigmatism Correction. The primary reason for picking the bow tie cavity is the need for astigmatism correction (with a minimal coma impact) which is necessary in order to create the smallest waist possible. This traditionally has been a problem for off-axis reflective optics being used in our design. [14, p.328] The general premise is shown in Figure 3.12. [14, p.328] The basic problem is that, in order to get the smallest focus size, the beam hitting the concave mirror has to be large, and therefore, a large off-axis angle is needed to keep the focus outside of the incoming

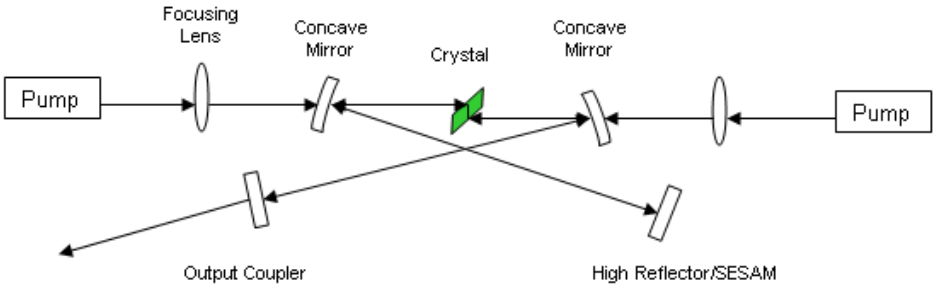

Figure 3.11: General bow tie cavity layout pumped from both sides of the cavity.

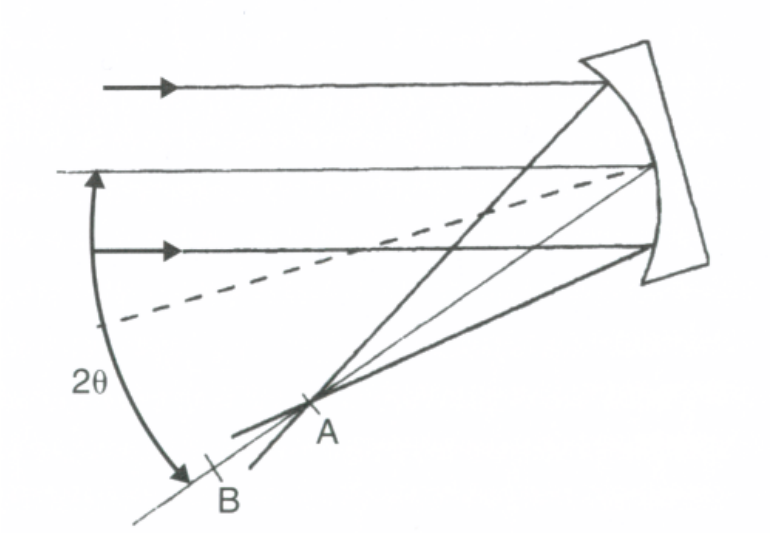

Figure 3.12: Off-axis focusing of a gaussian beam causing astigmatism. [14, p.328]

beam. This is then further complicated by the gain crystal itself which is where correction analysis begins.

When entering a crystal at Brewster's angle, the waists in the x and y axes begin to diverge. The primary difference, as represented in Figure 3.13, is that the waist in the y direction is effected by the index of refraction of the medium, whereas the x axis is not effected by the angle. The resulting waists are calculated with Equations

(3.1) and (3.2). [14, p329-330]

$$w_x = w_0\sqrt{1+\left(\frac{\lambda_l}{\pi w_0^2}\frac{d\sqrt{1+n^2}}{n^2}\right)^2} \tag{3.1}$$

$$w_y = nw_0\sqrt{1+\left(\frac{\lambda_l}{\pi w_0^2}\frac{d\sqrt{1+n^2}}{n^2}\right)^2} \tag{3.2}$$

The crystal can then be analyzed in terms of free space travel of the different portions of the beam as determined by Equations (3.3) and (3.4). [14, p.330]

$$d_x = d\frac{\sqrt{1+n^2}}{n^2} \tag{3.3}$$

$$d_y = d\frac{\sqrt{1+n^2}}{n^4} \tag{3.4}$$

Then by taking into account the focus of the mirror, the angle that would cause those waists to be equal at the focus can be determined via Equation 3.5 where R is the radius of curvature of the mirror, n is the index of refraction of the crystal, and d is half the distance through the crystal. [14, p.331]

$$\frac{2d}{R}\frac{\sqrt{n^4-1}}{n^4} = \frac{sin^2\theta}{cos\theta} \tag{3.5}$$

The result is an accurate, but surprisingly small, angle that is very component dependent. For example, for the 1-mm thick Yb:vanadate crystal, the angle turns out to be 11.5° using a mirror with a ROC of 50 mm.

3.2.2 System Components. Each system has the same basic components as illustrated in Figure 3.11. The multiple pump lasers, two concave mirrors, a SESAM or high reflector, and an output coupler are common to both systems. Choices on their properties are crystal specific, however, and need to be taken separately. Specific component manufacturers and model numbers are noted in Appendix B.

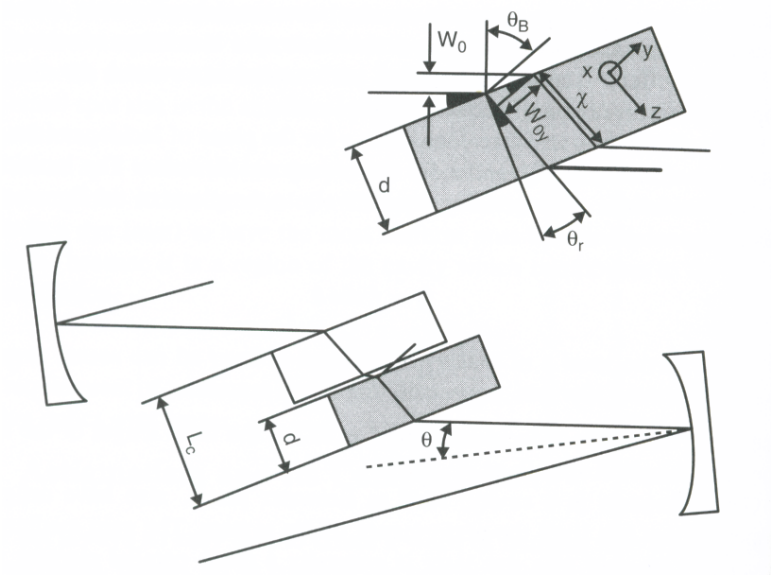

Figure 3.13: Analysis of differing path lengths in the x and y directions to allow correction. [14, p.330]

3.2.2.1 Cr:LiSAF Specific Components. The overall design for the Cr:LiSAF system is shown in Figure 3.14. The pump lasers chosen have an output power of 100 mW at a peak wavelength of 658 nm, close to the peak absorption of 670 nm. While optimum pumping is below 100 mW due to heat considerations, the ability to provide extra power on target along with the affordability of the diodes encouraged this design. The polarizing beam splitters are a general design with optimum wavelength transmission between 500 and 1200 nm. Focusing lenses with a 50-mm focal length were chosen to optimize the smallest spot size in the crystal. Other lenses, however, with different focal lengths were purchased in order to provide flexibility as design changes occurred.

The mirrors in the cavity had to be chosen by the two different wavelengths in the cavity. This specifically includes the concave mirrors which needed to transmit the 658-nm light but be a high reflector for the 850-nm laser light. What is important about all of these mirrors is that each is chirped for GVD correction at the lasing wavelength. This is unique, specifically for the concave mirrors, and is designed to reduce the size of the cavity. It is also important because, as of this writing, the

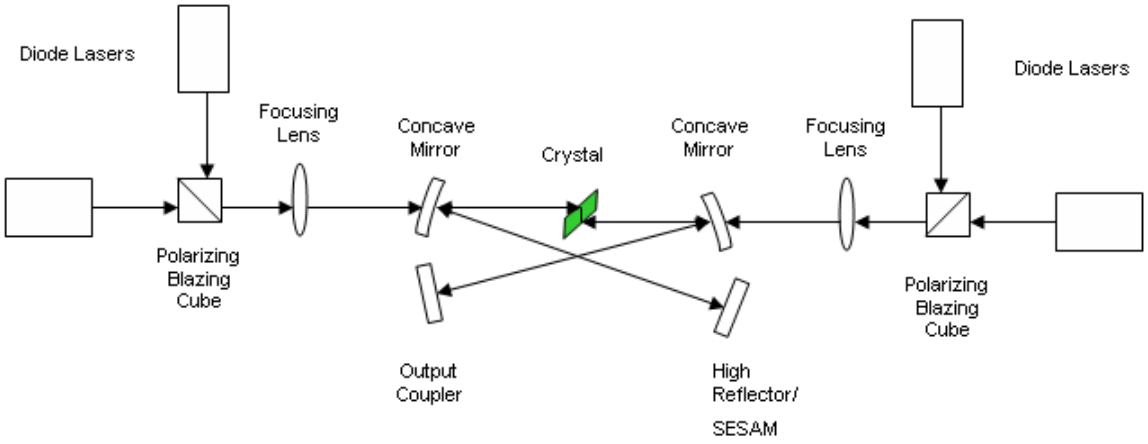

Figure 3.14: Design used as a basis for selecting components for the Cr:LiSAF system.

properties of a system with the concave mirrors being chirped has not been published. Mirrors with loss from 1-5% were chosen as output couplers. The SESAM was one of the latest designs as described in Chapter II with an unsaturated absorption of 4%.

The last major individual piece of equipment for the Cr:LiSAF system was the crystal mount itself. In order to ensure good thermal management, the mount was made with a copper alloy and contact with the crystal was maintained with indium foil. This is of increased importance due to the previously mentioned negative thermal expansion coefficient. Two designs were completed. The first is a clamp design shown in Figure 3.15 which is free standing, and the second design is shown in Figure 3.16 which was designed to fit into a standard 1 inch mount. The first mount was used for all research in this thesis.

3.2.2.2 Yb Specific Components. The design of the Yb based systems is shown in Figure 3.17. The lasers chosen were two fiber coupled diode lasers producing 450 mW of power at 976 nm. As a backup, two 4-W diode lasers were purchased if it became necessary to provide higher pumping power. The only portions of this laser system different from the Cr:LiSAF system are the prisms being used for GVD correction and the concave mirrors. The prisms chosen were 60° isosceles prisms which, while not at Brewster's angle, are within 0.5°. Due to the small separation between

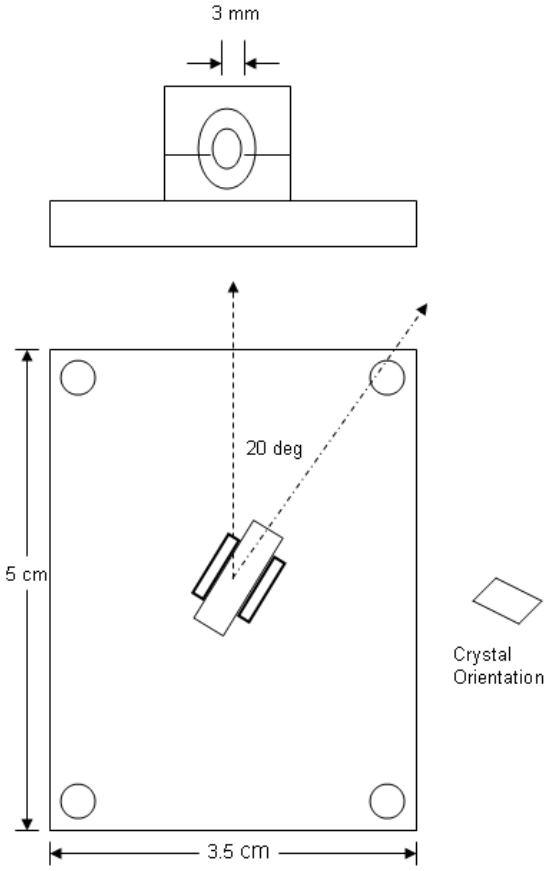

Figure 3.15: Primary crystal mount design for the Cr:LiSAF system.

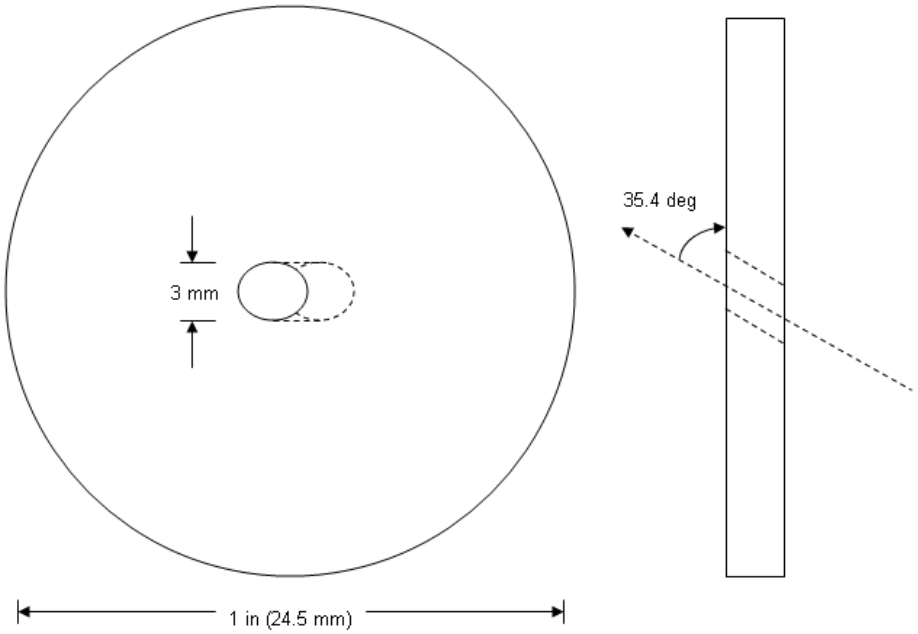

Figure 3.16: Secondary crystal mount design for the Cr:LiSAF system.

pump and lasing wavelengths, these mirrors were more specialized and, while allowing a lot of transmission, still only allowed approximately 85% of the pump light through. The SESAM is an excellent off-the-shelf system. The absorption is 1% and is designed to have a zero GVD for the 1064 nm as shown in Figure 3.18. [4] The mount for the Yb systems was very simplistic. The 1-mm-thick Yb:KGW and 2-mm-thick Yb:vanadate crystals were mounted in a piece of copper with a line milled in it for placement. The design for the 3-mm crystal is just a small 3-mm notch cut in a piece of aluminum.

3.3 Cavity Design

An example of the overall goal for the Cr:LiSAF system and Yb systems is shown in Figure 3.19. Several designs with a cavity length of less than 15 cm have shown to be successful at creating ultrafast pulse repetition rates. [16] This capability, combined with the small footprint, fits well with the previously stated design goals and prompted use of this design as a basis. The biggest limitation with accomplishing this design goal for both systems for this thesis was expense for the Yb systems. The

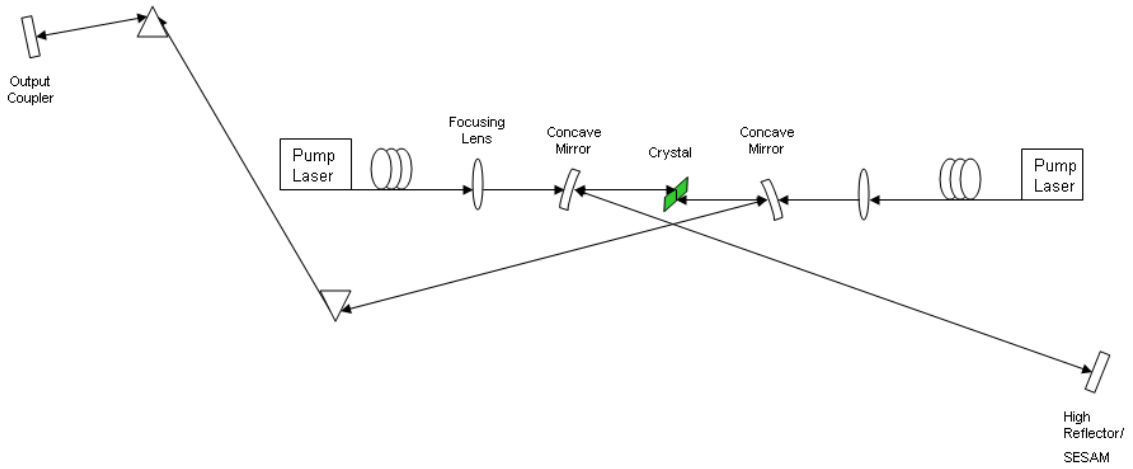

Figure 3.17: Design used as a basis for selecting components for the Yb systems.

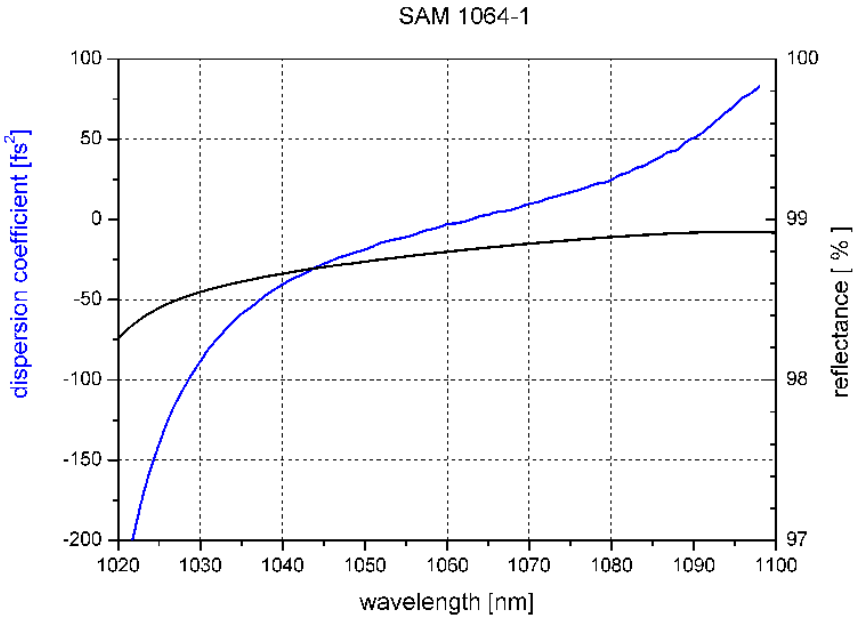

Figure 3.18: GVD and reflectance of a BATOP SAM-1064-1 saturable absorbing mirror.

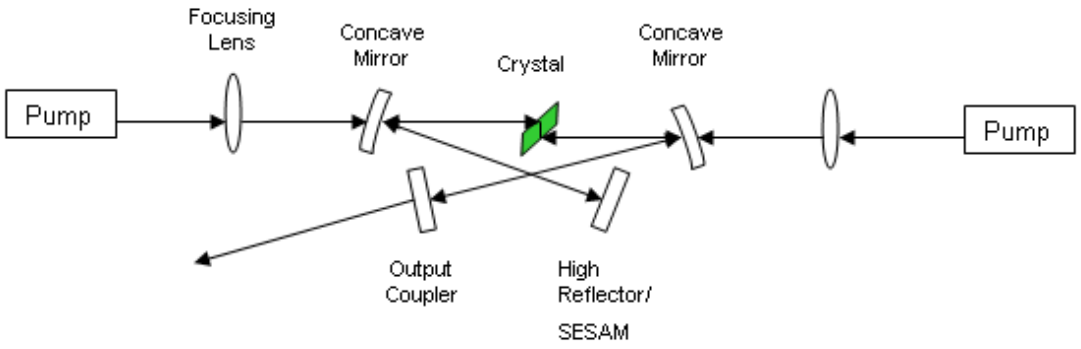

Figure 3.19: Overall goal for the Cr:LiSAF system and Yb system designs depending on expense.

initial designs were well proven and should have required little adjustment to properly function. This, however, did not occur due to improper components and crystal cut. This resulted in a continual evolution in the design and added unwanted complexity to both systems. The prime factor then became learning from mistakes with balancing the goals set. Overall, this prevented accomplishing all of our goals, but this can be easily overcome with component replacement.

Before moving on to the individual system evolutions, it is important to discuss the common elements in the systems used for setup and alignment. The first is placement of the focusing lenses on XYZ translation stages. This allows very fine beam steering outside of adjusting pump laser placement and is much more convenient. The next major commonality is that the two concave mirrors were put on X-translation stages, allowing movement towards and away from each other. The reason for this is that these two mirrors work together to get the proper focus inside the cavity and, as such, need to be at the proper separation to maintain this focus. The last major similarity is that the flat mirrors and SESAMs were mounted in tilt, translation, and tilt without translation mounts with as fine adjustment as possible. The obvious reason for this is that these mirrors have primary control over the angles in the cavity since the concave mirror angle is usually adjusted to the calculated astigmatism correction

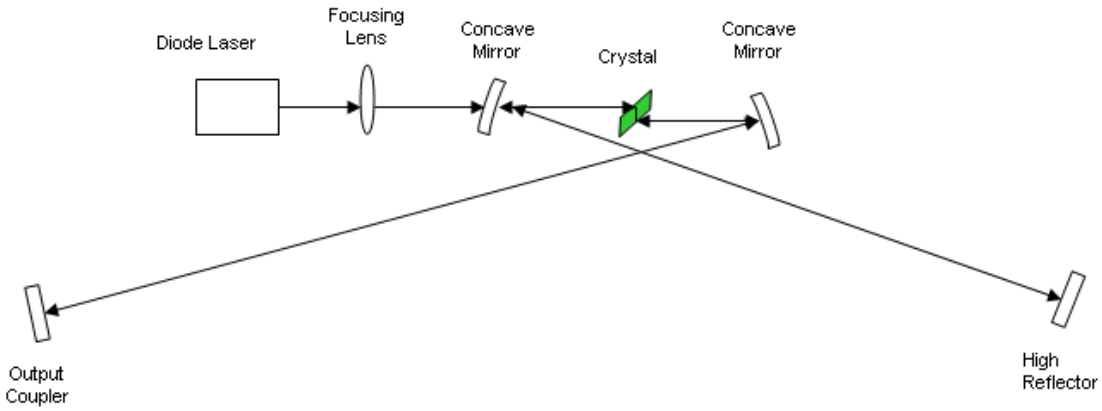

Figure 3.20: First working design of the Cr:LiSAF system.

and then left alone except for translation. These common elements contributed to the easy application of learned techniques to both systems.

3.3.1 Cr:LiSAF Evolution. Initial work with the Cr:LiSAF system used only one diode instead of the four planned. This decision was based off of previous published work and the limited availability of diode current drivers. [1, 2] A visual example is shown in Figure 3.20. This system, and a basis for the rest of the evolutions, uses 50-mm radius of curvature (ROC) concave mirrors resulting in a calculated angle of 9.2° for astigmatism correction. A 50 mm focal length lens, 99% output coupler, and a high reflector complete the component setup. One of the important things to note is the length of the arms of the cavity. Extending the arms is done to ensure a smaller spot size in the crystal and has the bonuses of easier angle placement and better feedback control when adjusting to get it to lase.

Primary alignment considerations focused on three aspects. First was space. In order to get a smaller cavity, and smaller spot sizes, the focal lengths of the components are small. The toughest aspect of interference was placing the mount in the cavity. This required an awkward setup with a kinematic stage and influenced the second mount design even though it was not used. The second alignment consideration was the placement of the concave mirrors. This is due to the fact that they are not

directly across from each other. Because the pump light is being put through at the crystal's Brewster angle, there is deviation from placement on one face of the crystal to the other face. If done correctly, the light should proceed down the center of the cylinder to the opposite face. The overall result is that there is a slight offset to these mirrors as can be seen in all of the cavity design figures. The last consideration is specific to the Cr:LiSAF system. Since the pump light and lasing wavelength are so far apart, they will bounce at different angles through the cavity. The result is that general alignment without the crystal in place is relatively inaccurate.

Work with this cavity progressed but the inability to get active lasing forced a change to the initial design. The primary basis for this decision was the belief that either the spot size on the crystal was too large or there was not enough power on target. The simplest solution was a four-diode design and adjusting the system as necessary. Important to note here is that the adjustments were complex. Getting the proper alignment of beams in the polarizing beam splitter and then keeping them overlapping past the crystal to the mirror on the same side as the pump diodes is difficult. Accomplishing this requires a general alignment in the crystal by looking at the beams immediately after combining in the beam splitter. With that accomplished, the next best place to look is at the concave mirror on the opposite side of the pump. Adjustments at this stage are best done by adjusting the beam splitter instead of the diodes. Once overlapping at this mirror, the next place to look is at the flat mirror that will be the next bounce. Normally, this should be close to desired overlap and very minute changes should be needed. Due to too high of losses on the concave mirrors, even with these changes, the tests proved unsuccessful.

The last design for the Cr:LiSAF system is that shown in Figure 3.21. The basis for this system was to remove a bounce of the laser light off a mirror in the system. By doing this, less loss is achieved in the cavity due to the removal of a mirror since the mirrors in this system proved to have a higher loss than expected. The only major component changes were a substitution of the right-hand-side concave mirror to one with a smaller ROC, and then moving it out to twice the focal length from the

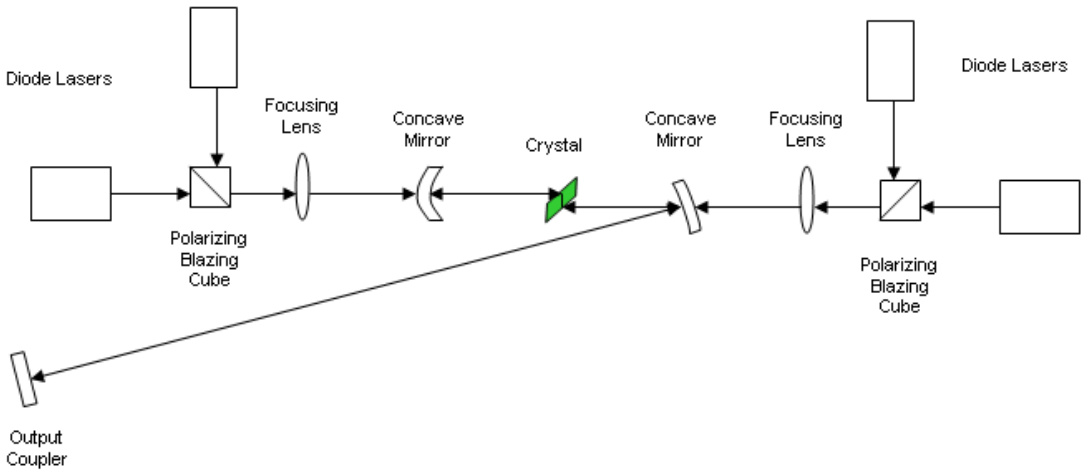

Figure 3.21: Asymmetric z cavity used as last cavity design for the Cr:LiSAF system.

crystal instead of at the focal length, setting up an optimum focus in the crystal. The other component that was changed was the output coupler which was replaced by a high reflector with 0.4% loss. This proved to be the most successful of the Cr:LiSAF systems and specific results will be discussed in Chapter IV.

3.3.2 Yb Evolution. The initial design for the Yb systems was very similar to the initial design for the Cr:LiSAF and is shown in Figure 3.22. Specifically, due to arrival time, the 3-mm thick Yb:KGW was used initially and provided some success. Two 50-mm ROC concave mirrors were used with a biconvex focusing lens with a focal length at 50 mm. With this setup, the angle for astigmatism correction was determined to be 13.6°. With this success, it was determined that it would be best to use a dual laser design pumping from both sides of the cavity to provide more power. Alignment procedures are somewhat similar to that of the Cr:LiSAF system without having to worry about overlap through a polarizing beam splitter. With the Yb systems, it is not possible to pump from the same side using a polarized combining process since the polarization dependence of the crystal is high. This system did lase well. Specific dimensions will be mentioned in Chapter IV.

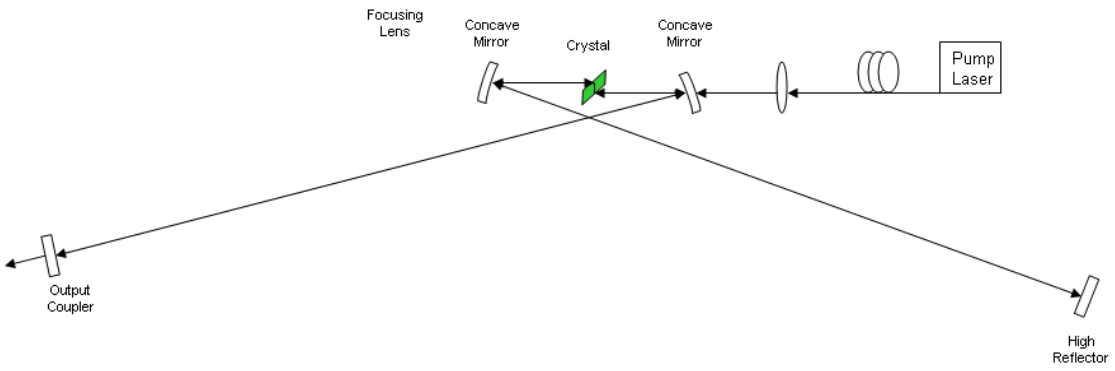

Figure 3.22: Initial working design for the Yb systems.

The next two evolutions of the system are tied together. The first was to change out the high reflector for the SESAM. Along with this, the right-hand concave mirror was changed to a 75-mm ROC and the left-hand concave mirror was changed to a 40-mm ROC mirror and moved to twice the focal length from the crystal. The arm containing the SESAM was shortened to twice the focal length of the 40-mm concave mirror in order to provide as small a beam size as possible to provide saturation. With this, the angle for astigmatism reduced to 11.5°. A schematic of the changes made is shown in Figure 3.23. One of the biggest problems at this point was interference from different components of the system. Because the correction angles are so small, the mount for the SESAM began interfering with the beam to the output coupler. The overall fix for this was moving the SESAM a little further away than twice the focus desired. This produced problems later but it was able to lase. There is one primary disadvantage in this movement. As a result of the shorted arm length, the spot size in the crystal becomes larger, meaning that some adjustment of the pump lasers is needed because the pump modes and the cavity modes need to be the same.

In order to provide further clearance from the beam, both concave mirrors were changed to 100-mm ROC mirrors. The left mirror was repositioned such that it was focused on the crystal and the SESAM was placed close to twice the focal length. These changes were quickly adjusted and with a little work the system lased. With this success, it was possible to move the prisms in for GVD correction as shown

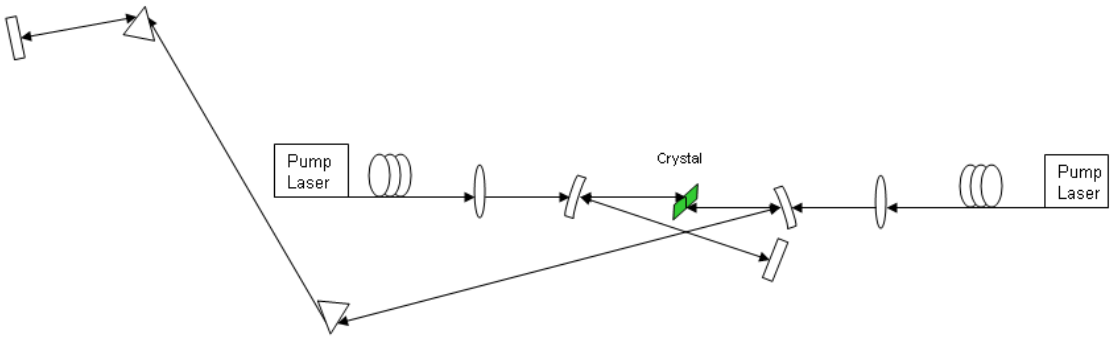

Figure 3.23: Adjustment made to Yb:KGW system in order to incorporate the SESAM.

in Figure 3.24. It is important to note that the beams going into the first prism and coming out of the second prism are parallel. This is a consequence of the GVD correction and the geometry needed along with the desire to reduce loss. Introduction of the prisms was accomplished by putting the first prism encountered on an X axis translation stage so it could be slowly moved into the beam. The second prism and second output coupler were then placed based off of the minimum deviation angle of the first prism. Special care was taken to ensure that the total length from the right concave mirror through the prisms to the second output coupler was the same as from the right mirror to the original output coupler. This is done in order to ease in realignment to get the system lasing. Lasing proved to be possible, but it was determined that it was unable to mode lock since the spot size on the SESAM was not small enough to saturate the semiconductor. Specific dimensions are included in Chapter IV.

Armed with this knowledge and several published articles, the push was to get the Yb:vanadate crystal into the system. [18, 22] The other reason for this was, since the doping of this crystal was less and it was physically thinner, it would be possible to get more power onto the SESAM. The first step behind this was resetting the cavity to that in Figure 3.22 except with two pumping lasers. The reason for this was essentially to step back to what was proven to work with the least amount of components involved. This system was worked on for an extended period of time. Due

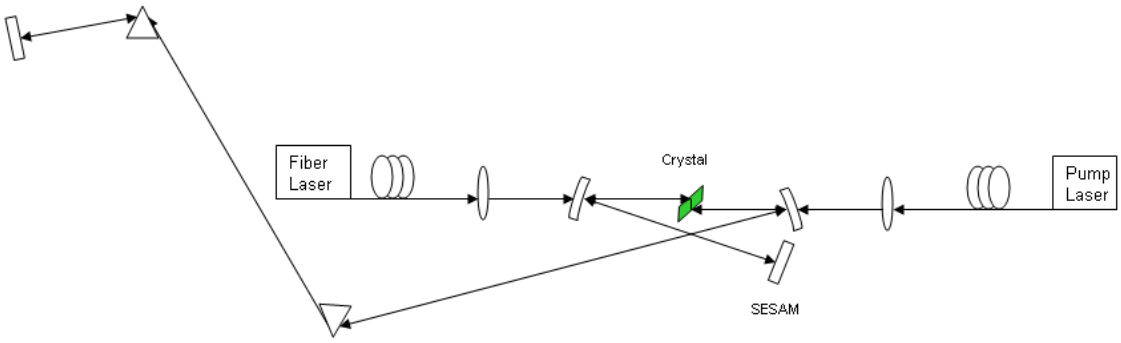

Figure 3.24: Layout with introduction of prism GVD correction to the Yb:KGW system.

to the inability to get lasing, it was determined, with contact from the manufacturer, that the crystals were cut wrong and no amount of moving the crystal would allow lasing. With this problem arising, the default was to move to the 1 mm thick Yb:KGW crystal. This was severely limited by time, and no progress was made except for some basic observations of the crystal.

3.3.3 General Techniques. The first step is alignment. The most important alignment factor is to get the pump beams centered in the concave mirrors from both sides. If this is not completed, added problems arise in that the beam angle changes direction coming off the mirror as it is translated back and forth. This can cause instability in the cavity and make accurate adjustments almost impossible. Another very specific technique that is extremely useful for ensuring proper alignment consists of putting an iris between a concave mirror and the flat mirror. This is part of the reason for the long arms of the bow tie. By doing this, it is then possible to adjust the iris down after aligning it to the beam from the concave mirror in order to see the reflected beam location from the flat mirror. This has the bonuses in that it reduces the intensity on the arm mirrors when it is important not to overload a detector and if adjustment of a concave mirror is necessary, an established realignment capability is present.

As far as a procedure to adjust the components of the system there really is nothing standard. The general goal is to make adjustments to get the maximum power detected at the output coupler. It is recommended to use a bandpass filter in front of the detector separating the pump and lasing wavelengths to ensure that the lasing wavelength is seen. This is important since they bounce at different angles, so it is possible to see an increase in power as the pump is focused better on the detector. If the wavelengths of the laser and pump are close, a mode-lock-in amplifier with an optical chopper is best to separate the pump and lasing wavelengths. The optimum location for the chopper is in front of the high reflector or SESAM in the system since only light making it from that mirror to the output coupler will be measured with the lock-in amplifier.

The best recommendation for adjustments is to establish a list in the order of component adjustment and stick to that procedure. This way, there is a logical progression and, if there is an abnormality, the culprit should be readily identifiable. Behind this is that several components are related and best adjusted together. The most obvious of these are the two concave mirrors as mentioned before. Other examples are the output coupler and high reflector or SESAM, and if pumping from both sides of the cavity, the focusing lenses. All of these can be very sensitive and care needs to be taken not to over-adjust them. Progress can be made, however, if an adjustment is made and then back tracked. The best way to work with this problem is to purposely adjust a component off of the maximum and use its related component to work it back up in power.

The last pre-lasing technique is based more on lab equipment and availability. When a system is about to lase, there is a small amount of instability, and depending on the detector, this might be seen as a minuscule jump with a return to normal due to integration time. If it is possible, a detector or monitor would be best if it had a manual setting that made a noise when overloaded. This ensures that, if it does momentarily lase, you know about it and can adjust it as necessary. This seems a

little innocuous but proved invaluable in getting systems up and running quickly after a component change.

A simple technique that can be used after the system is cw lasing is to tap the components. This provides a small amount of deflection which normally returns to the previous power level. By watching the power level it is possible to tell if the component is moving in the proper direction. This is most effective on the focusing lenses if using multiple lasers but it will work on all components. Another useful technique after lasing is accomplished is to let the system sit and run without adjustments for a little while. This allows all parts of the system to even out thermally and can provide an indication of whether or not heat is building up in components, most specifically the crystal. The key is stability. The more stable the system is cw the better it will be to mode lock.

These techniques may seem somewhat basic, but they are more specific to ultrashort pulsed lasers than other lab techniques. All of these techniques proved themselves and should help any other researchers when working on similar systems.

IV. Experimental Results

Experimental results are divided into two sections. The first section contains results gained from the work with small cavity lasers. The second section contains pulse data from the AFIT commercial Ti:sapphire laser. This second section was planned to be compared to the data received from the locally built small cavity lasers.

4.1 Small Cavity Results

4.1.1 Cr:LiSAF. As noted in Chapter III, the initial design of this system was modified by removing a mirror due to the incurred loss by the concave mirrors in the system. When the mirrors were purchased, the transmission percentage of the pump beam was specified. This had the disadvantage in that it affected the reflectivity of the lasing wavelength inside the cavity. Specifically this took the percentage of reflectance for 850 nm from around 99.5% to 98%. This effect on sustained lasing was drastic because of problems maintaining photons in the system. The key to this problem is that these two mirrors are *required* to be used and not optional. The reason for this purchase was to get the maximum pump efficiency but this came at the cost of cavity efficiency which was unable to initially be overcome.

Removing the mirror and accompanying "bounces" contributed to improving the system's lasing ability. A general layout of the modified system with dimensions is shown in Figure 4.1. In order to maximize power, it was determined that a thermoelectric cooler (TEC) was needed to control the temperature effects noted in Chapter III. The TEC was mounted underneath the copper mount and a power source provided a constant current. The resulting temperature change, though small, allowed more consistent and predictable lasing. With this configuration, the total power reaching the crystal was 140 mW, even after one of the diodes failed. Using a Rigrod analysis, an output power of 2.0 mW was achieved with a mirror providing 99.8% reflection. When a 99% output coupler was used the output power increased to 17 mW. The resulting pump efficiency improved to 17.1% from around 10%, better

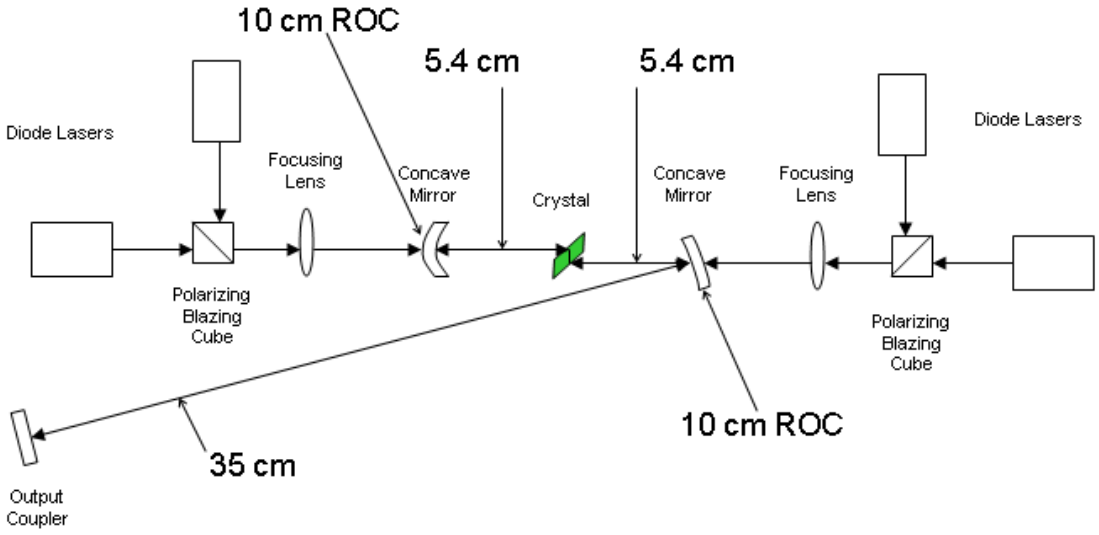

Figure 4.1: Final configuration of the Cr:LiSAF system with dimensions.

than expected. Despite this efficiency it was determined that it would not be effective to mode lock the laser.

The main problem with this system was the movement to the three mirror configuration. This resulted in the inability to use the planned SESAM for mode locking. The possibility of using KLM was discussed, but the availability of a medium to provide the necessary third order properties was limited. This resulted in an interesting, but unexplained effect. In order to reduce the overall footprint of the system the length of the arm was shortened. But this modification resulted in the system not lasing. This was puzzling and could be the result of several different factors, including astigmatism correction angle and focusing by the concave mirrors resulting in too large of a spot size in the crystal.

4.1.2 Yb:KGW. With the 3 mm thick crystal, this system was by far the most successful. Dimensions of the final designs with and without the prisms are shown in Figure 4.2 and Figure 4.3. Maximum cw power reached was 20.5 mW with 450 mW of pump power. This results in an efficiency of 4.3%. This was low but expected due to the length of the crystal since a large amount of the laser light is

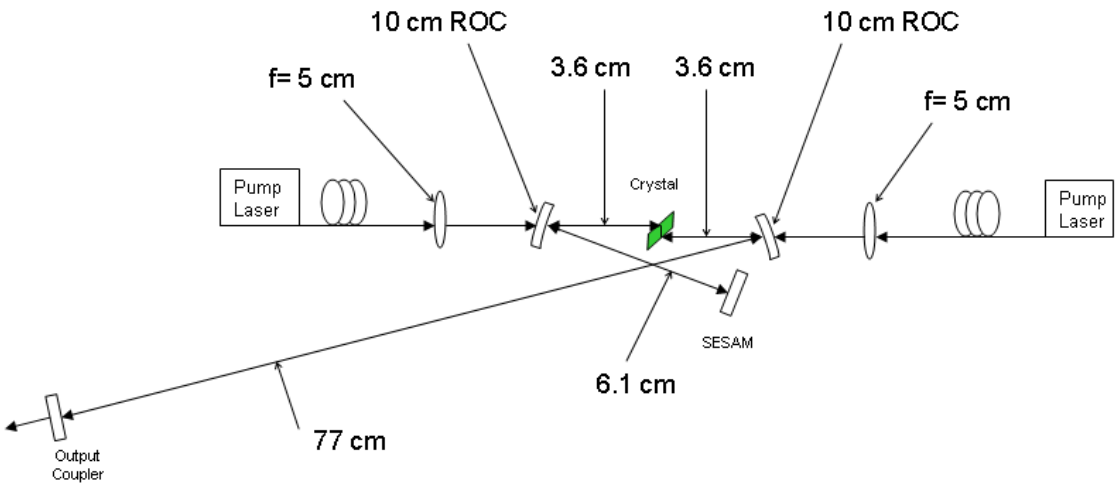

Figure 4.2: Final design of the 3 mm Yb:KGW system without the GVD correction prisms with dimensions.

reabsorbed and this is the crystal planned for higher power applications. Once the SESAM was put in this power went down to 12.3 mW due to a 1% loss by the SESAM under cw conditions.

While this was the most successful system tested, this is also where I made the biggest mistake. Once the system had good lasing stability I shortened the right hand arm in order to put in the SESAM. The main idea behind this was to reduce the footprint of the cavity, it resulted in being unable to get the smallest waist at the SESAM. The reason this is necessary is due to the amount of intensity needed to saturate the semiconductor on the surface. This SESAM has a saturation intensity of 90 μJ/cm^2. I used the basic assumptions of a cavity length of 90 cm, 350-mW power inside the cavity, and a diameter of 100 μm to determine the energy of a pulse per area would be 26.9 μJ/cm^2. Obviously, this beam radius is too large. Due to spacing issues it became obvious that the arm should have kept at its original length, put in a concave mirror in place of the SESAM, and put the SESAM at the focal point a little offset from the input beam as shown in Figure 4.4. If the beam radius had been reduced to 54 μm, it would have saturated the SESAM and straight mode locking should have been achieved.

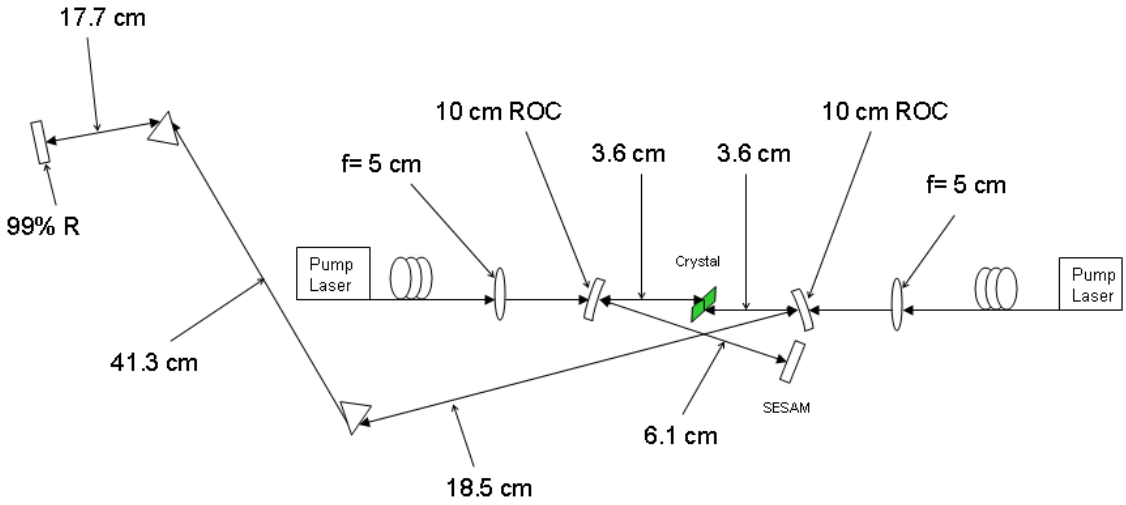

Figure 4.3: Final design of the 3 mm Yb:KGW system with the GVD correction prisms with dimensions.

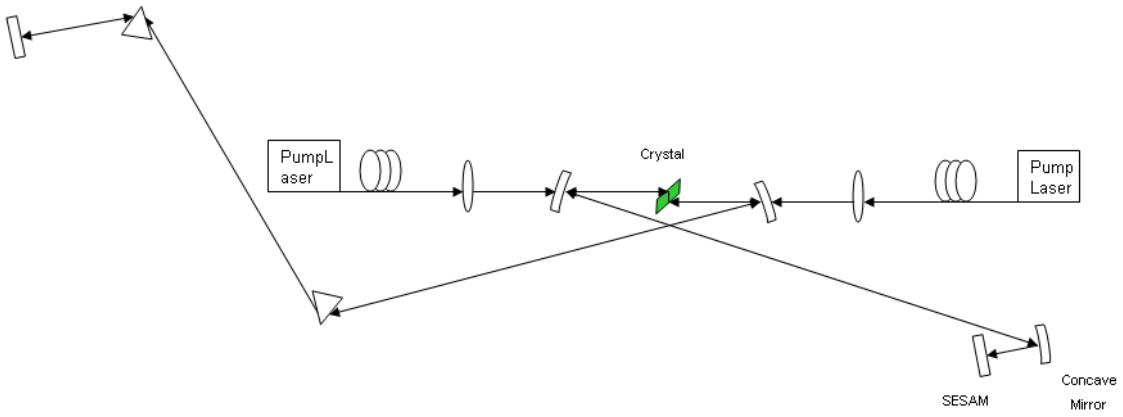

Figure 4.4: Design layout that should have been used in order to ensure mode locking with the SESAM.

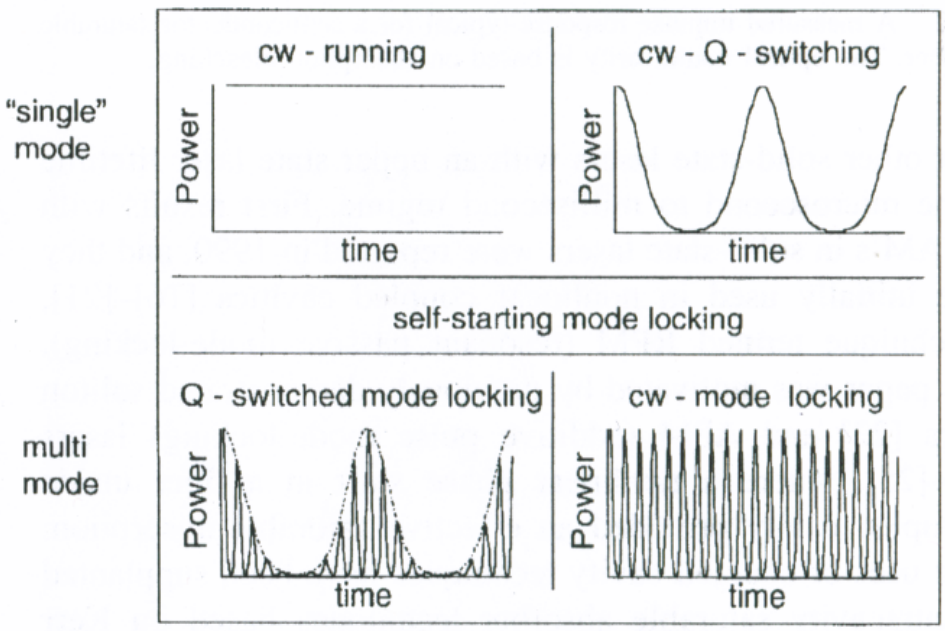

Figure 4.5: Example of operating modes of a laser. [15]

While this mistake was serious, laser pulsing was achieved. The type of pulsing that noted was Q-switched mode locking as illustrated in the lower left-hand corner of Figure 4.5. [15] What is also important, is that as one of the concave mirrors was moving, the system would mode lock. This is what also showed that the SESAM was not saturating. No good plots of this information were taken since this was a transient effect a digital oscilloscope was being used. This validated the design and the work done on this research. While not sustained these were the results being looked for. Movement to the 1-mm crystal was made after working with the Yb:vanadate, but due to time considerations little, was accomplished.

4.1.3 Yb:vanadate. The results from the Yb:vanadate system were disappointing as the system was unable to lase. This system is based off of the design and dimensions of the 3 mm Yb:KGW crystal since it was a proven design. After getting the system setup and fully aligned, there was no progress on increasing power. After working on this for an extended time, the manufacturer was contacted and it was determined that the crystal was cut incorrectly. No matter what orientation the

crystal is in, it will not lase. As soon as a new crystal is delivered, the system will be reset and retested.

4.2 Measurement Equipment

Important aspects of this study were the techniques for measuring pulsing while it is occurring and the several pieces of equipment used to accomplish this. The first are second harmonic generation (SHG) interferometric correlation devices. [14, p.466] These use the intensity of a pulse in order to create a measurement of the pulse based off of a reference signal. The second piece of equipment is a real-time spectral analyzer (RF spectrum analyzer) which does a fast Fourier transform (FFT) to look at the signal in the frequency domain.

4.2.1 Autocorrelator. There are several different types of autocorrelators. Most common, and the one used for these experiments, is an intensity autocorrelator. The basis of this analysis is that the system uses a reference pulse to base its analysis of the incoming pulse. The temporal profile of a pulse can be determined using Equation (4.1), where $I_r(t-\tau)$ is the reference pulse and $I_s(t)$ is the intensity profile of the incoming pulse. [14, p.458]

$$A_c(\tau) = \int_{-\infty}^{\infty} I_s(t) I_r(t-\tau) dt \tag{4.1}$$

Most often for pulses shorter than 1 ps, the reference pulse is the pulse itself. [14, p.459] This is accomplished normally by a Michelson interferometer such as that shown in Figure 4.6. [3] The pulse is split in two by the beam splitter and then reflected to a detector by separate mirrors. One of those separate mirrors is mounted on an adjustable mount, allowing for repositioning. By moving this mirror, the pulse can be compared to itself through the SHG crystal. An example is shown in Figure 4.7 where the reference pulse is the one denoted with the vertical dashed line. This reference pulse is the portion separated and reflected on the non-moving mirror.

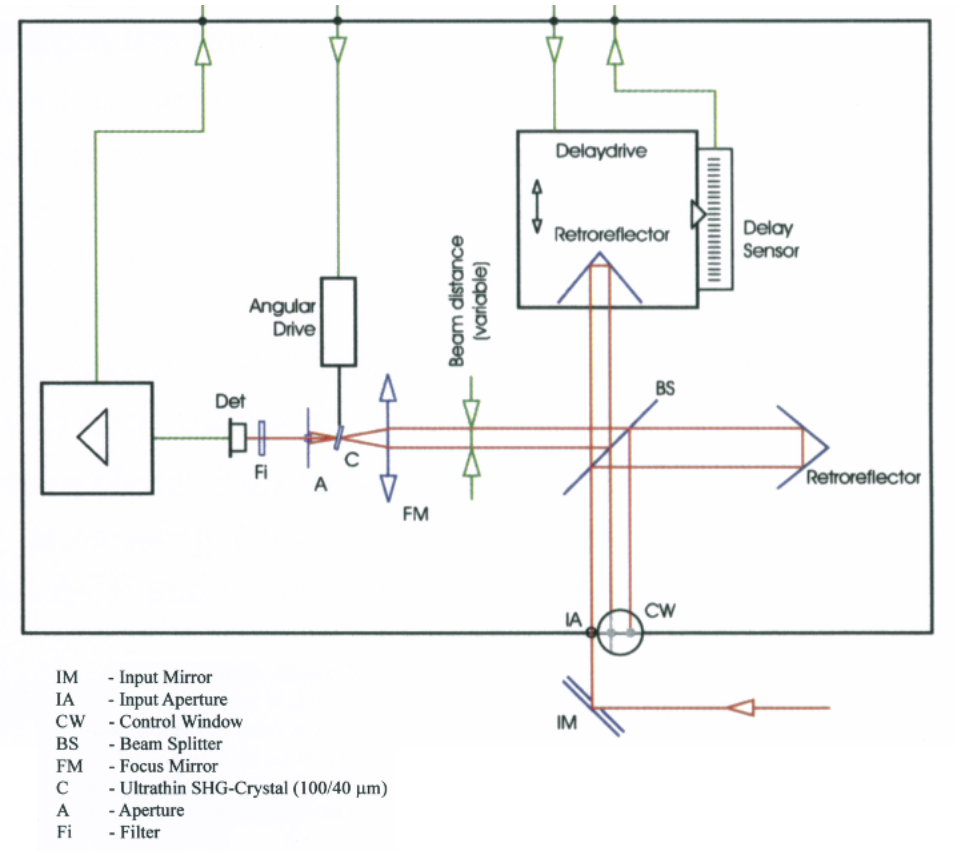

Figure 4.6: Setup of a Michelson interferometer in an autocorrelator. [3]

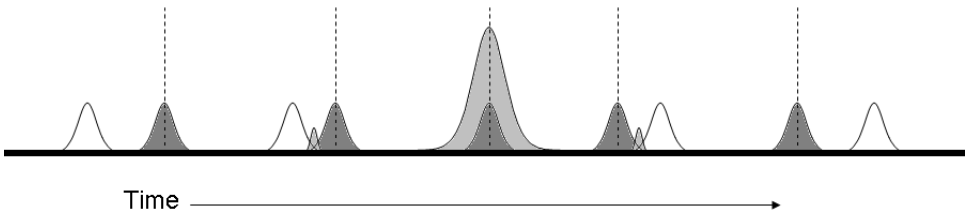

Figure 4.7: Example of pulse comparison in an intensity autocorrelator. The pulse is multiplied by the reference pulse shown with the dashed line which can be measured.

Table 4.1: General properties of Gaussian and sech^2 pulse shapes. [14, p.477]

$\mathcal{E}^2(t)$	$\lvert\mathcal{E}(\Omega)\rvert^2$	$\tau_p\Delta\nu$	$A_c(\tau)$	τ_{ac}/τ_p
e^{-t^2}	$e^{-\Omega^2}$	0.441	$e^{-t^2/2}$	1.414
$\text{sech}^2(t)$	$\text{sech}^2\left(\frac{\pi\Omega}{2}\right)$	0.315	$\frac{3\tau(ch\tau-sh\tau)}{sh^3\tau}$	1.543

The intensity autocorrelator has two major disadvantages. The first is due to the multiplication of the pulse and its reference as shown in Equation (4.1). As a result, there is a distortion at the edges causing a broadening of the autocorrelation in the time domain as presented. The solution for this is to assume a pulse shape and apply those properties to the autocorrelation. Table 4.2.1 gives the properties of Gaussian and sech^2 pulse shapes, which are most often used. [14, p.477] The second disadvantage is that there is no information on the frequency or modulation of the phase of the pulse. The solution for this is to use an instrument that uses interferometric correlation. This uses higher order interferometry patterns which can show qualitative properties of the phase and chirp. [14, p.462]

4.2.2 RF Spectrum Analyzer. An RF spectrum analyzer essentially takes the data given and provides the ability to view data in several different domains. For this experiment this was used to transfer the time domain information to the frequency domain. The result is a comb effect showing the Fourier transform of the time signal. An example of this type of data is shown in Figure 4.8. [14, p.284] The advantage that this has is the ease of ability to look at the pulse rate and portions of the phase. This can then be applied to the information from the autocorrelator to give the characterizations of the pulses.

4.3 Ti:sapphire

As noted before, the Ti:sapphire laser is the bedrock of solid state ultrashort pulsed laser systems. Pulses as short as 5.5 fs have been accomplished but most commercial systems, like the Coherent MIRA™ system being used here, have limits

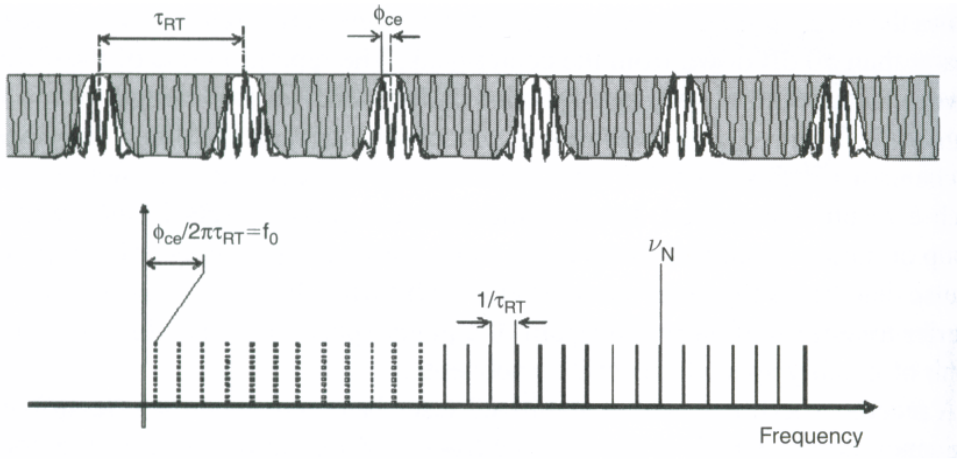

Figure 4.8: Example of the Fourier transform from time to frequency producing a comb pattern in the frequency domain. [14, p.284]

around 10 fs. [29] The purpose of this information initally was to compare to the results from the small cavity lasers. Since these lasers were unsuccessful at mode locking, actual pulse analysis defaulted to this comparison data. As a result no attempt was made to adjust the pulses for width or rate for full range analysis.

The first part of the analysis was temporal. Width of the pulses was determined by using an intensity autocorrelator as noted above. The resulting pulse view is shown in Figure 4.9. Time reference is in terms of the delay produced by the moving mirror. Measurements taken over a period of hours resulted in an average uncorrected width of 182.5±6.5 fs. Assuming a sech^2 pulse shape, the correction is 0.648 times the pulse width, resulting in a pulse width of 118.3±4.1 fs. Pulses from this laser are very consistent and that is expected from a commercial system. This can be seen by the pulse train measured shown in Figure 4.10. Overall, this is a useful pulse width and has been used to create terahertz radiation in the AFIT laboratory.

The more interesting and useful measurements were accomplished with the RF spectrum analyzer looking at the frequency domain. The reason for this is that this gives information about the cavity itself. The general frequency comb is shown in Figure 4.11 which almost directly relates to Figure 4.8. What is important is the difference between the different frequencies of the comb. A focused example is shown

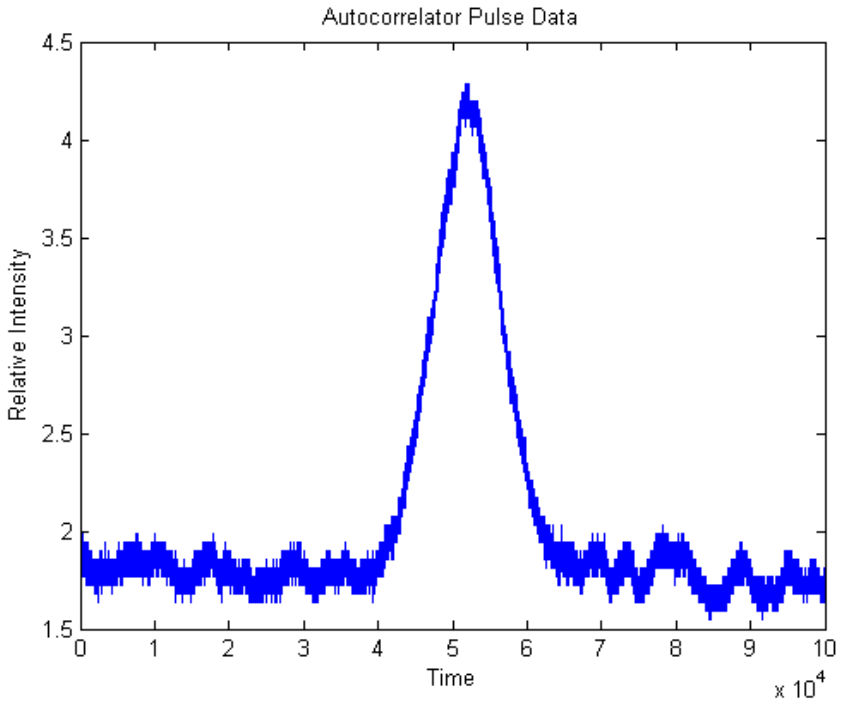

Figure 4.9: Autocorellator data from a commercial Ti:sapphire laser for a single pulse.

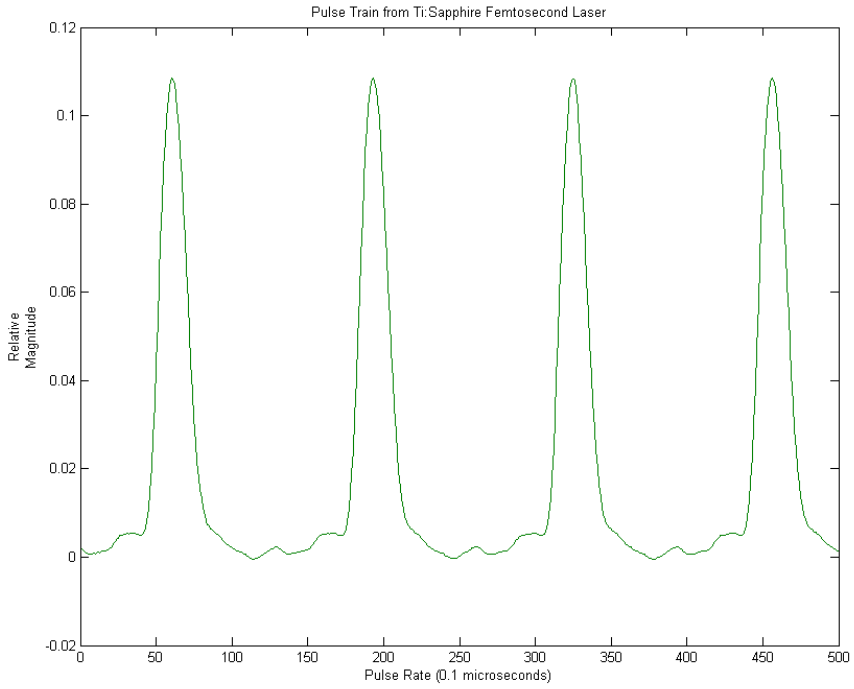

Figure 4.10: Measured pulse train from a commercial Ti:sapphire laser.

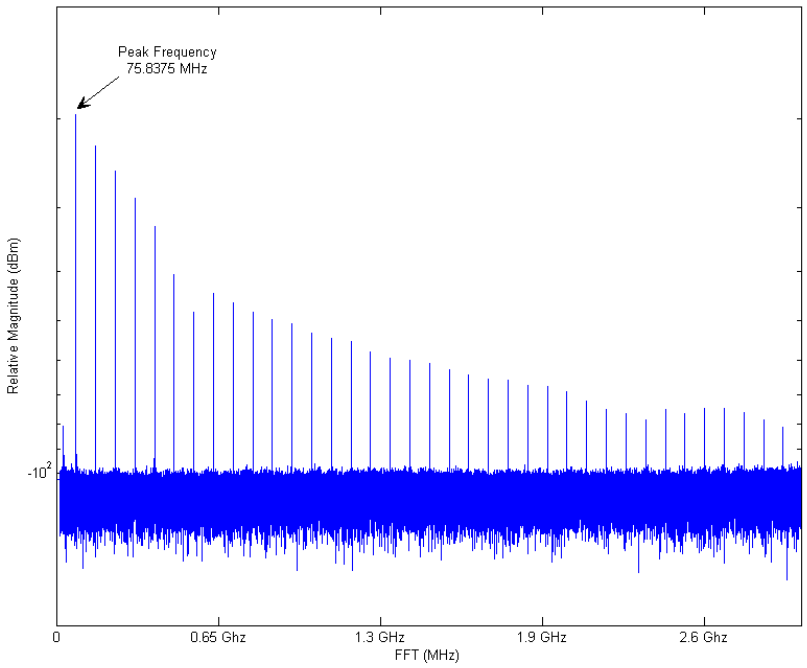

Figure 4.11: Plot of the frequency comb of the pulses from a commercial Ti:sapphire laser.

in Figure 4.12 showing a difference of 75.8 MHz. This separation gives a round trip time for a pulse to travel in the cavity using Equation 4.2.

$$\nu = \frac{c}{2L} \tag{4.2}$$

In this case it gives us a cavity length of 1.97 m. This is much longer than the small cavities that were designed and help emphasize that point that current lasers have a large footprint.

Another piece of information both domains give is an estimate in the number of modes in the cavity. This is accomplished via Equation 4.3 where τ_p is the pulse width and τ_{RT} is the round trip time. [14, p.279]

$$M \approx \frac{1}{\tau_p \tau_{RT}} \tag{4.3}$$

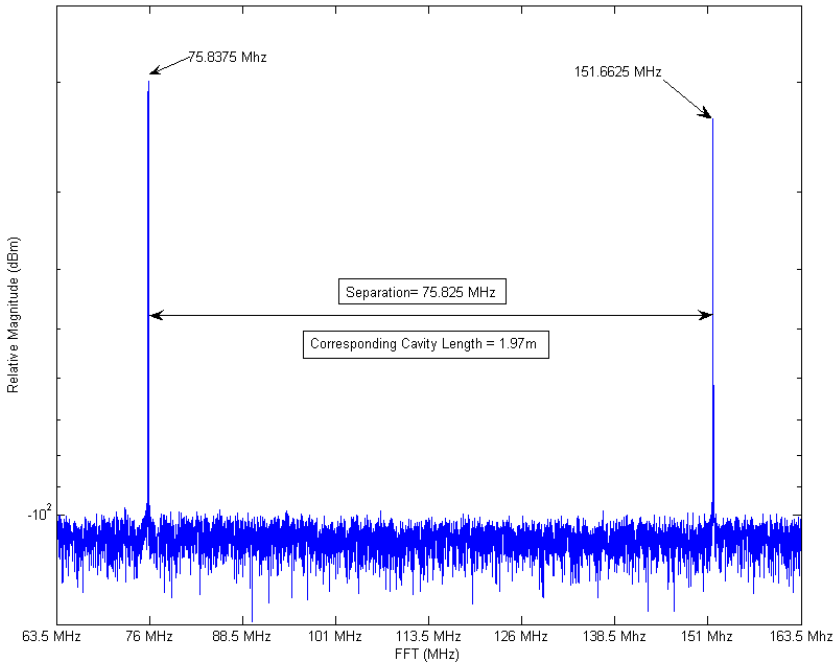

Figure 4.12: Plot of two of the frequencies of the comb showing separation and the resulting calculated cavity length.

In this cavity, this estimate comes out to be 1.11×10^5 modes. This is a large number of modes but provides a good example of how many modes in a cavity need to be locked to allow good pulsing. This comes with a little caveat in that this estimate assumes equally spaced modes.

Overall, this work on small-cavity fs pulsed lasers provides a great deal of data and experience for comparative purposes with other small cavity systems. This is provided as a short cut for future researchers.

V. Conclusions

The limiter overall was time. With each obstacle overcome, overall time was lost causing problems with the overall accomplishments. This does not mean, however, that it was not important and purposeful. The problems that occurred were due to physical components of the system and not the designs since the designs worked at a basic level. Pulsing was occurring and that is the proof of usefulness. Behind that, each system needs to be looked at for proper consideration.

5.1 Cr:LiSAF

The basis behind this system has a better track record as far as previous research than the Yb systems. This design was the more ambitious of the two used because there are newly available components, specifically chirped concave mirrors, that we wanted to use to push the boundaries providing a precedent. Successful pulsing with a completely chirped cavity is the next logical step for a Cr:LiSAF design. The system was well designed and thought out, and thus, provides an excellent basis for the next researcher to use. While the mirrors for this system keep the system from being overall successful, these components are easily replaced, and when they are the system should complete the desired goals laid out.

5.2 Yb Based Systems

These systems were the most successful in both design and components. The biggest success was the 3-mm Yb:KGW system which showed pulsing via Q-switching but was unable to mode lock due to inadequate saturation of the SESAM. This gave credit to the design work and proved that the only limiter on that system was pump power. The time working on the Yb:vanadate system was not wasted even though the crystal had been cut incorrectly. The design of the system and its relation to work with the 3-mm Yb:KGW system provides the most immediate possibilities once the manufacturer provides the correct crystal. While that is not documented here, it should be completed shortly. As noted, time was the enemy for work with the 1

mm Yb:KGW crystal. While there was suspicion that there might be a problem with the doping percentage of the Yb, further adjustment of the system should show that success, even if inefficient, is possible. This system is the baseline required for AFIT and can be used as a model for AFRL/SN.

5.3 Overall Conclusions

The only goal that was unsuccessful, even though it is major, was getting one of these systems mode locked. The other goals of understanding, component use, and providing a baseline system were completed. It has been shown that it was economically feasible to create a pulsed system with off-the-shelf components. These off-the-shelf components included two of the three crystals that were used since only the Yb:vanadate is a recent advancement in crystal design. While these systems are not yet portable, this should be corrected within the next six months with the Cr:LiSAF system. The only support needed is a current source, be it an electrical outlet or batteries. That is proof enough that there is a future of these systems anywhere they are needed be it on the battlefield or in the home.

This work is important because the systems were accurately designed and and then built two completely different laser systems for different purposes but with the necessary undercurrent of "extreme light." Each system has its advantages and detractors, but the usefulness of both systems cannot be denied. The significance of this research to AFIT and AFRL/SN is widespread and must be continued in the short term to create a cadre of experienced researchers. Ultrashort and ultrafast systems are a major path in the future of optics. The research here provides a couple of footprints down that path. It is now up to other researchers using their imaginations to clear that path of obstacles and make purposeful use of ultrashort and ultrafast small cavity pulsed lasers.

Appendix A. Common Solid State Crystals and Glasses

Table A.1: Properties of several laser materials involved in the development of femtosecond lasers. [35]

Materials	Emission band width	Minimum theoretical duration	Central emission peak	Absorption (usual pumping)	Emission cross section (10^{-20} cm^2)	Fluorescence lifetime	Thermal conductivity (undoped) W/m/K
Ti^{3+}:Sapphire	180 nm	3.6 fs	790 nm	500 nm	41	3.2 μs	34
Cr^{4+}:Mg_2SiO_4	150 nm	11 fs	1250 nm	1064 nm	20	3 μs	5
Cr^{4+}:$Y_3Al_5O_{12}$(YAG)	200 nm	11 fs	1450 nm	1064 nm	20	4 μs	11
Nd:glass	22 nm	53 fs	1053 nm	808 nm	4	360 μs	0.8
Cr^{3+}:$LiSrAlF_6$(LiSAF)	100 nm	7.6 fs	850 nm	670 nm	4.8	67 μs	3.1
Cr^{3+}:$LiCaAlF_6$(LiCAF)	100 nm	6 fs	760 nm	670 nm	1.3	175 μs	5
Yb^{3+}:$Y_3Al_5O_{12}$(YAG)	9 nm	124 fs	1031 nm	942 nm	2.1	951 μs	11
Yb^{3+}:glass	35 nm	31 fs	1020 nm	975 nm	0.05	1300 μs	0.8
Yb^{3+}:Y_2O_3	15 nm	75 fs	1031 nm	977 nm	0.9	850 μs	13.6
Yb^{3+}:Sc_2O_3	12 nm	95 fs	1042 nm	975 nm	1.3	800 μs	16.5
Yb^{3+}:$Ca_4GdB_3O_{10}$(GdCOB)	44 nm	26 fs	1044 nm	976 nm	0.35	2600 μs	2.1
Yb^{3+}:$Sr_3Y(BO_3)_3$(BOYS)	60 nm	18 fs	1025 nm	975 nm	0.3	1100 μs	1.8
Yb^{3+}:$KGd(WO_4)_2$(KGW)	25 nm	44 fs	1023 nm	981 nm	2.8	600 μs	3.3
Yb^{3+}:$KY(WO_4)_2$(KYW)	24 nm	46 fs	1025 nm	981 nm	3	600 μs	3.3
Yb^{3+}:$SrY_4(SiO_4)_3O$ (SYS)	73 nm	16 fs	1040 nm	979 nm	0.44	820 μs	2
Cr^{2+}:ZnSe	600 nm	11 fs	2500 nm	1600 nm	90	7 μs	16
Cr^{2+}:ZnS	500 nm	12 fs	2350 nm	1600 nm	140	4.5 μs	27.2
Ce^{3+}:$LiSrAlF_6$(LiSAF)	14 nm	6.2 fs	288 nm	270 nm	900	0.025 μs	3.1

Appendix B. Component Specifics

Table B.1: Equipment list for the Cr:LiSAF system.

#	Description	Manufacturer	Model #
2	5.5% doped Cr:LiSAF crystals	VLOC	973707
4	Diode Lasers 658nm/100mW	Blue Sky Research	VPSL0658-100X5-G
2	SESAM A=4% λ= 850nm	BATOP Optoelectronics	SAM 262-111a.2
2	50mm ROC concave mirror AR for 658 nm	CVI Laser	TNMS-800-900-0537-0.05cc-AR658
2	100mm ROC concave mirror AR for 658 nm	CVI Laser	TNM2-800-900-0537-0.10cc-AR658
1	Output coupler 99% reflectance	CVI Laser	PR1-850-99-0525
1	High reflectance output coupler	CVI Laser	TNM2-800-900
1	Focusing lens f=50.0mm AR coated for 658nm	Thorlabs Inc.	LB1471-B
1	Focusing lens f=60.0mm AR coated for 658nm	Thorlabs Inc.	LB1596-B
4	Laser diode mounting kits	Optima Precision Inc.	LDM-1100
4	Laser diode lens kits	Optima Precision Inc.	ADP-9056
4	Constant power laser drivers	Thorlabs, Inc.	LD1100
1	Precision current driver	ILX Lightwave	3207-B
1	Precision current driver	ILX Lightwave	LDC-3722
2	XYZ mounts	New Focus, Inc.	9066
3	X mounts	New Focus, Inc.	9042

Table B.2: Equipment list for the Yb systems.

#	Description	Manufacturer	Model #
1	5x5x3mm 5% doped Yb:KGW crystal	EKSPLA	custom
1	10x4x1mm 5% doped Yb:KGW crystal	EKSPLA	custom
1	10x10x2mm 2.6% doped Yb:vanadate crystal	EKSPLA	custom
2	SESAM A=1% λ=1064nm	Del Mar Photonics	SAM 342-IVa.30
2	Fiber diode lasers 976nm/450mW	JDS Uniphase	29-8000-500
2	Butterfly laser diode mounts	Thorlabs, Inc.	LM1452
2	Fiber mount with fiber holder	Newport Corp.	F-915T
1	Precision current driver	ILX Lightwave	3545
1	Thermoelectric temperature controller	Thorlabs, Inc.	TED200
1	Precision current driver	ILX Lightwave	LDC-3722
3	40mm ROC concave mirror AR for 981 nm	Rocky Mountain Inst. Co.	custom
3	50mm ROC concave mirror AR for 981 nm	Rocky Mountain Inst. Co.	custom
3	75mm ROC concave mirror AR for 981 nm	Rocky Mountain Inst. Co.	custom
1	Output coupler 99% reflectance	CVI Laser	PR1-1047-99-0512
1	High reflectance output coupler	CVI Laser	TNM2-800-900
1	Focusing lens f=50.0mm AR coated for 981nm	Thorlabs Inc.	LB1471-B
1	Focusing lens f=60.0mm AR coated for 981nm	Thorlabs Inc.	LB1596-B
1	Focusing lens f=75.0mm AR coated for 981nm	Thorlabs Inc.	LB1901-B
1	XYZ mounts	New Focus, Inc.	9066
1	X mounts	New Focus, Inc.	9062
3	X mounts	New Focus, Inc.	9044

Bibliography

1. Agate, B. "Compact Femtosecond Lasers". *Optics Communications*, 205:207–213, 2002.

2. Agate, B., B. Stormont, A. J. Kemp, C. T. A. Brown, U. Keller, and W. Sibbett. "Simplified cavity designs for efficient and compact femtosecond Cr:LiSAF lasers". *Optics Communications*, 205:207–213, April 2002.

3. Angewandte Physik & Elektronik (APE). *Pulse Check Autocorrelator Manual*. Available at http://www.ape-berlin.de.

4. BATOP Optoelectronics, Inc. "SAM Data Sheet SAM-1064-1-x, λ=1064 nm". Available at http://www.batop.de/products/saturable_absorber/SAM/pdf_sheets/1064nm/sam-1064-1.pdf.

5. Brown, C. T. A., M. A. Cataluna, A. A. Lagatsky, E. U. Rafailov, M. B. Agate, C. G. Leburn, and W. Sibbett. "Compact laser-diode-based femtosecond sources". *New Journal of Physics*, 175(6):1–19, November 2004.

6. Components, CVI Optical and Assemblies.

7. Components, CVI Optical and Assemblies. "Ultrfast Components: Technical Notes". Available at http://www.cvilaser.com/Common/PDFs/Ultrafast_mirrors_discussion.pdf.

8. Druon, F., S. Chénais, F. Balembois, P. Georges, R. Gaumé, P. H. Haumesser, G. Aka, B. Viana, and D. Vivien. "Diode-pumped femtosecond oscillators based on new ytterbium doped borates crystals". R. Lessard, G. Lampropoulos, and G. Schinn (editors), *Applications of Photonic Technology 5*, volume 4833, 906–914. Proceedings of SPIE, 2004.

9. EKSPLA Ltd., Photonics Division.

10. GmbH, RP Photonics Consulting. "Titanium-sapphire lasers". Encyclopedia of Laser Physics and Technology, July 2006. Available at http://www.rp-photonics.com/titanium_sapphire_lasers.html.

11. Hecht, Eugene. *Optics*. Addison Wesley, San Francisco, CA, fourth edition, 2002.

12. Hohmuth, R., G. Paunescu, J. Hein, C. H. Lange, and W. Richter. "Saturable Absorber Mirrors for Passive Mode-locking". Poster summary.

13. International Atomic Energy Agency. *Ultra-intense Laser Plasma Interactions Related To Fast Ignitor In Inertial Confinement Fusion*, 17, October 1998.

14. Jean-Claude Diels, Wolfgang Rudolph. *Ultrashort Laser Pulse Phenomena: Fundamentals, Techniques, and Applications on a Femtosecond Time Scale*. Academic Press, Burlington, MA, second edition, 2006.

15. Keller, U., K. Weingarten, F. Kärtner, D. Kopf, B. Braun, I. Jung, R. Fluck, C. Hönninger, N. Matuschek, and J. Aus der Au. "Semiconductor Saturable Absorber Mirrors (SESAM's) for Femtosecond to Nanosecond Pulse Generation in Solid-State Lasers". *Journal of Selected Topics in Quantum Electronics*, volume 2, 435–451. Institute of Electrical and Electronics Engineers (IEEE), 1996.

16. Kemp, A. J., B. Stormont, B. Agate, C. T. A. Brown, U. Keller, and W. Sibbett. "Gigahertz repetition-rate from directly diode-pumped femtosecond Cr:LiSAF laser". *Electronics Letters*, 37(24), November 2001.

17. Kisel, V. E., A. E. Troshin, V. G. Shcherbitsky, N. V. Kuleshov, V. N. Matrosov, T. A. Matrosava, M. I. Kupchenko, F. Brunner, R. Paschotta, F. Morier-Genoud, and U. Keller. "Femtosecond pulse generation with a diode-pumped Yb^{3+}:YVO_4 laser". *Opt. Soc. of America*, 30(10), May 2005.

18. Kisel, V. E., A. E. Troshin, N. A. Tolstik, V. G. Shcherbitsky, N. V. Kuleshov, V. N. Matrosov, T. A. Matrosava, and M. I. Kupchenko. "Spectroscopy and continuous-wave diode-pumped laser action of Yb^{3+}:YVO_4". *Optics Letters*, 29(21), November 2004.

19. Kuze, S., D. du Boulay, N. Ishizawa, N. Kodama, M. Yamaga, and B. Henderson. "Structures of $LiCaAlF_6$ and $LiSrAlF_6$ at 120 and 300K by synchroton X-ray single-crystal diffraction". *Journal of Solid State Chemistry*, 177:3505–3513, April 2004.

20. Laboratory., Jet Propulsion. "Global Positioning System (GPS)". Mission and Spacecraft Library: Program Statement. Available at http://samadhi.jpl.nasa.gov/msl/Programs/gps.html.

21. Laboratory, Lawrence Livermore National. "The Amazing Power of the Petawatt". Program Information, March 2000. Available at http://www.llnl.gov/str/MPerry.html.

22. Lagatsky, A. A., A. R. Sarmani, C. T. A. Brown, W. Sibbett, V. E. Kisel, A. G. Selivanov, I. A. Denisov, A. E. Troshin, K. V. Yumashev, N. V. Kuleshov, V. N. Matrosov, T. A. Matrosova, and M. I. Kupchenko. "Yb^{3+}-doped YVO_4 crystal for efficient Kerr-lens mode locking in solid-state lasers". *Optics Letters*, 31(23):3234–3236, December 2005.

23. Major, A., V. Barzda, P. Piunno, S. Musikhin, and U. Krull. "Development of femtosecond Yb:KGW laser for applications in optical DNA sensor technology". W. Chan, K. Yu, U. Krull, R. Hornsey, B. Wilson, and R. Weersink (editors), *Photonic Applications in Biosenseing and Imaging*, volume 5969. Proceedings of SPIE, 2005.

24. Payne, S., W. Krupke, L. Smith, W. Kway, L. D. DeLoach, and J. Tassano. "752 nm Wing-Pumped Cr:LiSAF Laser". *IEEE Journal of Quantum Electronics*, 28(4):1188–1196, April 1992.

25. Payne, S. A., L. K. Smith, R. J. Beach, B. H. T. Chai, J. H. Tassano, L. D. DeLoach, W. L. Kway, R. W. Solarz, and W. F. Krupke. "Properties of Cr:$LiSrAlF_6$ crystals for laser operation". *Applied Optics*, 33(24):5526–5536, August 1994.

26. Pujol, M.C., M. Rico, C. Zaldo, R. Solé, V. Nikolov, X. Solans, M. Aguiló, and F. Díaz. "Crystalline structure and optical spectroscopy of Er^{3+}-doped $KGd(WO_4)_2$". *Applied Physics B*, 68:187–197, 1999.

27. Rohwetter, P., K. Stelmaszczyk, L. Wöste, R. Ackerman, G. Méjean, E. Salmon, J. Kasparian, J. Yu, and J.P. Wolf. "Filament-induced remote surface ablation for long range laser-induced breakdown spectroscopy operation". *Spectrochinica Acta Part B*, March 2005.

28. Roquemore, Mel and Jim Gord. ""Extreme Light" Science and Applications of Ultrafast, Ultraintense Lasers". AFIT Seminar, October 2006.

29. RP Photonics, Inc. "Titanium-sapphire lasers". Encyclopedia of Laser Physics and Technology, January 2007. Available at http://www.rp-photonics.com/titanium_sapphire_lasers.html.

30. Saleh, Bahaa E. A. and Malvin Carl Teich. *Fundamentals of Photonics*. John Wiley & Sons, Inc., New York, NY, first edition, 1991.

31. Siegman, Anthony E. *Lasers*. University Science Books, Sausalito, CA, first edition, 1986.

32. Stelmaszczyk, K., P. Rohwetter, G. Méjean, J. Yu, E. Salmon, J. Kasparian, R. Ackerman, J.P. Wolf, and L. Wöste. "Long-distance remote laser-induced breakdown spectroscopy using filamentation in air". *Applied Physics Letters*, 85(18):3977–3979, November 2004.

33. Szipocs, R. and A. Kohazi-Kis. "Theory and design of chirped dielectric laser mirros". *Applied Physics B*, 65:115–135, 1997.

34. Verdeyen, Joseph T. *Laser Electronics*. Prentice Hall, Upper Saddle River, NJ, third edition, 1995.

35. Viana, B., J. Petit, R. Gaumé, D. Vivien, F. Druon, F. Balembois, and P. Georges. "Yb^{3+} doped laser materials for high power or ultrafast applications". A. Sennaroglu, J. Fujimoto, and C. Pollock (editors), *Solid State Lasers and Amplifiers*, volume 5460, 145–156. Proceedings of SPIE, Bellingham, WA, 2004.

36. VLOC. "Cr-doped Colquiriite (Cr:LiSAF, Cr:LiSGaF & Cr:LiCAF) Laser Crystals". Product Information Guide, October 2006. Available at http://www.vloc.com/PDFs/OtherGainMaterials/Cr_LiSAF_LiSGaF_LiCAF.pdf.

37. Wikipedia Foundation, Inc. "Atomic clock". The Free Encyclopedia, December 2006. Available at http://en.wikipedia.org/wiki/Atomic_clocks.

38. Wikipedia Foundation, Inc. "Borosilicate glass". The Free Encyclopedia, December 2006. Available at http://en.wikipedia.org/wiki/Borosilicate_glass.

39. Wikipedia Foundation, Inc. "Kerr-lens modelocking". The Free Encyclopedia, November 2006. Available at http://en.wikipedia.org/wiki/Kerr-lens_modelocking.

40. Wikipedia Foundation, Inc. "Ring laser gyroscope". The Free Encyclopedia, October 2006. Available at http://en.wikipedia.org/wiki/Ring_laser_gyroscope.

41. Wikipedia Foundation, Inc. "Sagnac effect". The Free Encyclopedia, November 2006. Available at http://en.wikipedia.org/wiki/Sagnac_effect.

42. Wikipedia Foundation, Inc. "Sellmeier Equation". The Free Encyclopedia, September 2006. Available at http://en.wikipedia.org/wiki/Sellmeier_Equation.

43. Wikipedia Foundation, Inc. "Ti-sapphire laser". The Free Encyclopedia, November 2006. Available at http://en.wikipedia.org/wiki/Ti-sapphire_laser.

REPORT DOCUMENTATION PAGE

Form Approved
OMB No. 0704-0188

PLEASE DO NOT RETURN YOUR FORM TO THE ABOVE ORGANIZATION.

1. REPORT DATE *(DD-MM-YYYY)*	2. REPORT TYPE	3. DATES COVERED *(From - To)*
22-03-2007	Master's Thesis	Sep 2006-Mar 2007

4. TITLE AND SUBTITLE
Portable Diode Pumped Femtosecond Lasers

5a. CONTRACT NUMBER

5b. GRANT NUMBER

5c. PROGRAM ELEMENT NUMBER

6. AUTHOR(S)
Jones, David A., Captain, USAF

5d. PROJECT NUMBER

5e. TASK NUMBER

5f. WORK UNIT NUMBER

7. PERFORMING ORGANIZATION NAME(S) AND ADDRESS(ES)
Air Force Institute of Technology
Graduate School of Engineering Management (AFIT/EN)
2950 Hobson Way, WPAFB OH 45433-7765

8. PERFORMING ORGANIZATION REPORT NUMBER
AFIT/GAP/ENP/07-04

9. SPONSORING/MONITORING AGENCY NAME(S) AND ADDRESS(ES)
N/A

10. SPONSOR/MONITOR'S ACRONYM(S)

11. SPONSOR/MONITOR'S REPORT NUMBER(S)

12. DISTRIBUTION/AVAILABILITY STATEMENT
APPROVED FOR PUBLIC RELEASE; DISTRIBUTION UNLIMITED

13. SUPPLEMENTARY NOTES

14. ABSTRACT

This thesis discusses the work to make ultrashort pulsed lasers smaller and more economical. While sharing many of the basic properties of normal beam optics there are some specific properties in both creating and exploiting those pulses that must be understood. The discussion will focus on mode locking as the primary way of producing ultrashort pulses. Particular attention will be paid to intracavity group velocity dispersion and how to correct it inside the cavity. The discussion then turns to the basis of our work including initial cavity design and component selection with focus on the specific crystals used in the solid state laser. The rest of the experiment setup is based on evolution of the designs in order to get the systems lasing and then mode locked. Results from the work on the small cavity systems are compared to data taken from a commercial titanium-sapphire laser with emphasis on current measurement techniques. Overall conclusions include the impact of both equipment and the crystals used in the solid state cavity to generate ultrashort pulses. While not fully successful, the groundwork has been laid for future research.

15. SUBJECT TERMS
Lasers, Optics, Mode Locking, Pulsed, Solid State, Cr:LiSAF, Yb:KGW

16. SECURITY CLASSIFICATION OF:			17. LIMITATION OF ABSTRACT	18. NUMBER OF PAGES	19a. NAME OF RESPONSIBLE PERSON
a. REPORT	b. ABSTRACT	c. THIS PAGE			Matthew J. Bohn, Lt Col, USAF
U	U	U	UU	105	19b. TELEPHONE NUMBER *(Include area code)* 937-255-3636

Reset

Standard Form 298 (Rev. 8/98)
Prescribed by ANSI Std. Z39.18

INSTRUCTIONS FOR COMPLETING SF 298

1. REPORT DATE. Full publication date, including day, month, if available. Must cite at least the year and be Year 2000 compliant, e.g. 30-06-1998; xx-06-1998; xx-xx-1998.

2. REPORT TYPE. State the type of report, such as final, technical, interim, memorandum, master's thesis, progress, quarterly, research, special, group study, etc.

3. DATES COVERED. Indicate the time during which the work was performed and the report was written, e.g., Jun 1997 - Jun 1998; 1-10 Jun 1996; May - Nov 1998; Nov 1998.

4. TITLE. Enter title and subtitle with volume number and part number, if applicable. On classified documents, enter the title classification in parentheses.

5a. CONTRACT NUMBER. Enter all contract numbers as they appear in the report, e.g. F33615-86-C-5169.

5b. GRANT NUMBER. Enter all grant numbers as they appear in the report, e.g. AFOSR-82-1234.

5c. PROGRAM ELEMENT NUMBER. Enter all program element numbers as they appear in the report, e.g. 61101A.

5d. PROJECT NUMBER. Enter all project numbers as they appear in the report, e.g. 1F665702D1257; ILIR.

5e. TASK NUMBER. Enter all task numbers as they appear in the report, e.g. 05; RF0330201; T4112.

5f. WORK UNIT NUMBER. Enter all work unit numbers as they appear in the report, e.g. 001; AFAPL30480105.

6. AUTHOR(S). Enter name(s) of person(s) responsible for writing the report, performing the research, or credited with the content of the report. The form of entry is the last name, first name, middle initial, and additional qualifiers separated by commas, e.g. Smith, Richard, J, Jr.

7. PERFORMING ORGANIZATION NAME(S) AND ADDRESS(ES). Self-explanatory.

8. PERFORMING ORGANIZATION REPORT NUMBER. Enter all unique alphanumeric report numbers assigned by the performing organization, e.g. BRL-1234; AFWL-TR-85-4017-Vol-21-PT-2.

9. SPONSORING/MONITORING AGENCY NAME(S) AND ADDRESS(ES). Enter the name and address of the organization(s) financially responsible for and monitoring the work.

10. SPONSOR/MONITOR'S ACRONYM(S). Enter, if available, e.g. BRL, ARDEC, NADC.

11. SPONSOR/MONITOR'S REPORT NUMBER(S). Enter report number as assigned by the sponsoring/ monitoring agency, if available, e.g. BRL-TR-829; -215.

12. DISTRIBUTION/AVAILABILITY STATEMENT. Use agency-mandated availability statements to indicate the public availability or distribution limitations of the report. If additional limitations/ restrictions or special markings are indicated, follow agency authorization procedures, e.g. RD/FRD, PROPIN, ITAR, etc. Include copyright information.

13. SUPPLEMENTARY NOTES. Enter information not included elsewhere such as: prepared in cooperation with; translation of; report supersedes; old edition number, etc.

14. ABSTRACT. A brief (approximately 200 words) factual summary of the most significant information.

15. SUBJECT TERMS. Key words or phrases identifying major concepts in the report.

16. SECURITY CLASSIFICATION. Enter security classification in accordance with security classification regulations, e.g. U, C, S, etc. If this form contains classified information, stamp classification level on the top and bottom of this page.

17. LIMITATION OF ABSTRACT. This block must be completed to assign a distribution limitation to the abstract. Enter UU (Unclassified Unlimited) or SAR (Same as Report). An entry in this block is necessary if the abstract is to be limited.